Forest Stand Hydrological Recovery of Snow Accumulation and Ablation Investigated Using Simultaneous Localization and Mapping (SLAM) Enabled LiDAR

by

Cydne Rae Potter
B.Sc., University of Victoria, 2016

A Thesis Submitted in Partial Fulfillment
of the Requirements for the Degree of

MASTER OF SCIENCE

In the Department of Geography

We acknowledge and respect the Lək̓ʷəŋən (Songhees and Esquimalt) Peoples on whose territory the university stands, and the Lək̓ʷəŋən and W̱SÁNEĆ Peoples whose historical relationships with the land continue to this day.

Forest Stand Hydrological Recovery of Snow Accumulation and Ablation Investigated Using Simultaneous Localization and Mapping (SLAM) Enabled LiDAR

by

Cydne Rae Potter
B.Sc., University of Victoria, 2016

Supervisory Committee

Dr. Daniel Peters, Co-Supervisor
Department of Geography

Dr. Olaf Niemann, Co-Supervisor
Department of Geography

Abstract

Forest-snow interactions were analyzed using fine-resolution mobile terrestrial LiDAR in four stands representing increasing forest maturity ranging from a recently replanted clearcut to a mature forest in the interior cedar – hemlock biogeoclimatic zone of the southern Selkirk Mountain range in British Columbia, Canada. LiDAR-derived models representing peak snow depth and daily ablation were used to assess the impact of sampling intensity on stand-level averages and to determine sampling distances required to capture between-stand differences and within-stand variability. The process of hydrological recovery, a term which describes the return of snow accumulation and ablation processes in regenerating forests to pre-disturbance conditions, was investigated at the scale of individual trees and for the full stand. Outcomes from this study better quantify the influence of tree growth on peak SWE and ablation rate at both the tree and stand level for north aspect mixed conifer stands. The process of negative ablation recovery in early juvenile stands reported in previous studies is herein clearly observed. The methods used increase transferability of outcomes to stands where canopy characteristics (i.e., height, crown cover, and heterogeneity) differ from the reference sites considered here.

Table of Contents

Table of Contents

List of Tables

List of Figures

Acknowledgements

The work presented herein would not have been possible without the unyielding support, motivation, and assistance provided by the following people: Dr. Kim Green, who started me down this path in the first place and who spent many hours organizing and carrying equipment, setting up field surveys, and collecting snow density measurements which supported this project; my supervisors, Dr. Daniel Peters and Dr. Olaf Niemann who somehow remained committed to supporting this project, even when family and life kept me from it; my children, Agnes and Noah Lord; my loving parents, Gregory and Jacqueline Potter; and my loving dog Otis, who kept my feet warm while I sat at the desk for many long hours.

Funding

Funding for this work was provided by the Natural Sciences and Engineering Research Council of Canada (NSERC) CCIP grant 517639-2017 - Building an Innovative Forestry Technology Sector, Selkirk Innovates, and Innovate BC. Industry partners contributing to the funding of this work include Kalesnikoff, INTERFOR, SIFCO, ATCO, BCTS, Cooper Creek Cedar Ltd., Nakusp Community Forest (NACFOR), Timberland Consultants Ltd., Tolko Industries Ltd., and Woodlot Forestry Services Ltd.

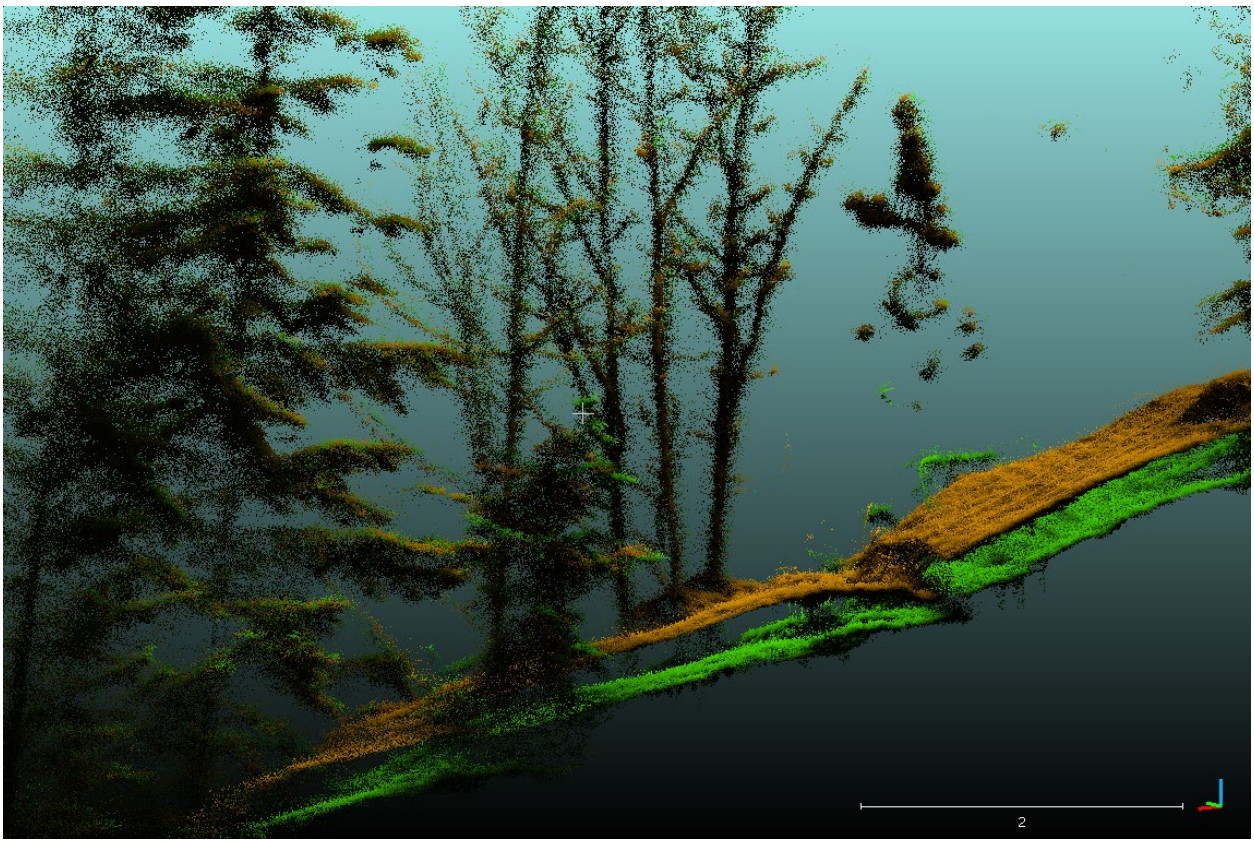

1-meter cross section of two aligned LiDAR pointclouds showing the change in snow surface elevation between March 21 (brown) and April 8 (green).

CHAPTER 1: Introduction

1.1 Introduction

In many watersheds located in cold regions around the world, annual snow melt is the most significant hydrological event in the year and can account for as much as 80% of the total runoff (Ellis et al., 2011; Dixon et al., 2014). Accurate determination of snowpack properties, such as snow water equivalence (SWE) and timing of snowpack ablation are thus crucial for understanding and predicting annual water supplies (Varhola et al., 2010; Dong, 2018) and the potential for flood events (Ellis et al., 2011; Dickerson-Lange et al., 2017). For instance, an early and rapid seasonal snowmelt in watersheds with high accumulation of SWE can result in large-scale flooding and can impact annual water storage within a watershed (Moore and Wondzell, 2005).

Forest canopies influence snow accumulation depths and ablation rates by intercepting falling snow and by controlling the balance between incoming shortwave and emitted long-wave radiation reaching the snow surface (Varhola et al., 2010, Ellis et al., 2010). Snow interception by the forest canopy acts as a significant control on the annual peak SWE of the underlying snowpack (Hudson, 2000; Varhola et al., 2010; Dickerson-Lange et al., 2017; Déry et al., 2014) resulting in accumulations that are up to 40% less than that measured in adjacent clearcuts (Winkler et al., 2005). Decreased snow interception from reductions in forest cover has been shown to result in greater snow accumulation depths and peak SWE (Ellis et al., 2010; Hudson, 2000; Varhola et al., 2014; Boon, 2007).

The net available energy reaching a snowpack is the primary driver of snow melt (Ellis et al., 2011; Varhola et al., 2010). Forest canopies act to reduce incoming shortwave radiation, which effectively reduces the net energy available for driving snow melt processes (Ellis et al., 2011; Varhola et al., 2010; Hudson, 2000; Boon, 2007). In stands which have been altered by either logging or natural (pest or fire) disturbance, reduction in the percentage of canopy closure has been shown to lead to earlier and increased rates of snow melt (Hudson, 2000). These changes to the hydrological behavior of a watershed are most evident where a forest stand or watershed has experienced an extensive reduction in forest cover (Hudson, 2000; Winkler and Boon, 2015).

As juvenile and replanted stands regenerate, their evolving forest structure increasingly affects snow accumulation and melt processes until hydrologically, they resemble a mature forest (Winkler and Boon, 2015; Hudson, 2000). This process is what is referred to as “hydrological recovery”, and is a measure used by forestry companies and resource planners to help determine the degree to which prior

and planned forest harvest may impact the hydrological behavior of a watershed (Winkler and Boon, 2015; Green and Alila, 2012).

While research has shown that forest structure influences snow accumulation and ablation (Varhola et al., 2010; Dickerson-Lange et al., 2017; Winkler et al., 2005), the degree of influence each of these variables play across climate zone boundaries is still poorly understood. Hydrological recovery models developed for recovering stands in British Columbia have focused on climate zones located in the southern coast (Hudson, 2003) where rainfall plays a large role in the annual hydrology, as well as in the southern interior where snowfall represents a larger percentage of the annual precipitation (Winkler and Boon, 2015).

There is no simple model that defines the relationship between snow accumulation or melt processes and forest maturity across all regions. It is therefore crucial to develop a methodology whereby these relationships can be easily quantified at the forest stand and watershed levels to better model hydrological responses to forest removal for lumber and/or degradation from natural disturbances.

Hydrological recovery models developed in British Columbia (Winkler and Boon, 2015; Hudson, 2000) and Ontario (Buttle et al., 2005) have focused on estimations of stand-level SWE and ablation rates derived from point-sampling-based field surveys of snowpack depth and density. These samples are measured at points distributed at even intervals along either a linear snow course or grid within a study area (Winkler and Boon, 2015, Hudson, 2003; Hardy and Hansen-Bristow, 1990). Although informative, these methods often fail to accurately represent the spatial variability of the snowpack, particularly in areas with a high degree of topographic variability, or in areas which are difficult or unsafe to sample (Winkler et al., 2005; Deems et al., 2006). The inherent uncertainty in resulting estimations of stand-level SWE translate into uncertainty in the development of hydrological recovery models and in model outcomes.

Advancements in LiDAR technology have led to an increase in the use of aerial (Hopkinson et al., 2012; Kostadinov et al., 2019; Deems et al., 2013; Zheng et al., 2016), terrestrial (Grunewald et al.,2010), or handheld LiDAR (Bauwens et al., 2016; Ryding et al., 2015) for creating high-precision surface elevation models and more accurate spatial estimations of snow depth and SWE. While Aerial platforms allow for LiDAR measurements of snowpack to be carried out across large areas, the prohibitive costs associated with operating these platforms often limits the frequency of repeated snowpack surveys

throughout the accumulation and ablation periods (Hopkinson et al., 2012; Deems et al., 2013; Zheng et al, 2016). Additionally, the potentially low ground point densities measured by aerial LiDAR under dense forest canopy can limit the ability to consider the relationship between individual trees on snowpack variability (Harpold et al., 2014).

Recent developments in Simultaneous Localization and Mapping (SLAM) based mobile terrestrial LiDAR platforms offer an alternative to the high costs associated with aerial surveys (Ryding et al., 2015). Handheld SLAM systems have the potential to increase the precision of surface models in areas where high canopy closure may reduce the number of LiDAR returns measured from above the canopy (Bauwens et al.; Qian et al, 2016; Ryding et al., 2015). The applicability of SLAM LiDAR for estimating snowpack properties and variability, and for improving for our understanding of hydrological recovery has yet to be explored in British Columbia.

The purpose of this thesis research is to develop a methodology which utilizes SLAM-enabled mobile terrestrial LiDAR to quantify the process of hydrological recovery on peak SWE and ablation rates in forested, mountainous watersheds in the Interior Cedar-Hemlock (ICH) Biogeoclimatic Ecosystem Classification (BEC) zone of British Columbia (BC) (Figure 1-1). This methodological-focused research aims to provide information to improve hydrological recovery models used for resource planning purposes specific to climate zones, at a watershed scale.

There are fourteen BEC zones in BC which identify regions with similar climate and vegetative characteristics (BC Ministry of Forests, 2016). The ICH BEC zone is a highly productive ecological zone which primarily lies at lower elevations in the foothills of the Columbia Mountains and is characterized by cool wet winters and warm dry summers (Ketchison et al., 1991). As much as 50% of the precipitation in the ICH falls as snow, making snow melt an important contributor to the hydrological regime of watersheds in this zone (Ketchison et al, 2016). The ICH has the greatest range of tree species out of all of the BEC zones and is the second most productive in BC for wood fiber production (BC Ministry of Forests, 2016). While the following research will only provide a snapshot of how recovering stands on mid-elevation slopes in the ICH BEC zone influence snow accumulation and ablation processes, this research will help to establish the efficacy of this methodology as a tool for determining the relationships between forest regeneration and hydrological recovery across aspects, elevations, and regions.

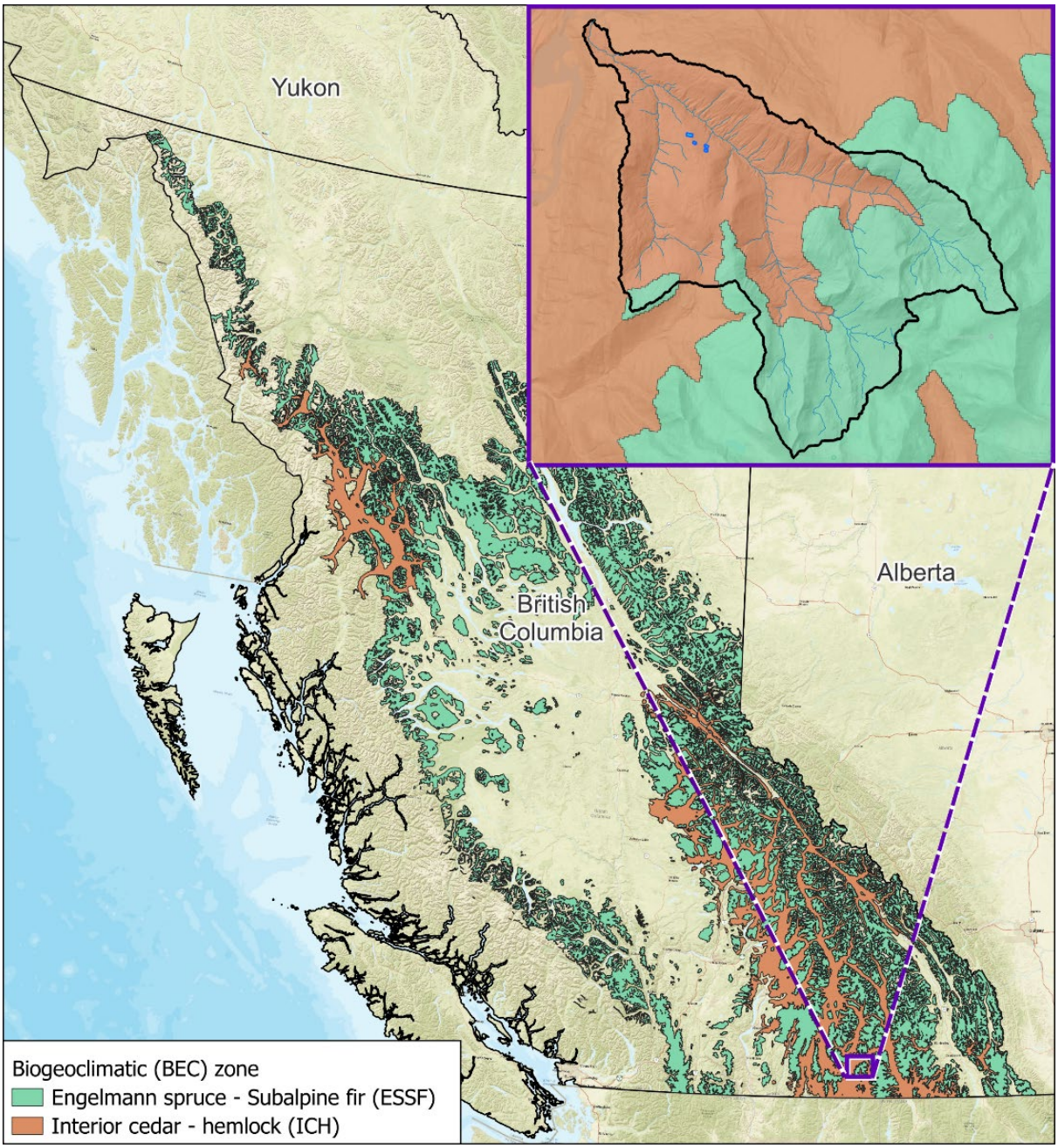

Figure 1-1 The Rover Creek watershed, located in the Bonnington Range of the southern Selkirk Mountains of British Columbia, Canada. Biogeoclimatic (BEC) zones in the Rover Creek watershed include the Engelmann spruce – subalpine fir (ESSF) BEC zone (teal) and the interior cedar – hemlock (ICH) BEC zone (orange) which encompasses the area in this study [study sites shown in blue, inset map].

1.2 References

Bauwens, S., Bartholomeus, H., Calders, K., & Lejeune, P. (2016). Forest Inventory with Terrestrial LiDAR: A Comparison of Static and Hand-Held Mobile Laser Scanning. *Forests*, *7*, 127. https://doi.org/10.3390/f7060127

BC Ministry of Forests (2016). The Ecology of the Interior Cedar-Hemlock Zone. Victoria, BC. Retrieved from https://www.for.gov.bc.ca/hfd/pubs/docs/bro/bro48.pdf

Boon, S. (2007). Snow accumulation and ablation in a beetle-killed pine stand in Northern Interior British Columbia. *BC Journal of Ecosystems and Management*, *8*(3), 1–13.

Buttle, J, M., Oswald, C.J., and Woods, D.T. (2005). Hydrologic Recovery of Snow Accumulation and Melt Following Harvesting in Northeastern Ontario. *62nd Eastern Snow Conference. Waterloo, ON, Canada 2005*.

Deems, J.S., Fassnacht, S.R., Elder, K.J (2006). Fractal Distribution of Snow Depth from Lidar Data. *Journal of Hydrometeorology, 7, 285-29.*

Deems, J. S., Painter, T. H., & Finnegan, D. C. (2013). Lidar measurement of snow depth: A review Lidar measurement of snow depth: a review. *Journal of Glaciology*, *59*, 467–479. https://doi.org/10.3189/2013JoG12J154

Déry, S., Knudsvig, H., Hernández-Henríquez, M., & Coxson, D. (2014). Net Snowpack Accumulation and Ablation Characteristics in the Inland Temperate Rainforest of the Upper Fraser River Basin, Canada. *Hydrology*, *1*(1), 1–19. https://doi.org/10.3390/hydrology1010001

Dickerson-Lange, S. E., Gersonde, R. F., Hubbart, J. A., Link, T. E., Nolin, A. W., Perry, G. H., … Lundquist, J. D. (2017). Snow disappearance timing is dominated by forest effects on snow accumulation in warm winter climates of the Pacific Northwest, United States. *Hydrological Processes*, *31*(10), 1846–1862. https://doi.org/10.1002/hyp.11144

Dixon, D., Boon, S., & Silins, U. (2014). Watershed-scale controls on snow accumulation in a small montane watershed, southwestern Alberta, Canada. *Hydrological Processes*, *28*(3), 1294–1306. https://doi.org/10.1002/hyp.9667

Dong, C. (2018). Remote sensing, hydrological modeling and in situ observations in snow cover research: A review. *Journal of Hydrology*, *561*(February), 573–583. https://doi.org/10.1016/j.jhydrol.2018.04.027

Ellis, C. R., Pomeroy, J. W., Brown, T., & Macdonald, J. (2010). Simulation of snow accumulation and melt in needleleaf forest environments. *Hydrology and Earth System Sciences*, *14*(1995), 925–940. https://doi.org/10.5194/hess-14-925-2010

Ellis, C. R., Pomeroy, J. W., Essery, R. L. H., & Link, T. E. (2011). Effects of needleleaf forest cover on radiation and snowmelt dynamics in the Canadian Rocky Mountains. *Can. J. For. Res.*, *41*, 608–620. https://doi.org/10.1139/X10-227

Green, K. C., & Alila, Y. (2012). A paradigm shift in understanding and quantifying the effects of forest harvesting on floods in snow environments. *WATER RESOURCES RESEARCH*, *48*(August), 1–21. https://doi.org/10.1029/2012WR012449

Grünewald, T., Schirmer, M., Mott, R., & Lehning, M. (2010). Spatial and temporal variability of snow depth and ablation rates in a small mountain catchment. *Cryosphere*, *4*(2), 215–225. https://doi.org/10.5194/tc-4-215-2010

Hardy, J.P. and K.J. Hansen-Bristow. (1990). Temporal accumulation and ablation patterns in forests representing varying stages of growth. Proc. 58th West. Snow Conf., Sacramento, Calif., pp. 23–24.

Harpold, A., Guo, Q., Molotch, N., Brooks, P., Bales, R., Fernandez-Diaz, J., … Lucas, R. (2014). LiDAR-derived snowpack data sets from mixed conifer forests across the Western United States. *Water Resources Research*, *50*(October 2013), 1–7. https://doi.org/10.1002/2013WR013935.

Hopkinson, C., Collins, T., Anderson, A., Pomeroy, J., & Spooner, I. (2012). Spatial snow depth assessment using LiDAR transect samples and public GIS data layers in the Elbow River watershed, Alberta. *Canadian Water Resources Journal*, *37*(2), 69–87.

Hudson, R. (2000). Snowpack recovery in regenerating coastal British Columbia clearcuts. *Canadian Journal of Forest Research*, *30*, 548–556.

Hudson, R. (2003). *Using Combined Snowpack and Rainfall Interception Components to Assess Hydrologic Recovery of a Timber-Harvested Site: Working Toward an Operational Method*. Forest Service of British Columbia

Ketcheson, M. V., Braumandl, T. F., Meidinger, D., G. Utzig, G., Demarchi, D. A., & B.M. Wikeem, B. M. (1991). *ECOSYSTEMS OF BRITISH COLUMBIA*. Victoria, BC. Retrieved from https://www.for.gov.bc.ca/hfd/pubs/docs/srs/srs06/chap11.pdf

Kostadinov, T. S., Schumer, R., Hausner, M., Bormann, K. J., Ga, R., Mcgwire, K., … Harpold, A. A. (2019). Remote Sensing of Environment Watershed-scale mapping of fractional snow cover under conifer forest canopy using lidar. *Remote Sensing of Environment*, *222*, 34–49. https://doi.org/10.1016/j.rse.2018.11.037

Moore, R. D., & Wondzell, S. M. (2006). Physical Hydrology and the Effects of Forest Harvesting in the Pacific Northwest: A Review. *Journal of the American Water Resources Association,* 04065, 763–784.

Qian, C., Liu, H., Tang, J., Chen, Y., Kaartinen, H., & Kukko, A. (2016). An Integrated GNSS / INS / LiDAR-SLAM Positioning Method for Highly Accurate Forest Stem Mapping. *Remote Sensing*, *9*(3), 1–16. https://doi.org/10.3390/rs9010003

Ryding, J., Williams, E., Smith, M. J., & Eichhorn, M. P. (2015). Assessing Handheld Mobile Laser Scanners for Forest Surveys. *Remote Sensing*, *7*, 1095–1111. https://doi.org/10.3390/rs70101095

Sammartano, G., & Spanò, A. (2018). Point clouds by SLAM-based mobile mapping systems: accuracy and geometric content validation in multisensor survey and stand-alone acquisition. *Applied Geomatics*, *10*, 317–339.

Varhola, A., Coops, N. C., Bater, C. W., Teti, P., Boon, S., & Weiler, M. (2010). The influence of ground- and lidar-derived forest structure metrics on snow accumulation and ablation in disturbed forests. *Canadian Journal of Forest Research*, *40*(4), 812–821. https://doi.org/10.1139/X10-008

Varhola, A., Coops, N. C., Alila, Y., & Weiler, M. (2014). Exploration of remotely sensed forest structure and ultrasonic range sensor metrics to improve empirical snow models. *Hydrological Processes*, *28*(15), 4433–4448. https://doi.org/10.1002/hyp.9952

Winkler, R., & Boon, S. (2015). *Revised Snow Recovery Estimates for Pine- dominated Forests in Interior British Columbia*. Ministry of Forests, Lands, and Natural Resource Operations. Kamloops, BC.

Winkler, R. D., Spittlehouse, D. L., & Golding, D. L. (2005). Measured differences in snow accumulation and melt among clearcut, juvenile, and mature forests in southern British Columbia. *Hydrological Processes*, *19*(1), 51–62. https://doi.org/10.1002/hyp.5757

Zheng, Z., Kirchner, P. B., & Bales, R. C. (2016). Topographic and vegetation effects on snow accumulation in the southern Sierra Nevada: a statistical summary from lidar data. *The Cryosphere*, *10*, 257–269. https://doi.org/10.5194/tc-10-257-2016

Zheng, Z., Molotch, N. P., Oroza, C. A., Conklin, M. H., & Bales, R. C. (2018). Spatial snow water equivalent estimation for mountainous areas using wireless-sensor networks and remote-sensing products. *Remote Sensing of Environment*, *215*(October 2017), 44–56. https://doi.org/10.1016/j.rse.2018.05.029

CHAPTER 2: Literature Review

The following literature review was undertaken to ascertain the existing body of research pertaining to two main themes: 1) Research relating to the current understanding of snow-forest interactions, and how these relate to hydrological recovery in snow-dominated watersheds; 2) Application of the emerging LiDAR technology to obtain snow depth and SWE across large areas.

2.1 Forest-snow relationships and hydrological recovery

The relationships between forest cover and below-canopy snowpack accumulation/ablation have been investigated over the past century in a variety of forest types and geographic locations. The earliest documented publication included in this review was undertaken by C.A. Connaughton in 1935, who investigated differences in snow accumulation and melt between clearcut, replanted, and virgin forest stands in the Boise River Watershed (Connaghton, 1935). In the decades following this pioneering work, studies have investigated these relationships using similar comparisons between either forested areas and openings or between stands with differences in forest maturity (Troendle and Meiman, 1984; Winkler and Boon, 2015; Buttle et al., 2005; Hudson, 2000; Talbot and Plamondon, 2002; Jones, 2000, etc.).

Although the above studies encompass a range of forest types and BEC zones, most are situated in southwestern Canada (Winkler and Moore; 2006; Winkler and Boon; 2015; Hudson, 2000) or in the northwestern of the United States (Dickerson-Lange et al., 2015; Hardy and Hansen-Bristow, 1990; Elder et al., 1991; Storck et al, 2002; Musselman et al, 2008; Troendle and Meiman, 1984). A handful of other studies have been carried out in other regions, including eastern Canada (Buttle et al., 2005; Talbot and Plamondon, 2002), Sweden (Odin and Degermark, 1990; Löfvenius et al., 2003), and Czechia (Hotovy and Jenicek, 2020).

Regardless of location, each of these studies focused on the specific topographic, climatic, and vegetation characteristics of their areas. Authors from several of these studies acknowledge that transferability of specific study outcomes to other climate regions, forest types, and to watersheds with different topographic characteristics should be done with caution (Winkler and Boon, 2015; (Musselman et al, 2008; Hudson, 2000). However, as outlined below, some general relationships between forests and below-canopy snowpack are consistent between the studies.

2.1.1 Forest-snow relationships

In snow-dominated watersheds, annual water supplies, stream flow magnitude and streamflow longevity are influenced by forest cover (Winkler and Boon, 2015; Varhola et al., 2010). In these watersheds, forest cover acts to control ground-level snow accumulation through canopy interception, whereby up to 60% of cumulative snowfall has been shown to be intercepted and up to 40% sublimated from the canopy (Hedstrom and Pomeroy, 1998). Forest cover also influences the timing and rate of snow melt through canopy shading (Winkler et al., 2005; Ellis et al., 2011). Forestry-related disturbances which reduce the canopy closure or stand heights can alter the hydrologic regime of the watershed (Hudson; 2000). Forest harvesting has been shown to lead to increased annual water yields and peak flows, as well as extend period of summer low flows (Moore and Wondzell, 2005; Hudson, 2000). These hydrological effects have been observed at the stand, hillslope, and watershed scales (Hudson, 2000; Moore and Wondzell, 2005). While the relationships between forest cover and snow accumulation/ablation have been confirmed by numerous studies, study outcomes highlight the complexity of these relationships and the high degree of variability between regions, stand types, and year (Varhola et al., 2010).

It should be noted that ablation processes are generally considered in terms of changes in stand-level SWE, rather than snow depth, as these measures quantify the loss of water volume (Winkler et al., 2005; Ellis et al., 2011). SWE is calculated by multiplying snow depth by snow density, which is a better measure for comparisons of snowpack between areas with different or non-uniform snow densities. However, ripening of the snowpack prior to the onset of melt typically reduces the variability in snow density so that the major source in variation in SWE is directly related to the variation in snow depth (Elder et al., 1991). As such, studies investigating forest-snow ablation relationships use either SWE or depth, according to the study design or snow sampling methodologies used.

Vegetation controls on snow accumulation

In general, canopy interception during the accumulation period results in reduced ground-level accumulation depths and associated SWE below the forest canopy compared to in the openings (Moore and Wondzell, 2005; Varhola et al., 2010; Troendle and Meiman, 1984; Buttle et al, 2005). In the northwest US and southwestern Canada, Moore and Wondzell summarized regional study outcomes which identified snow accumulation in cutblocks as having between 30% to 50% more snow than in the surrounding forested areas. Additionally, Hudson (2000) found that there was approximately twice as

much snow in young stands with canopy heights under 3.5m than there was in the surrounding old growth.

As stands begin to regenerate and achieve juvenile height and canopy closure characteristics, the increasing interception capacity in these juvenile stands begins to influence ground-level accumulation. Winkler and Moore (2006) measured April 1 SWE in the Thompson Okanagan region of British Columbia in adjacent clearcut, juvenile, and mature stands and found that snow accumulation in the clearcut was 16% higher than in juvenile stand and 47% higher than in the mature forest.

Differences in canopy interception capacity are able to explain most of the difference in ground level accumulation between forested areas and clearcuts (Troendle and Meiman, 1984). However, when considering the variability of the snowpack between years, there are greater differences in below-canopy snowpack depths observed in forested areas than in either clearcuts or natural openings (Winkler and Moore, 2006). In these forested areas, trees and low vegetation can act to trap snow, while preferential deposition controlled by the variability of the forest canopy can also influence differences in ground-level accumulation of the snowpack, resulting in greater between-year differences (Buttle et al., 2005; Troendle and Meiman, 1984).

Vegetation controls on ablation

Snow ablation, which is the combined loss of the snowpack resulting from melt, sublimation, and evaporation, is driven by the net radiation reaching the surface (Ellis et al., 2010; Ellis et al., 2011). This net radiation includes the total balance of incoming and outgoing shortwave radiation (solar), the total incoming and outgoing longwave radiation (re-emitted) from the snowpack and surrounding vegetation, as well as sensible and latent heat fluxes (Ellis et al., 2010; Hotovy and Jenicek, 2000). In forested stands, the canopy acts to reduce incoming shortwave radiation (Varhola et al., 2010) while also increasing the incoming long-wave radiation re-emitted from the canopy to the snowpack surface (Ellis et al., 2010).

Forest removal can result in an increase in incoming shortwave radiation while also causing increased outgoing longwave radiation leaving the snowpack (Ellis et al. 2010). The relative amount of incoming and outgoing shortwave and longwave radiation varies according to hillslope aspect, canopy cover, and to a lesser degree, vegetation height (Ellis et al., 2011; Hotovy and Jenicek, 2020; Davis et al. 1997). Together, these variables control the net energy driving snowmelt rates and timing. According to a summary of study outcomes in the pacific northwest presented by Moore and Wondzell (2005),

snowmelt rates are typically 30% to 100% higher in openings compared to forested areas, as the increase in incoming shortwave radiation tends to outweigh longwave energy losses.

Many of the studies investigating forest-ablation relationships were conducted in study sites situated on flat terrain, where slope aspect was not considered (Stork et al., 2002; Hudson; 2000; Winkler and Boon; 2015). In these studies, Storck et al (2002) found that the combination of reduced snow accumulation through canopy interception, paired with increased longwave radiation from the canopy, resulted in earlier snow disappearance in forested stands than in the open sites. However, Löfvenius et al. (2003) observed earlier snow disappearance in clearcut stands compared to stands characterized by multilayered shelterwood due to a large increase in incoming solar radiation.

Studies which utilize flat references sites to investigate the relationship between forest cover and ablation are of course not representative watersheds in mountainous regions, where forested and disturbed stands are situated on slopes encompassing a range of aspects. Ellis et al (2011) considered the role of aspect plays in determining both the timing and rate of snow melt in the Marmot Creek Research Basin located in southwestern Alberta. This study showed that topographic shading on north aspects causes a reduction to total incoming shortwave radiation compared to south aspects. This study found that topographic reductions in incoming shortwave energy on north aspects was offset by increased longwave radiation emitted from the canopy. This was found to result in earlier snow melt in forested areas and delayed melt in the openings, where longwave energy loss resulted in an energy deficit (Ellis et al., 2011). On south aspects where there is no topographic shading, the reduction in shortwave energy is found only in forested areas, which causes a delayed and slower ablation rate in forested stands compared to openings (Ellis et al., 2011).

Vegetation influence on within-stand variability

The majority of research investigating forest – snow relationships has focused on stand-level differences in measures of snow depth, SWE, or ablation rate between open, juvenile, or mature stands. However, within-stand variability of the snowpack may also be an important consideration, particularly when establishing the transferability of study outcomes from reference sites with known stand heights, tree spacing, and canopy cover to stands and geographic areas where snow accumulation and melt are influenced by microtopography or variable canopy cover (Winkler and Moore, 2006; Elder et al., 1991). As such, within-stand variability and tree-scale controls on below crown accumulation and ablation have been explored in studies which consider the snowpack surrounding individual trees (Musselman et al.,

2008; Hardy et al., 1997), and in small (4m radius) survey plots located in stands with varying degrees of maturity (Winkler and Moore, 2006).

Although canopy interception in conifer forests has been shown to result in reduced sub-canopy accumulation at the scale of the stand (Buttle et al., 2005), individual tree crowns can also cause a localized, below-crown reduction adjacent to the tree bole, creating a feature known as a tree well (Mussleman et al., 2008). Snow depth in these tree wells increases nonlinearly with distance away from the individual tree boles to a distance equal to the radius of the individual tree crown (Musselman et al., 2008; Winkler and Moore, 2006). Hardy et al. (1997) found that the snow depth adjacent to the tree bole was approximately 20% of the undisturbed surrounding snowpack. The distribution of individual trees and their respective tree wells within a stand can result in a spatially heterogenous snowpack (Hardy et al., 1997). This complexity is important when considering the relationship between stand maturity and snow accumulation, as increasing tree density in a stand may result in stand-scale reductions in snow accumulation.

Ablation processes in both forested and recently replanted stands can also be complex, with differential melting causing increased within-stand variability of SWE as the melt season progresses (Hotovy and Jenicek, 2000; Löfvenius et al., 2003; Odin and Degermark, 1990). Hotovy and Jenicek (2000) investigated the impact of forest disturbance on the net energy balance at the snow surface in stands with different canopy structures using a CNR4 Net Radiometer established within each stand. They found that in recently replanted clearcuts characterised by smaller trees, longwave radiation from individual trees could be detected up to distances of approximately 5m. This longwave radiation can drive snowmelt near the tree base, exposing them to more incoming shortwave radiation both directly, and reflected from the surrounding snowpack (Odin and Degermark, 1990; Löfvenius et al., 2003). This process has the potential to accelerate the ablation rates adjacent to smaller trees and can result in stand-level melt rates which exceed those seen in unplanted clearcuts and natural openings (Löfvenius et al., 2003).

2.1.2 Hydrological recovery

In snow-dominated watersheds, the recovery of SWE and ablation processes are collectively referred to as hydrological recovery; a term which describes the restoration of hydrological characteristics to pre-disturbance conditions (Winkler and Boon, 2015; Buttle et al., 2005; Hudson, 2000; Talbot and Plamondon, 2002; Jones, 2000). Hydrological recovery is expressed as a positive trend increasing from 0% for clearcut to 100% for a regenerated mature stand. Although numerous studies have investigated stand-level differences in snow accumulation and melt according to forest maturity (Buttle et al., 2000; Murray and Buttle, 2003; Winkler et al., 2005; Winkler and Moore, 2006; Varhola et al.,2010; Broxton et al., 2015; Konstantinos et al., 2018), few studies have specifically addressed the process by which disturbed and regenerating stands recover hydrologically (Winkler and Boon; 2015; Buttle et al., 2005; Hudson, 2000; Talbot and Plamondon, 2002).

To date, hydrological recovery for snowmelt dominated watersheds has primarily been studied in 5 geographic areas. These studies include the following: Hardy and Hansen-Bristow (1990) considered the recovery of peak snow accumulation and ablation according to canopy cover in the Gallatin National Forest of Montana (USA); Hudson (2000) investigated snowpack recovery of peak SWE and ablation in the coastal mountains of British Columbia (Canada); Talbot and Plamondon (2002) focused on the recovery of melt rates in Montmorency Forest in Quebec (Canada); Buttle et al (2005) focused on snowpack recovery of peak SWE and ablation in the boreal forest of northeastern Ontario (Canada); Buttle et al (2018) considered hydrological recovery in deciduous forest stands in the Boreal Shield Ecozone in the Algoma region of central Ontario; and Winkler and Boon (2015) created updated models of hydrological recovery of peak SWE and ablation in the Thompson-Okanagan region of British Columbia (Canada).

All of these studies rely on stand-averaged values of SWE or changing SWE derived from traditional snow-sampling methods at select points and averaging these measured values for the entire stand. These averaged values were measured for stands encompassing a range of forest maturity at the time of assumed (April 1st) peak SWE and at some point later in the melt season or at the time of snow-disappearance. With the assignment of 0% recovery for clearcut stands and 100% for mature forest, the percentage of recovery in regenerating juvenile stands was determined according to stand height and canopy cover by comparing the percentage of change from the clearcut condition (Hudson, 2000; Winkler and Boon, 2015; Buttle et al., 2005).

The resulting recovery values were plotted against either stand height or canopy cover to derive empirical models representing the process of recovery for each of these study areas (Hudson, 2000;

Winkler and Boon, 2015; Buttle et al., 2005). Hudson (2000) determined that using a Chapman-Richards curve fitted to data points representing recovery according to stand height resulted in the best representation of the process of hydrological recovery. This method of curve fitting was also used in the subsequent studies by Buttle et al (2005) and Winkler and Boon (2015).

Hydrological recovery begins when a regenerating stand is able to intercept snowfall and reduce incoming solar radiation (Winkler et al, 2015). The initiation of recovery and the rate at which it progresses differs between studies and geographic locations. Hardy and Hansen-Bristow (1990) found no measurable recovery for trees under 13 years in age. The authors also determined that a 41% recovery of peak SWE and 48% recovery of ablation rate was reached once the stand was 10 to 14m tall. The rate of recovery was observed to differ depending on whether a stand was replanted or left to regenerate naturally. For instance, in Montana, hydrological recovery in replanted stands was determined to occur within approximately 35 years but would take 79 years in a naturally regenerating stand (Hardy and Hansen-Bristow, 1990).

Hudson (2000) estimated that in coastal BC, 50% hydrological recovery was reached when stands were 4 m in height and had a canopy density of 20%; while full recovery was reached by the time the stand was 20 m and a canopy density of 95%. In Montmorency Quebec, Talbot and Plamondon (2002) determined that hydrological recovery reaches 50% when a stand is 4 m in height and full recovery at 10 m. The latter study considered paired stands (by maturity) on north versus south aspects and found that snow melt rates, and recovery, were not consistent across aspects. Buttle et al (2005) found that in Ontario, the recovery rate of peak SWE was faster than the recovery of ablation rate. Buttle found that when a stand is 15 years in age, peak SWE had recovered by 80% but had only reached an ablation recovery of 50%. Winkler and Boon (2015) determined that recovery of peak SWE and ablation in the Thompson-Okanagan region (BC) only began once the trees had grown to heights greater than 3 m. In Winkler and Boon (2015), recovery curves were developed according to stand height, showing that the hydrological recovery of the stand reaches 10% when a stand is 5 m, and over 80% when the stand has reached 15 m in height.

In the studies of Winkler and Boon (2015) and Buttle et al. (2005), an initial period of increased melt rate in the clearcut condition was observed compared to adjacent small trees in very young stands. This observation suggested the likelihood of a period of negative recovery (Winkler and Boon; 2015; Buttle et al, 2005) for recently replanted stands. These studies considered hydrological recovery

averaged for the stand and thus lack the precision required to determine the process by which recovery transitions from negative to positive as a stand matures.

The literature review above reveals that the processes and rates of hydrological recovery in snow-dominated watersheds vary by forest type, topography, and geographic region. While the current research does provide a methodological framework for deriving models of recovery in regenerating stands, it is clear that more research is needed to develop methods which can be more broadly applied, or which can be adjusted to account for the unique characteristics of individual watersheds (Hudson, 2000; Moore and Wondzell, 2005; Winkler and Boon, 2015; Musselman et al, 2008). Advancement of hydrological recovery science will therefore depend on the acquisition of representative measures of snowpack depth and density which can effectively quantify the unique snowpack and forest stand characteristics of a watershed.

2.2 Traditional and LiDAR-based snow surveys

The ability to accurately quantify snow depth distributions within a watershed using traditional manual sampling methods is limited by challenges related to ease of access, the lengthy time involved in collecting a representative sample (Harder et al., 2020), and safety considerations (Deems et al., 2006; Harder et al., 2020). This is particularly true in mountainous terrain, where steep slopes and deep snow accumulations limit accessibility (Deems et al., 2006). As the variability of the snowpack can have a large influence on stand or watershed calculations of mean SWE, it is therefore critical to explore methods which may more effectively capture this variability (Dong, 2018).

Increasingly, remote sensing using satellite or aerial platforms is being used to quantify the spatiotemporal distributions of snow depth to better estimate the snow water equivalence stored in a watershed, and to predict snow melt rates and timing (Painter et al., 2016; Zheng et al., 2018). While the presence or absence of snow can be determined for unvegetated areas using optical remote sensing platforms and satellite imagery, these remote sensing methods are not suited for observing the presence of snow beneath forest canopy and within vegetation (Kostadinov et al., 2019).

Light detection and ranging (LiDAR) is an active remote sensing method which can effectively measure a continuous surface of snow or the bare terrain with a high degree of horizontal and vertical precision, even in forested areas (Hopkinson et al., 2004; Varhola et al., 2010; Dharmadasa et al., 2024; Musselman et al., 2008). LiDAR calculates distances based on the time elapsed between a transmitted and returned laser pulse (Kostadinov et al., 2019; Deems et al., 2006). As the laser pulse travels, it

interacts with vegetation, terrain, or snow and is reflected back to the sensor (Zheng et al., 2016). The measured returns result in a three-dimensional point cloud which can be used to produce fine-resolution digital terrain and snow surface elevation models, which in turn can be used for the development of models representing snow depth (Hopkinson et al., 2012). Additionally, LiDAR point clouds can be used to derive tree or stand-level height and canopy cover measures representing the overlying vegetation which can be used to investigate forest-snow relationships (Hopkinson et al., 2012; Zheng et al., 2016).

LiDAR is a relatively new tool in the snow survey toolkit. Some of the earliest work investigating the utility of LiDAR for quantifying measures of snow depth in a forested watershed were carried out by Hopkinson et al. (2001). In this early work, the authors investigated the utility of aerial LiDAR for mapping the distribution of snow depth in a variable forest stand. In the 2 decades following this early work, improvements to LiDAR sensors, and the introduction of more platform options for LiDAR surveys have led to its increased use.

2.2.1 Traditional methods for quantifying snow depth and SWE

In studies reviewed in Section 2.1.1 and 2.1.2, only a single value for stand-level snow depth/SWE or ablation was used to investigate the process of hydrological recovery or for comparing differences in snow accumulation or ablation according to stand age. The assigned value for the stand in each study was derived using traditional snow-survey methods. For instance, snow depth or density was recorded at only a single location within the stand in some studies. Single point snow depths can be measured using an optical snow-depth sensor (Dickerson-Lange et al., 2017) or with an acoustic depth sensor (Dickerson-Lange et al., 2015). Snowpack density or SWE can be measured using a snow pillow (Déry et al., 2014) or weighing lysimeter (Storck et al., 2002). These index locations are typically situated in flat, protected areas unaffected by wind, slope, or aspect (Grünewald and Lehning, 2015). In mountainous environments where variable topography and vegetation cover influence the distribution of snow accumulation and ablation processes (Ellis et al., 2011), these single point measures are unlikely to accurately represent the stand.

Several studies have employed traditional point-based sampling methods using snow depth probes or snow tubes to collect measures of snowpack depth or density either along an equally spaced snow course or transect (Buttle et al., 2005; Dickerson-Lange, 2017; Hudson, 2000; Storck et al., 2002,

Löfvenius et al., 2003), or by using a sampling grid design with sampling points measured every 10m to 20m (Winkler et al., 2005; Winkler and Boon, 2015; Dickerson-Lange et al., 2017; Hardy and Hansen-Bristow, 1990; Talbot and Plamondon, 2002). The spacing of these sampling points and the sample sizes used are largely based on established snow-survey standards or on previous studies (Winkler and Spittlehouse, 1995 Hardy and Handsen-Bristow, 1990). For example, Winkler and Boon (2015) used a combination of data collected in grids spaced at 10 m and 15 m. These sampling distances were chosen according to outcomes from a power analysis undertaken by Spittlehouse and Winkler (1996) which was based on 3 years of SWE measurements collected from this study area. This power analysis determined the sampling intensity required to identify hydrologically significant differences in snow accumulation and ablation according to stand maturity.

Single values of stand-level depth or SWE are typically determined by calculating the mean value from all samples measured in each snow course or grid-based snow survey (Dickerson-Lange, 2017; Dickerson-Lange et al., 2015; Buttle et al., 2005; Winkler and Moore, 2006; Winkler and Boon, 2015). These average values are used for identifying stand-level peak SWE, and also for determining ablation rates by calculating the average change in SWE across a date range (Winkler and Boon (2015).

Accurately representing stand-level snow depth or SWE is crucial for limiting the uncertainty introduced to between-stand comparisons of snow accumulation and ablation, or for developing models representing the process of hydrological recovery. It should be noted that some uncertainties in these stand-level measures have been identified related to both sampling design and measurement error (Winkler and Spittlehouse, 1995). Perhaps one of the largest sources of uncertainty is related an inability of traditional point-sampling methods to accurately capture within-stand variability. As noted in section 2.1.1 the distribution of trees in coniferous stands can influence stand-level averages by controlling the distribution and overlap (or not) of individual tree wells (Mussleman et al., 2008). Snow depth variability has been shown to be greater in forested areas than in the openings, due to these localized controls (Storck et al., 2002). Sampling distances of 10m to 20m are also unlikely to capture this within stand variability, as these sampling distances are often greater than tree well diameters, particularly in juvenile stands (Winkler and Moore, 2006).

Sampling methods which more effectively capture this within-stand variability in coniferous forests have the potential not only to more accurately predict seasonal snow water storage (Grünewald and Lehning, 2015) but may also aid the development of more accurate models of hydrological recovery (Winkler and Boon, 2015).

2.2.2 LiDAR platforms

The majority of LiDAR-based snow surveys have utilized aerial platforms to carry the LiDAR scanner, although sub-canopy LiDAR surveys have also been performed for smaller areas using either terrestrial laser scanners (TLS) or handheld mobile terrestrial LiDAR units. The platform-type chosen for these studies has depended on study objectives, the LiDAR technology available at the time of the study, and the detail of ground surface or overlying vegetation being considered. For large geographic areas such as a full watershed basin, aerial platforms are typically preferred, as they can cover the full basin area within a relatively small window of time (Kostadinov et al., 2019; Deems et al., 2013). However, the costs associated with operating aircraft can be prohibitive (Deems et al., 2013). For studies investigating sub-canopy snowpack and vegetation interactions at finer resolutions, TLS and handheld mobile terrestrial LiDAR platforms may be preferred, as these survey methods produce LiDAR point clouds with higher point densities, capturing a greater level of detail of the snowpack surface and surrounding vegetation (Bhardwaj et al., 2016; Harder et al., 2020).

Aerial platforms (not including UAVs)

Aerial LiDAR surveys have an advantage over other platform options due to the ability to cover large areas in a single day (Deems et al., 2013). In an aerial survey, the LiDAR sensor is mounted onto an airframe, such as a fixed wing aircraft (Deems et al., 2006; Hopkinson et al., 2001; Hopkinson et al., 2012; Tinkham et al., 2011), helicopter (Varhola et al., 2010) or using high-altitude aircraft. High altitude LiDAR has primarily been collected either by the Airborne Snow Observatory (ASO) (Painter et al., 2016; Raleigh and Small, 2017) or by the National Center for Airborne Laser Mapping (NCALM) (Kostadinov et al., 2019; Kirchner, 2014; Zheng et al., 2016; Harpold et al., 2014). An inertial measurement unit (IMU) is integrated along with the LiDAR sensor to account for the movement of the airframe (roll, pitch, and yaw), and a global positioning system (GPS) is incorporated to geolocate the resulting pointcloud relative to global coordinate systems (Painter et al., 2016; Deems et al., 2013).

Aerial LiDAR surveys are carried out by flying parallel and overlapping flightlines to ensure that a continuous ground surface is measured (Hopkinson et al., 2012). The point density of the resulting point cloud is controlled by a combination of factors relating to the survey design. LiDAR beams emitted from the sensor spread with distance through beam divergence (Deems et al., 2006). The height of the platform above the ground controls the spread (and density) between measured points. The flight

pattern used, along contour or perpendicular to the terrain slope, will also affect beam divergence and the resulting spread of LiDAR returns (Deems et al, 2013). Finally, the speed of the aircraft determines the number of emitted LiDAR pulses reaching the survey area (Sullivan et al., 2023).

Although subject to the combined influences of survey design, aircraft altitude, and aircraft speed, LiDAR surveys are able to produce ground-measured point densities of between 2 and 20 points/m^2 (Tinkham et al., 2012; Harpold et al., 2014). Typical spatial resolutions of gridded digital elevation models (DEMs) representing bare ground or snow surface produced from aerial LiDAR are between 1 and 1.5 m, depending on the density of ground returns (Varhola et al., 2010; Deems et al, 2006; Sullivan et al, 2023). In forested areas, aerial LiDAR surveys have been shown to have accuracies up to 10 cm root mean squared error (Deems et al., 2013), while mean snow depths derived from these DEMs have been determined to be within 0.13 m of field-based measurements (Hopkinson et al., 2012).

Unmanned aerial vehicles (UAVs)

In recent years, the development of lightweight LiDAR sensors has allowed for their increased use on lower-cost unmanned aerial vehicles (UAVs) (Bhardwaj et al., 2016). Although UAV-based LiDAR surveys are limited in their ability to cover extensive areas, their lower flight altitudes and slower flight speeds produce higher-density point clouds between 10 and 100 times greater than is typical for aerial surveys (Dharmadasa et al., 2024; Sullivan et al., 2023; Harder et al. 2020). Lower flight altitudes also allow for greater canopy penetration, making UAV based snow surveys more effective for use in studies considering the variability of snowpack depth under forest canopies (Sullivan et al., 2023). The lower costs associated with UAV LiDAR surveys compared to other aerial LiDAR platforms also allows for the potential to conduct more frequent surveys throughout the ablation period.

Terrestrial Laser Scanners (TLS)

Several snow surveys have relied on relatively low-cost terrestrial laser scanners (TLS) to conduct fine-resolution measures of snowpack variability or to investigate tree effects on below-canopy snow accumulation (Egli et al., 2012; Mendoza et al., 2020; Currier et al., 2019; Hancock et al., 2014; Revuelto et al., 2015). Although the LiDAR coverage area in TLS surveys can be limited due to the smaller range of the scanner (eg <500 m or <1500 m depending on the wavelength used) and the stationarity of the TLS platform (Deems et al., 2013), multiple scans can be carried out in a site from more than one

position, and subsequently tied together using common points established in the scan area prior to carrying out the survey (Bauwens et al., 2016). The accuracy of the measured snow surface or ground elevation is typically very high as positional errors are not introduced from a moving platform (Egli et al., 2012; Deems et al., 2013). The close scanning range of these ground-level surveys produces point clouds with much larger point densities than in either aerial or UAV LiDAR surveys (Revuelto et al., 2015).

One of the potential limitations of the stationary survey design is the inability to scan the snow surface or surrounding vegetation from more than one direction (Bauwens et al., 2016). Single scan TLS surveys have little utility, as the resulting pointclouds lack completeness in their representation of the measured area (Bauwens et al., 2016; Egli et al., 2012). Topographic or vegetative occlusion prevents emitted laser pulses from "seeing" behind individual trees or topography. To compensate for this, multiple scans are set up throughout the study area, and the resulting pointclouds from the individual scans are tied together using common points (Revuelto et al., 2015; Deems et al., 2013). This process is time consuming compared to mobile platforms, but the resulting point clouds can be used to build snow depth models with an accuracy of within 0.05 m across a distance of 250 m (Egli et al., 2012).

Mobile terrestrial LiDAR

Mobile terrestrial LiDAR platforms integrate a lightweight shorter-range (approximately 100 m) LiDAR unit with an inertial measurement unit (IMU) to allow for hand-held, portable, high-precision ground-level scans (Ryding et al., 2015; Bauwens et al., 2016). These platforms allow for the scan to be carried out from multiple directions during a single survey (Ryding et al., 2015). Resulting pointclouds have similar point densities and spatial accuracies to those created using TLS while also reducing occlusion-based signal loss (Ryding et al., 2015; Bauwens et al., 2016).

Recent developments in simultaneous localization and mapping (SLAM) technology have been incorporated into several mobile terrestrial LiDAR sensors (Qian et al., 2016). SLAM technology relies on combined distance and platform positions measured with the IMU paired with object recognition algorithms to produce three-dimensional point clouds with a high degree of internal accuracy (Qian et al., 2016; Bauwens et al., 2016). SLAM-integrated Mobile terrestrial LiDAR accuracies are greatest in complex environments, such as forested areas, where object recognition is able to utilize many common points within a scan (Qian et al., 2016). Internal accuracy of the resulting pointcloud is further improved by its lack of reliance on GPS positioning, which makes these platforms well suited to snow-surveys in forested areas where GPS signals may otherwise introduce positional error (Qian et al., 2016).

2.2.3 LiDAR-derived snow depths and error sources

LiDAR-derived snow depth models are created by calculating the elevation difference between paired snow-on and snow-free (bare ground) digital elevation models (Helficht et al., 2012; Hopkinson et al., 2004, Kostadinov et al., 2019; Painter et al., 2016; Deems and Painter, 2006). The result is a continuous surface representing snow depth for the scanned area which is unbiased by errors associated with traditional manual sampling methods (Mendoza et al., 2020; Raleigh and Small, 2017). Although Sullivan et al. (2023) found that the mean difference between snow depths produced from UAV-LiDAR scans and in-situ point measures of snow depth was not significant, uncertainties in LiDAR-derived snow depths can exist. These uncertainties result from issues related to the LiDAR platform being used, error introduced through the post-processing georectification of the resulting pointcloud, survey design, topography, vegetation, and through the process of creating the digital elevation models used to derive snow depths (Bhardwaj et al., 2016; Deems et al., 2013; Sullivan et al., 2023; Harder et al., 2020).

Positional errors: platform and topographic considerations

Positional error can be introduced to LiDAR pointclouds in a variety of ways, depending on the platform used to carry out the LiDAR survey. In aerial LiDAR surveys, positional errors can be attributed to poorly corrected positional data related to the inertial navigation system, which accounts for the movement of the airframe (roll, pitch, and yaw), or from boresight errors related to the position of the LiDAR sensor relative to integrated INS and GPS systems (Deems et al, 2013). Error in both aerial and ground-based (TLS and mobile terrestrial LiDAR) can also be introduced during post-processing georectification of the point cloud, which aims to align the pointcloud with global coordinate systems (Deems et al., 2013). One source of snow depth error which can be introduced regardless of the platform used results from poor co-registration of the snow on and snow free scans used to determine snow depth (Revuelto et al., 2015; Deems et al., 2013). This poor alignment can result from the positional errors listed above, but can also occur during post-processing co-registration, particularly for LiDAR scans conducted without integrated GPS systems (Revuelto et al., 2015).

LiDAR surveys are typically designed to maintain scan angles relative to the topography which allow for evenly distributed and regularly spaced ground surface returns (Bater and Coops, 2009). For aerial LiDAR surveys in mountainous terrain with steep slopes, small positional errors in horizontal space can translate to large vertical errors (Hopkinson et al., 2012). These vertical errors can be amplified if the

topography causes spreading of the LiDAR footprint; a situation referred to as beam divergence (Kostandinov et al., 2019; Baltsavias, 1999). Beam divergence has been found to result in vertical errors of up to 50 cm (Baltsavias, 1999). These positional errors can be minimized by designing flight plans account for the influence of the topography (Evans et al., 2009; Helfricht et al., 2012; Kostadinov et al., 2019). Flight plans which run parallel to elevation contours allow the LiDAR to scan the slope at a perpendicular angle, which ultimately reduces the influence of beam divergence (Deems and Painter, 2006; Deems et al, 2013). Despite efforts to reduce vertical uncertainty in mountainous areas, some studies have simply masked out areas with steep slopes to avoid incorporating the resulting positional error into any further analysis (Kostadinov et al., 2013; Hopkinson et al., 2012; Zheng et al., 2016; Tinkham et al., 2012). Kostadinov et al. (2019) found that the uncertainty in elevation increased dramatically for areas where slope gradients were 30° or greater.

Positional error using SLAM-enabled mobile terrestrial LiDAR platforms result either from poor georectification of the resulting pointcloud during post-processing, or from drift errors related to the integration of the LiDAR and inertial navigation system which increase throughout the duration of the scan (Ryding et al., 2015; Qian et al., 2016; Bauwens et al., 2016). These drift errors can be mitigated by performing the scan in a loop, where the starting and ending point of the scan are coincident (Bauwens et al., 2016).

Vegetation impacts on LiDAR snow depths

Vegetation impacts the accuracy of LiDAR-derived snow depth models by intercepting the incoming LiDAR pulse, resulting in fewer LiDAR returns from the snow surface or bare ground (Hopkinson et al., 2012; Zheng et al., 2016; Harpold et al., 2014; Dharmadasa et al., 2024; Harder et al., 2020). In aerial LiDAR surveys, this signal occlusion can result from dense overhead forest canopy or from the ground level vegetation (Dhamadasa et al., 2024; Zheng et al., 2016; Varhola et al., 2010). Snow depth models derived from aerial LiDAR scans have been shown to have uncertainties of 10 cm or more in forested areas compared to in openings (Harpold et al., 2014; Deems et al., 2013). Dense below-canopy ground vegetation has also been shown to reduce the number of LiDAR returns resulting from ground-based TLS or mobile terrestrial LiDAR surveys (Dharmadasa et al., 2024; Currier et al., 2019).

The degree of canopy penetration by LiDAR collected from an aerial platform depends largely on the canopy gap structure, but is also influenced by the signal strength, the scan angle, and the LiDAR pulse repetition frequency (Painter et al., 2016; Deems et al., 2013). Decreased canopy penetration

reduces the number of ground or snow surface points measured by the sensor, which can decrease the ability of LiDAR to accurately detect the natural variability of the surface below the vegetation (Painter et al., 2016). In a study by Harpold et al. (2014) which investigated the effects of canopy occlusion on sub-canopy snow detection using an aerial platform (twin-engine Piper PA-31 Chieftain), the authors found that up to 23% of the study area represented by dense canopy cover lacked any LiDAR returns from the underlying snow surface.

Low-lying vegetation such as lower tree branches and shrubs also introduce error into snow depth measurements by artificially elevating the apparent elevation of the snow surface by intercepting falling snow and preventing it from reaching the ground surface (Hopkinson et al., 2012; Painter et al., 2016). Low-lying vegetation can be difficult to distinguish from the surface of the snow using standard point cloud ground classification algorithms (Mendoza et al., 2020; Kostadinov et al., 2019). Seasonal changes in vegetation, most notably the resurgence of low shrubs or seasonal grasses in spring and summer may prevent ground points from the underlying terrain to be well represented in the digital terrain model representing the snow-free surface (Kostadinov et al., 2019). This summer vegetation affects the accuracy of the digital surface model used to establish the depth of snow above the ground from DSMs produced at the time of peak snow accumulation (Kostadinov et al. 2019).

One approach for addressing these potential errors includes masking out areas where low vegetation and lower-lying branches might introduce elevation error, or where branches can be confused for snow surface during times of peak accumulation (Kostadinov et al., 2019; Painter et al., 2016; Zheng et al., 2016). However, masking these areas requires a greater degree of interpolation between the remaining points, which effectively replaces one source of uncertainty with another (Painter et al., 2016).

A more proactive approach to addressing these potential errors is to increase the number of ground or snow points measured from the surface (Deems et al., 2013; Harder et al., 2020). For aerial LiDAR surveys, this can be accomplished by reducing the scan angle, increasing the laser pulse rate (Evans et al., 2009), decreasing the speed and/or altitude of the aerial platform, or increasing the overlap of individual flight lines (Deems and Painter, 2006; Currier et al., 2019; Kostadinov et al., 2019; Deems et al.; 2013; Sullivan et al., 2023; Harder et al., 2020). TLS and mobile terrestrial LiDAR systems allow for a higher density of sub-canopy points to be recorded at the ground or snow surface by eliminating signal loss related to canopy occlusion (Bauwens et al., 2016). Handheld mobile terrestrial LiDAR surveys can be designed to minimize vegetation-related signal loss by establishing a walking path which enables scanning the area of interest from multiple angles (Ryding et al., 2015). As the platform

speed is controlled by the walking pace of user, point densities in mobile terrestrial LiDAR scans can be increased by walking more slowly (Ryding et al., 2015).

Digital Elevation Model: ground classification and interpolation

Uncertainty in LiDAR-derived snow depths are often related to elevation errors contained within the two DEMs used to create the snow depth model (Guo et al., 2010; Deems et al., 2006; Bater and Coops, 2009, Dharmadasa et al., 2024). Elevation errors in these DEMs can result from either poor-quality ground/snow surface classification outcomes (Evans and Hudak, 2007) or from interpolation methods used to create a continue surface between sparse ground or snow points (Guo et al., 2010; Sullivan et al., 2023).

Ground classification is applied to LiDAR pointclouds in an effort to differentiate LiDAR returns which represent the ground surface from those representing the overlying vegetation (Silva et al., 2018; Sithole and Vosselman, 2004; Tinkham et al., 2011 Pingle et al., 2013). There are several ground classification algorithms available which utilize a variety of methodologies (Silva et al., 2018). The choice of ground classifier used can depend on operational costs of the software (proprietary vs open-source), processing efficiency, the ability of a classifier to effectively identify topographic complexity or slope angle, and the ability to account for inherent point density characteristics (Silva et al., 2018). Ground classification algorithms have been specifically developed for use with aerial LiDAR datasets (Sithole and Vosselman, 2004) which typically have lower ground point densities than from ground-based TLS or mobile terrestrial LiDAR surveys. To date, there are no studies which have investigated the performance outputs of available ground classifiers on higher-density sub canopy LiDAR.

The elevation uncertainty resulting from interpolation between ground or snow points to create a continuous surface model relates to the interpolation method used, as well as to the distance between individual points (Bater and Coops, 2009; Guo et al., 2010; Sullivan et al., 2023; Hopkinson et al., 2012; Deems et al., 2013). Many studies have relied on triangular irregular network (TIN) or nearest neighbor interpolation methods as these methods are efficient and retain the point position integrity of the original data (Guo et al., 2010; Hopkinson et al., 2012). However, in areas with steep terrain, or where ground vegetation may greatly influence the distribution of ground returns, more complex interpolation methods may be used such as kriging (Kirchner, 2014, Deems et al., 2006; Dharmadasa et al., 2024), inverse distance weighting (IDW), or spline-based interpolation (Guo et al., 2010; Deems et al., 2006; Bater and Coops, 2009, Dharmadasa et al., 2024). While spline and IDW interpolation have been found

to retain more complex topography between points, these interpolation methods have also been found to introduce artificial smoothing to the original dataset (Bater and Coops, 2009). While it is important to consider the potential errors introduced through interpolation, there is a general consensus that when the distances between ground or snow surface points are consistently small, the interpolation method used is unlikely to have a large impact on the accuracy of the resulting DEM (Dharmadasa et al., 2024; Guo et al., 2010).

2.2.4 References

Baltsavias EP (1999). Airborne laser scanning: basic relations and formulas. ISPRS J. Photogramm. Rem. Sens, 54(2–3), 199–214 (doi: 10.1016/S0924-2716(99)00015-5)

Bater, C., & Coops, N. (2009). Evaluating error associated with lidar-derived DEM interpolation. Computers and Geosciences, 35, 289–300. https://doi.org/10.1016/j.cageo.2008.09.001

Bauwens, S., Bartholomeus, H., Calders, K., & Lejeune, P. (2016). Forest Inventory with Terrestrial LiDAR: A Comparison of Static and Hand-Held Mobile Laser Scanning. Forests, 7. https://doi.org/10.3390/f7060127

Bhardwaj, A., Sam, L., Bhardwaj, A., & Martín-Torres, F. J. (2016). LiDAR remote sensing of the cryosphere: Present applications and future prospects. Remote Sensing of Environment, 177, 125–143. https://doi.org/10.1016/j.rse.2016.02.031

Broxton, P. D. (2019). Improving Snow Water Equivalent Maps with Machine Learning of Snow Survey and Lidar Measurements Water Resources Research. Water Resources Research, 55, 3739–3757. https://doi.org/10.1029/2018WR024146

Buttle, J, M., Oswald, C.J., and Woods, D.T. (2005). Hydrologic Recovery of Snow Accumulation and Melt Following Harvesting in Northeastern Ontario. 62nd Eastern Snow Conference. Waterloo, ON, Canada 2005.

Buttle, J. M., Beall, F. D., Webster, K. L., Hazlett, P. W., Creed, I. F., Semkin, R. G., & Jeffries, D. S. (2018). Hydrologic response to and recovery from differing silvicultural systems in a deciduous forest landscape with seasonal snow cover. Journal of Hydrology, 557, 805–825. https://doi.org/10.1016/j.jhydrol.2018.01.006

Connaughton, C.A. (1935). The Accumulation and Rate of Melting of Snow as Influenced by Vegetation, Journal of Forestry, Volume 33, Issue 6, June 1935, Pages 564-569, https://doi.org/10.1093/jof/33.6.564

Currier, W. R., Justin, P., Mazzotti, G., Jonas, T., Deems, J. S., Bormann, K. J., … Hiemstra, C. A. (2019). Comparing Aerial Lidar Observations with Terrestrial Lidar and Snow - Probe Transects from NASA's 2017 SnowEx Campaign Water Resources Research. Water Resources Research, 55, 6285–6294. https://doi.org/10.1029/2018WR024533

Davis, R. E., Hardy, J. P., Ni, W., Woodcock, C, McKenzie, J. C, Jordan, R. & Li, X. (1997). Variation of snow cover ablation in the boreal forest: a sensitivity study on the effects of conifer canopy. J. Geophys. Res. 102:29389-29395.

Deems, J. S., & Painter, T. H. (2006). Lidar measurement of snow depth: accuracy and error sources. Proceedings of the 2006 International Snow Science Workshop: Telluride, Colorado, USA, International Snow Science Workshop, 330, 330–338.

Deems, J., Fassnacht, S., & Elder, K. (2006). Fractal Distribution of Snow Depth from Lidar Data. Journal of Hydrometeorology, 7, 285–297.

Deems, J. S., Painter, T. H., & Finnegan, D. C. (2013). Lidar measurement of snow depth: A review Lidar measurement of snow depth: a review. Journal of Glaciology, 59(July). https://doi.org/10.3189/2013JoG12J154

Déry, S., Knudsvig, H., Hernández-Henríquez, M., & Coxson, D. (2014). Net Snowpack Accumulation and Ablation Characteristics in the Inland Temperate Rainforest of the Upper Fraser River Basin, Canada. Hydrology, 1(1), 1–19. https://doi.org/10.3390/hydrology1010001

Dharmadasa, V., Kinnard, C., & Bara, M. (2024). A new interpolation method to resolve under-sampling of UAV-lidar snow depth observations in coniferous forests. Cold Regions Science and Technology, 220(April 2023). https://doi.org/10.1016/j.coldregions.2024.104134

Dickerson-Lange, S. E., Lutz, J. A., Gersonde, R., Martin, K. A., Forsyth, J. E., & Lundquist, J. D. (2015). Water Resources Research. https://doi.org/10.1002/2015WR017873.Received

Dickerson-Lange, S. E., Gersonde, R.F., Hubbart, J.A., Link, T.E., Nolin, A.W., Perry, G.H., Roth, T.R., Wayand, N.E. & Lundquist, J.D. (2017). Snow disappearance timing is dominated by forest effects on snow accumulation in warm winter climates of the Pacific Northwest, United States. Hydrol. Process. 31, 1846–1862.

Dong, C. (2018). Remote sensing, hydrological modeling and in situ observations in snow cover research: A review. Journal of Hydrology, 561(April), 573–583. https://doi.org/10.1016/j.jhydrol.2018.04.027

Egli, L., Jonas, T., Grünewald, T., Schirmer, M., & Burlando, P. (2012). Dynamics of snow ablation in a small Alpine catchment observed by repeated terrestrial laser scans. Hydrological Processes, 26,1574–1585. https://doi.org/10.1002/hyp.8244

Elder, K., Dozier, J., & Michaelsen, J., (1991). Snow accumulation and distribution in an Alpine Watershed. Water Resources Research, Vo. 27, No.7, 1541-1552.

Ellis, C. R., Pomeroy, J. W., Brown, T., & Macdonald, J. (2010). Simulation of snow accumulation and melt in needleleaf forest environments. Hydrology and Earth System Sciences, 14(1995), 925–940. https://doi.org/10.5194/hess-14-925-2010

Ellis, C. R., Pomeroy, J. W., Essery, R. L. H., & Link, T. E. (2011). Effects of needleleaf forest cover on radiation and snowmelt dynamics in the Canadian Rocky Mountains. Can. J. For. Res., 41, 608–620. https://doi.org/10.1139/X10-227

Evans JS and Hudak AT (2007) A multiscale curvature algorithm for classifying discrete return LiDAR in forested environments. IEEE Trans. Geosci. Remote Sens., 45(4), 1029–1038. doi:10.1109/TGRS.2006.890412

Evans, J. S., Hudak, A. T., Faux, R., & Smith, A. M. S. (2009). Discrete Return Lidar in Natural Resources: Recommendations for Project Planning, Data Processing, and Deliverables. Remote Sensing, 1, 776–794. https://doi.org/10.3390/rs1040776

Grünewald, T., & Lehning, M. (2015). Are flat- field snow depth measurements representative? A comparison of selected index sites with areal snow depth measurements at the small catchment scale. Hydrological Processes, 29, 1717–1728. https://doi.org/10.1002/hyp.10295

Guo, Q., Li, W., Yu, H., & Alvarez, O. (2010). Effects of Topographic Variability and Lidar Sampling Density on Several DEM Interpolation Methods. Photogrammetric Engineering & Remote Sensing, 76(June), 701–712.

Hancock, S., Essery, R., Reid, T., Carle, J., Baxter, R., Rutter, N., & Huntley, B. (2014). Characterising forest gap fraction with terrestrial lidar and photography: An examination of relative limitations. Agricultural and Forest Meteorology, 190, 105–114. https://doi.org/10.1016/j.agrformet.2014.01.012

Harder, P., Pomeroy, J. W., & Helgason, W. D. (2020). Improving sub-canopy snow depth mapping with unmanned aerial vehicles: lidar versus structure-from-motion techniques. The Cryosphere, 14, 1919–1935.

Hardy, J., Davis, R. E., Hardy, J. P., Davis, R. E., Jordan, R., Li, X., … Ni, W. (1997). Snow melt modeling at the stand scale in a boreal jack pine forest Snow ablation modeling at the stand scale in a boreal jack pine forest. Journal of Geophysical Research Atmospheres, https://doi.org/10.1029/96JD03096

Hardy, J.P. and K.J. Hansen-Bristow. (1990). Temporal accumulation and ablation patterns in forests representing varying stages of growth. Proc. 58th West. Snow Conf., Sacramento, Calif., pp. 23–24.

Harpold, A., Guo, Q., Molotch, N., Brooks, P., Bales, R., Fernandez-Diaz, J., … Lucas, R. (2014). LiDAR-derived snowpack data sets from mixed conifer forests across the Western United States. Water Resources Research, 50(October 2013), 1–7. https://doi.org/10.1002/2013WR013935.

Hedstrom, N., Pomeroy, J., 1998. Measurements and modelling of snow interception in the boreal forest. Hydrological Processes, 12, 1611–1625.

Helfricht, K., Sch, J., Seiser, B., Fischer, A., & St, J. (2012). Snow accumulation of a high alpine catchment derived from LiDAR measurements. Advances in Geosciences, 32, 31–39. https://doi.org/10.5194/adgeo-32-31-2012

Hopkinson, C., Sitar, M., Chasmer, L., Gynan, C., Agro, D., Enter, R., Foster J, Heels N, Hoffman C, Nillson J & Sant Pierre, R. (2001). Mapping the spatial distribution of snowpack depth beneath a variable forest canopy using airborne laser altimetry. In Proceedings of the 58th Eastern Snow Conference, Ottawa, Ontario, Canada: USA, Eastern Snow Conference (pp. 253–264) (Accessed from http://geography.tamu.edu/class/aklein/esc/proceedings/2001/Hopkinson_2.pdf)

Hopkinson, C., Sitar, M., Chasmer, L., & Treitz, P. (2004). Mapping snowpack depth beneath forest canopies using airborne lidar. Photogrammetric Engineering & Remote Sensing, 70(3), 323–330. https://doi.org/10.14358/PERS.70.3.323

Hopkinson, C., Collins, T., Anderson, A., Pomeroy, J., Spooner, I., Hopkinson, C., … Spooner, I. (2012). Spatial Snow Depth Assessment Using LiDAR Transect Samples and Public GIS Data Layers in the Elbow River Watershed, Alberta Spatial Snow Depth Assessment Using LiDAR Transect Samples and Public GIS Data Layers in the Elbow River. Canadian Water Resources Journal, 37(2), 69–87. https://doi.org/10.4296/cwrj3702893

Hudson, R. (2000). Snowpack recovery in regenerating coastal British Columbia clearcuts. Canadian Journal of Forest Research, 30(4), 548.

Jones, J. A. (2000). Hydrologic processes and peak discharge response to forest removal, regrowth, and roads in 10 small experimental basins, Western Cascades, Oregon, Water Resources Research, 36(9), 2621–2642.

Kirchner, P. B., Bales, R. C., Molotch, N. P., Flanagan, J., & Guo, Q. (2014). LiDAR measurement of seasonal snow accumulation along an elevation gradient in the southern Sierra Nevada, California. Hydrology and Earth System Sciences, 18, 4261–4275. https://doi.org/10.5194/hess-18-4261-2014

Konstantinos, A.M., Storck, P., & Lettenmaier, D. P. (2009). Modeling snow accumulation and ablation processes in forested environments, Water Resources Research, 45:5, 1–13. https://doi.org/10.1029/2008WR007042

Kostadinov, T. S., Schumer, R., Hausner, M., Bormann, K. J., Ga, R., Mcgwire, K., … Harpold, A. A. (2019). Watershed-scale mapping of fractional snow cover under conifer forest canopy using lidar. Remote Sensing of Environment, 222(2019), 34–49. https://doi.org/10.1016/j.rse.2018.11.037

Löfvenius, M., Lundmark, M., & Lundmark T., (2003) Snow and soil frost depth in two types of shelterwood and a clear-cut area, Scandinavian Journal of Forest Research, 18:1, 54-63, DOI: 10.1080/02827581.2003.10383138Mendoza, P. A., Shaw, T. E., & Mcphee, J. (2020). Spatial Distribution and Scaling Properties of Lidar - Derived Snow Depth in the Extratropical Andes Water Resources Research. Water Resources Research, 56(2013), 1–23. https://doi.org/10.1029/2020WR028480

Moore, R. D., & Wondzell, S. M. (2006). Physical Hydrology and the Effects of Forest Harvesting in the Pacific Northwest: A Review. Journal of the American Water Resources Association, 04065, 763–784.

Murray, C. D., & Buttle, J. M. (2003). Impacts of clearcut harvesting on snow accumulation and melt in a northern hardwood forest. Journal of Hydrology, 271, 197–212.

Musselman, K. N., Molotch, N. P., & Brooks, P. D. (2008). Effects of vegetation on snow accumulation and ablation in a mid-latitude sub-alpine forest. Hydrological Processes, 22(April), 2767–2776. https://doi.org/10.1002/hyp

Odin, H. & Degermark, C. (1990). The spring in the forest terrain at Svartberget, northern Sweden. Geogr. Ann. 72A: 167-178.Painter, T. H., Berisford, D. F., Boardman, J. W., Bormann, K. J., Deems, J. S., Gehrke, F., Winstral, A. (2016). The Airborne Snow Observatory: Fusion of scanning lidar, imaging spectrometer, and physically-based modeling for mapping snow water equivalent and snow albedo. Remote Sensing of Environment, 184, 139–152. https://doi.org/10.1016/j.rse.2016.06.018

Pingel, T. J., Clarke, K. C., & Mcbride, W. A. (2013). ISPRS Journal of Photogrammetry and Remote Sensing An improved simple morphological filter for the terrain classification of airborne LIDAR data. ISPRS Journal of Photogrammetry and Remote Sensing, 77, 21–30. https://doi.org/10.1016/j.isprsjprs.2012.12.002

Qian, C., Liu, H. Tang, J., Chen, Y., Kaartinen, H., Kukko, A., Zhu, L., Lian, X., Chen, L. & Hyppa, J. (2016). An integrated GNSS/INS/LiDAR-SLAM positioning method for highly accurate forest stem mapping. Remote Sensing, 9:3. doi:10.3390/rs9010003

Raleigh, M. S., & Small, E. E. (2017). Snowpack density modeling is the primary source of uncertainty when mapping basin-wide SWE with lidar. Geophysical Research Letters, 44, 3700–3709. https://doi.org/10.1002/2016GL071999

Revuelto, J., Lopez-Moreno, J., Azorin-Molina, C., & Vincent-Serrano, V. (2015). Canopy influence on snow depth distribution in a pine stand determined from terrestrial laser data. Water Resources Research, 51, 3476–3489. https://doi.org/10.1002/2014WR016496.Received

Ryding, J., Williams, E., Smith, M. J., & Eichhorn, M. P. (2015). Assessing Handheld Mobile Laser Scanners for Forest Surveys. Remote Sensing, 7, 1095–1111. https://doi.org/10.3390/rs70101095

Silva, C. A., Klauberg, C., Maria, Â., Hentz, K., Paula, A., Corte, D., … Liesenberg, V. (2018). Comparing the Performance of Ground Filtering Algorithms for Terrain Modeling in a Forest Environment Using Airborne LiDAR Data. Floresta e Ambiente, 25(2). https://doi.org/http://dx.doi.org/10.1590/2179-8087.015016

Sithole, G., & Vosselman, G. (2004). Experimental comparison of filter algorithms for bare-Earth extraction from airborne laser scanning point clouds. Photogrammetry & Remote Sensing, 59, 85–101. https://doi.org/10.1016/j.isprsjprs.2004.05.004

Spittlehouse, D.L., and Winkler, R.D. (1996). Forest Canopy Effects on Sample Size Requirements in Snow Accumulation and Melt Comparisons. Presented at the 64th Western Snow Conference. Bend, Oregon.

Storck, P., D. P. Lettenmaier, and S. M. Bolton, (2002). Measurement of snow interception and canopy effects on snow accumulation and melt in a mountainous maritime climate, Oregon, United States, Water Resour. Res., 38(11), 1223, doi:10.1029/2002WR001281.

Sullivan, F. B., Hunsaker, A. G., Palace, M. W., & Jacobs, J. M. (2023). Evaluating the Effects of UAS Flight Speed on Lidar Snow Depth Estimation in a Heterogeneous Landscape. Remote Sensing, 15(5091).

Talbot, J., & Plamondon, A. P. (2002). The Diminution of Snowmelt Rate with Forest Regrowth as an Index of Peak Flow Hydrologic Recovery Montmorency Forest Quebec, 59th EASTERN SNOW CONFERENCE, Stowe, Vermont.

Tinkham, W. T., Huang, H., Smith, A. M. S., Shrestha, R., Falkowski, M. J., Hudak, A. T., … Marks, D. G. (2011). A Comparison of Two Open-Source LiDAR Surface Classification Algorithms. Remote Sensing, 3, 638–649. https://doi.org/10.3390/rs3030638

Troendle, C.A. and J.R. Meiman, (1984). Options for Harvesting Timber to Control Snowpack Accumulation. Proceedings of the 52nd Western Snow Conference (Sun Valley, Idaho), Colorado State University, Fort Collins, Colorado, pp. 86-97.

Varhola, A., Coops, N., Weiler, M., & Moore, R. D. (2010). Forest canopy effects on snow accumulation and ablation: An integrative review of empirical results. Journal of Hydrology, 392, 219–233. https://doi.org/10.1016/j.jhydrol.2010.08.009

Winkler R.D. and Boon, S., (2015), Revised Snow Recovery Estimates for Pine-Dominated Forests in Interior British Columbia. B.C. Ministry of Forests, Lands and Natural Resource Operations, Extension Note 116 (https://www.for.gov.bc.ca/hfd/pubs/docs/en/EN116.PDF).

Winkler, R. D., & Moore, R. D. (2006). Variability in snow accumulation patterns within forest stands on the interior plateau of British Columbia. Hydrological Processes, 20, 3683–3695. https://doi.org/10.1002/hyp. 6382

Winkler, R.D., Spittlehouse, D.L. and Golding, D.L. (2005), Measured differences in snow accumulation and melt among clearcut, juvenile, and mature forests in southern British Columbia. Hydrol. Process., 19: 51-62. https://doi.org/10.1002/hyp.5757

Winkler, R.D., Spittlehouse, D.L. and Golding, D.L. (1995), The Importance of Sample Size in Forest/Clearcut Snow Accumulation Comparisons. Mountain hydrology, Peaks and Valleys in Research and Applications. Proceedings from a conference, May 16-19, 1995, Vancouver, British Columbia.

Zheng, Z., Kirchner, P. B., & Bales, R. C. (2016). Topographic and vegetation effects on snow accumulation in the southern Sierra Nevada: a statistical summary from lidar data. The Cryosphere, 10, 257–269. https://doi.org/10.5194/tc-10-257-2016

Zheng, Z., Ma, Q., Qian, K., & Bales, R. C. (2018). Canopy Effects on Snow Accumulation: Observations from Lidar, Canonical-View Photos, and Continuous Ground Measurements from Sensor Networks. Remote Sensing, 10. https://doi.org/10.3390/rs10111769

CHAPTER 3: Research Statement and Thesis Organization

3.1 Research needs

Studies which have endeavoured to quantify the process of hydrological recovery in snow-dominated watersheds have relied on traditional snow survey methodologies which utilize manual point-based measurements of SWE and melt rate to determine stand-level averages. These studies have been limited to a very small range of geographic regions and forest types. Authors of these previous works acknowledge that transferability of outcomes to watersheds or regions with different climate, topographic, or forest characteristics should be done with caution, as these outcomes represent the specific characteristics of the study areas and reference stands considered. To better quantify the process of hydrological recovery across a larger range of forest and stand types, it is necessary to develop methodologies which can efficiently measure snowpack SWE, ablation, and forest stand metrics.

Little is known about how increased sampling intensity might impact the stand-level measures of SWE or ablation rate used to investigate recovery. Traditional point-based snow surveys are also unlikely to capture measures of within-stand snowpack variability or the influence which tree height and canopy cover variability within a stand might have on measures of stand-level recovery. The availability of LiDAR for snow depth investigations provides a new opportunity to consider a larger range of forest and stand types at a spatial resolution not considered in previous work. The uniquely high-precision LiDAR scan outputs produced from sub-canopy mobile terrestrial LiDAR scans allow for ultra-fine resolution consideration of within stand variability.

3.2 Research objectives and Thesis format

This paper-based thesis aims to expand on previous works which investigated the process by which regenerating stands recover hydrologically using point-based samples of snowpack depth, peak annual SWE, and ablation rate through the use of fine-resolution digital snow depth models produced from mobile terrestrial LiDAR. In Chapter 2, a two-part literature review presents the current body of research pertaining to 1) forest and snow relationships, and how these relationships have been used for quantifying the process of hydrological recovery in snow-dominated watersheds, and 2) Traditional and LiDAR-derived snow depth, methodologies, and limitations. Due to the novelty of the higher-precision mobile terrestrial LiDAR dataset used here, the following objectives were identified.

Objective 1 is addressed in a stand-alone journal style manuscript, presented in chapter 4.

1) The Effect of Snow Sampling Intensity on Resulting Estimates of Peak Snow Depth and Daily Ablation on North Aspect Slopes in the Rover Creek Watershed

Objective 2 is similarly addressed in a stand-alone journal manuscript (published in Hydrological Processes, https://doi.org/10.1002/hyp.15247) presented in chapter 5.

2) Investigating Hydrological Recovery in Regenerating Coniferous Stands in Snow-Dominated Watersheds Using SLAM-Enabled Mobile Terrestrial LiDAR

Finally, this thesis concludes with Chapter 6, which summarizes the research findings presented in chapters 3, 4, and 5 and discusses limitations of this study and areas for future research.

CHAPTER 4: The Effect of Snow Sampling Intensity on Resulting Estimates of Peak Snow Depth and Daily Ablation on North Aspect Slopes in the Rover Creek Watershed

4.1 Introduction

In forested mountainous watersheds where the main annual hydrological event is related to snow processes, the ability to accurately quantify peak snow water storage and its ablation is crucial for estimating annual water supplies (Wetlaufer et al, 2016; Broxton et al., 2019) and for assessing the risk for drought or flood (Ganjkhanlo et al., 2019). Traditional methods used to quantify snow water storage have relied on a variety of methods, such as manual point-based measures of snow depth and snow water equivalent (SWE) (Broxton et al., 2019; Watson et al., 2006; Egli et al., 2009), automated snow pillows (López-Moreno et al., 2020), and hydrological models which rely on such point measurements and in some cases remotely sensed datasets (Magnusson et al., 2018; Clark et al., 2011). Long term monitoring locations are often situated on flat terrain and in stands with homogenous forest cover (Grünewald and Lehning, 2015, Elder et al., 2009), which are unlikely to reflect the higher degree of spatial variability in snow depth found in topographically complex mountainous regions (Ganjkhanlo et al., 2020; Deems et al, 2006; Trujillo et al., 2007; Kuchment and Gelfan, 2001; Trujillo and Lehning, 2015).

Point-based sampling remains the most commonly used method for studies investigating the relationships between forest disturbance or stand maturity to differences in snow accumulation and ablation (Winkler and Boon, 2015; Hudson, 2000; Buttle et al., 2005; Talbot and Plamondon, 2002); an important relationship used for estimating the hydrological impacts of forestry-related or natural (fire/pest) disturbance. Many of these studies rely on calculations of stand-averaged snow depth and SWE measured either in a regularly spaced sampling grid or along a transect using snow depth gauges or snow core sampling methods (Egli et al., 2009; Winkler and Boon, 2015; Spittlehouse and Winkler, 1996; Grünewald and Lehning, 2015). These point-based surveys introduce uncertainties associated with sampling bias, failure to capture the variability of the snowpack between sample points, operator error, error (+/- 1cm SWE) associated with the snow tube itself, changing snowpack conditions (density) throughout the lengthy manual sampling process, and the inability to sample the same location twice due to sampling induced disturbance of the snowpack (Spittlehouse and Winkler, 1996; Shae and Jamieson, 2010). The uncertainty related to snowpack variability has been shown to decrease by

increasing the sample size, and by decreasing the distance between sample points (McCreight et al, 2014; Spittlehouse and Winkler, 1996; Trujillo and Lehning, 2015).

Few studies have investigated the role that sampling intensity (sample size and point sampling distance) plays in deriving accurate calculations of snowpack depth/SWE, or for determining measurable or hydrologically significant differences in snow depth or peak SWE between stands according to the level of stand maturity (Winkler et al, 1995; Spittlehouse and Winkler, 1996). One study by Spittlehouse and Winkler (1996) used an ANOVA-F power analysis to identify sample sizes required to identify specific differences in snow depth (effect sizes) between a clearcut, juvenile, and mature stand. This previous work was related to snow survey data collected from 64 data points spread at 15m point sampling distances to calculate stand-averaged SWE in each stand. However, one inherent weakness of the ANOVA-F test is that the power of a sample of a given size to identify measured differences (in snow depth, SWE, melt rate) between two samples determined from the test result assumes that the mean and standard deviation representing each sample (stand) is accurate (Nemec, 1991). As the mean and standard deviation depend on the values measured and associated sample size, these values will differ as sample sizes change, and can be influenced by sampling bias, which is common in areas where complex terrain limits easy access to regularly or randomly-spaced sampling locations. Reducing the uncertainty in stand-level calculations of snowpack depth and variability is therefore crucial for accurate estimations of required sampling intensities used to identify between-stand differences.

LiDAR-based snow surveys offer an opportunity to more accurately quantify the continuous snow depth across large areas at a fine (sub meter) spatial resolution without disrupting the snowpack. Such surveys greatly reduce the uncertainties introduced by using stand-level averages and standard deviations calculated from point-based samples. This study utilizes ultra-fine resolution models of snow depth derived from mobile terrestrial LiDAR to determine the sampling intensity (sample size and point sampling distance) and spatial resolution of gridded snow depth models required for effective characterization of within-stand snow depth variability and between-stand measured differences in snow depth and daily ablation according to differences in stand maturity.

4.1.1 Study Area

The study area is located in the Rover Creek watershed, approximately 25 kilometers southwest of the town of Nelson in the Selkirk Mountains of British Columbia, Canada (Figure 4-1). The study area is located on north aspect slopes, where vegetation has been shown to have a larger influence on snow accumulation and melt (Dickerson-Lange et al., 2023; Ellis et al., 2011). Four adjacent sites representing increasing forest maturity were selected to investigate how stand maturity might influence the sampling sizes and point sampling distances required to effectively quantify stand-level measures of peak snow accumulation (depth), melt rate (ablation), and within-stand peak depth variability. These sites included a recently replanted clearcut stand with trees averaging 2.7 m (J2), two juvenile stands with average heights of 11.5 m (J10) and 14.8 m (J15), and one mature stand with an average tree height of 37.6 m (M). All four sites have similar topographic characteristics (slope gradient, aspect, and elevation) to limit the primary variable controlling between-stand differences in snow accumulation and ablation to differences in forest maturity. Sites have moderate slope gradients ranging from 27% to 60% and are located between 950 to 1050 m above sea level (ASL) within the Interior Cedar and Hemlock (ICH) biogeoclimatic subzone (BC FLNRO, 2021), where much of the forestry-related disturbance in the interior of British Columbia is focused.

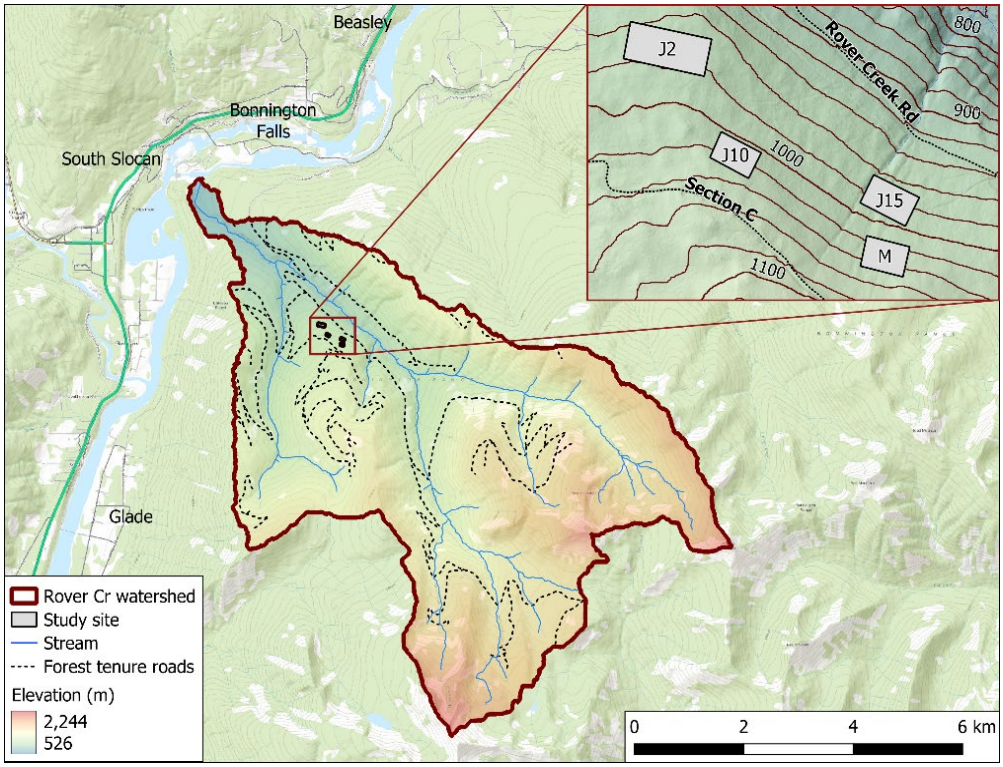

Figure 4-1 The study area, including sites J2, J10, J15, an M, located within the Rover Creek Watershed in the southern Kootenay region of British Columbia, Canada.

The Rover Creek watershed was selected both for its proximity to Castlegar, BC, where the study was based, and also for the ease of access to the study site locations. Road access to the study area was maintained by the nearby Snowwater Ski Lodge, which enabled easy access to the study sites, allowing repeated (every 2-3 day) data collection from peak snow accumulation (March 21, 2019) to the end of the melt period (April 24, 2019).

4.2 Data and Methods

4.2.2 Data Collection

LiDAR surveys

LiDAR scans of the snow surface/ground was measured in each study site using a GeoSLAM ZEB-Horizon handheld mobile LiDAR scanner (https://www.faro.com/en/Products/Hardware/GeoSLAM-ZEB-Horizon-RT). The ZEB-Horizon utilizes Simultaneous Location and Mapping (SLAM) technology to produce point clouds with a high degree of internal accuracy (1 to 3 cm) through the integration of an Inertial Measurement Unit (IMU) (Bauwens et al., 2016). The ZEB-Horizon LiDAR operates at a wavelength of 905 nm and has a reported operational distance of 100 m and effective range of approximately 40 to 50 m.

Survey loops were established within each study site (J2, J10, J15, and M) which incorporated a 100 m snow course. This looped survey design is a requirement in SLAM LiDAR surveys for reducing the influence of drift error on resulting point clouds by matching the start and end location in each LiDAR scan. This design also allows for the site area and individual features to be measured from multiple sides and angles as the user walks along the survey loop, reducing the potential for data voids or lower point densities associated with topographic or vegetative occlusion.

In order to allow for the accurate co-registration of LiDAR point clouds produced from the repeated surveys in each site, between 3 and 6 ground control points (GCPs) were established along the looped walking paths to be incorporated into each of the resulting scan outputs. These control points consisted of styrofoam spheres attached to the ends of bamboo rods which were fastened to large trees or stumps within the scan area using steel strapping. These GCPs were held in place throughout the duration of the study period.

LiDAR scans were performed in each site approximately every 2 to 3 days from the time of peak snow accumulation (March 21, 2019) to the end of the site-specific ablation period (March 31, 2019 in site M to April 24, 2019 in site J10) when the ground was snow-free. For each of the scan dates, all sites were measured within a 4-hour time window. The resulting LiDAR outputs allowed for consideration of peak snow accumulation and also the melt rates between individual scan dates.

Manual snow course / SWE sampling

A snow course with 10 sample locations spread at 10 m intervals was established adjacent to the LiDAR survey path in each study site (J2, J10, J15, and M). Following established snow survey methods (Winkler et al. (2005), Hudson (2000), Dixon et al. (2014)), snow water equivalence (SWE) and depth were measured within 30 minutes of each LiDAR scan using a standard Federal snow tube equipment. Snow cores were collected on the upslope side of the snow course in order to reduce disturbance to the snow sampling area. Repeated snow surveys were collected within 1 m of the marked sampling location.

4.2.3 Data Processing

GeoSLAM ZEB Horizon Data Processing

The GeoSLAM ZEB Horizon produces LiDAR data files in a data format which can only be viewed and processed using GeoSLAM's proprietary HUB software (https://knowledge.faro.com/Software/GeoSlam/GeoSLAM_Hub). For this study, all of the individual GeoSLAM data files were converted to the more commonly used LAS LiDAR format for all further classification, processing, and analysis.

LiDAR pointclouds for all survey dates in each of the 4 sites were co-registered (aligned) in CloudCompare using the styrofoam GCPs established in each site. The aligned spheres for all co-registered scans in each site had a root mean squared error (RMSE) of less than 0.03 m.

LiDAR Classification

Co-registered point clouds were classified using the ground classification tools available in TerraScan (TerraSolid, 2016) to isolate LiDAR points relating to either the snow surface or bare ground from those relating to overlying vegetation. Default ground classification parameters in TerraScan, which optimize classification accuracy in aerial LiDAR, were adjusted to account for the high point densities associated with terrestrial LiDAR surveys. Each LiDAR point cloud was classified individually to ensure that the site-specific terrain angles were accounted for within the classification parameters. The iteration distance parameter was set to 0.1 m and the iteration angle was set to 10° for all study sites.

4.2.4 LiDAR derivatives (DSMs, Depth, SWE models, Ablation models)

LiDAR points representing the snow surface or ground classification identified using the TerraScan ground classifier (class 2) were used to derive gridded surface models (DSMs) representing the snow surface elevation for each of the LiDAR scans. The spatial resolution of these DSMs was decided based on both quantitative measures of stand-level point densities and point spacing identified using LASinfo (https://rapidlasso.de/lasinfo/) (Table 4-1) as well as by qualitatively assessing the distribution of any data voids or gaps in the resulting snow/ground classifications by visually inspected the snow/ground classification in CloudCompare (CloudCompare.org) (Figure 4-2). The 0.1 m spatial resolution chosen for gridding the DSMs ensures that the vast majority of the resulting DSM grid cells are populated with measured snow surface elevations averaged for the grid cell. Simple linear interpolation was used to fill LiDAR data voids in order to produce a continuous surface representing the snow surface elevation. Linear interpolation was chosen based on study outcomes investigating the accuracy of interpolation methods used to derive models of snowpack depth presented by Kučerova and Jeniček (2014).

Gridded models of snow depth

The ground (snow) surface LiDAR classification was used to produce DSMs with a grid resolution of 0.1 m of the snow surface (DSMs) for each snow-on scan date, and of the bare ground (DSMg) once the site became snow free. These DSMs were used to produce gridded models of snow depth by subtracting the elevation of the DSMg from each DSMs.

Conversion of snow depth to SWE

Using snow depth to SWE relationships established from the snow course data collected concurrently with the LiDAR scans in each site, the gridded snow depth models were converted to gridded models representing SWE.

Gridded ablation rate

Gridded models of ablation rate were produced from the SWE models by averaging the daily decrease in SWE between March 21, 2019 and March 28, 2019. This date range was selected as it captured a period of increased melt rates prior to the date at which the mature stand (site M) became snow-free (March 31, 2019) and before the snowpack in the remaining sites became patchy. Rasterized SWE grid cells which became snow-free during the time range considered were masked out to avoid introducing an artificial slowing of the melt rate (Clark et al., 2011; Murray and Buttle, 2003) for the stand by including these grid cells in calculations of stand-level averages.

4.2.5 Point sampling

Previous studies undertaken to determine the sample sizes required to identify between stand differences in peak snow accumulation (SWE) and ablation (melt) between stands with different levels of forest maturity (clearcut, juvenile, and mature) have used ANOVA F tests to investigate the power that samples of a given size have for identifying these measured stand-level differences. However, the stand-averaged values of peak SWE or melt rate and associated calculations of variance used in these analyses were themselves calculated from averages of a point-based sampling design, with sampling points spread at either 10 m or 15 m intervals.

In order to determine the impact point sample spacing has on the resulting calculations of stand-averaged snow depth, ablation, and the associated measure of coefficient of variation, the gridded snow depth model representing peak depth (March 21, 2019) and the daily ablation rate model representing the melt period between March 21 and March 28 were sampled at distances ranging from 0.1 m to 15 m (Figure 4-3). Sample distances were decreased by 1m increments from 15 m to 1 m. Below the 1 m sampling distance, the point spacing was carried out at 0.5 m, 0.25 m, and 0.1 m sampling distances.

The resulting stand-averaged mean values, and associated coefficient of variation were plotted to provide a qualitative assessment of how sample size might impact these measures (Figures 4-4 and 4-5).

4.2.6 Power analysis

The power analyses applied here to identify required sample sizes and point sampling distances able to detect observed between-site differences utilizes the two-sample t-test for samples of different sizes (Cohen, 1988) provided in the pwr package in R (Champely, 2020; R core team, 2020). The one sample t-test available in the 'pwr' package was also used for identifying point sampling distances and sample sizes required to identify within-stand depth variability according to a range of effect sizes. T-tests were selected instead of using an ANOVA F test as the sample sizes differ between the four sites, as do the sample variances in both snow depth and daily ablation. Prior to running one or two-sample t-tests, the rasterized snow depth models and ablation models were tested for normality using the Shapiro Wilks test in R. This test produced $p < 0.05$ for all sample dates up to April 16 in sites J2, J10 and J15, and up to March 28 in site M. After these dates these distributions no longer met this assumption consistently due to reduced sample sizes resulting from patchy snow, although visual inspections of histograms for these later dates appear to be approximately normally distributed.

Factors that determine power for identifying differences between two samples, or variations away from a sample mean include the sample size (n), the level of significance deemed important for the test results (α), and the effect size (d). For this study effect size (d) equals the measured stand-level difference between sites or differences in depth within the site that contributes to within-stand snow depth variability (Nemec, 1991). Power can be increased by lowering the level of significance, increasing the sample size, or increasing the effect size (Winkler and Spittlehouse, 1995).

Power analysis for peak snow depth measurements

One-sample t-test to quantify within-stand variability

Rasterized (gridded) models of snow depth derived from each LiDAR scan date were used to calculate stand-averaged mean snow depth and standard deviation. These stand-level descriptive statistics were used to determine the sample sizes and point sampling distances which would have the power to identify within-stand variability in peak snow depth for a range of effect sizes (differences in snow depth). For both the one-sample and two-sample t-tests available in the pwr package, the user supplies parameter values for all known variables in order to solve for one remaining unknown variable. These variables include the sample size (n), the effect size (Cohen's d), the power of the test (90%), and the significance level ($\alpha = 0.05$). For this study, the unknown variable is sample size (n), so all other values are supplied to solve for n.

Using the one-sample t-test available in the pwr package, the sample sizes and point sampling distances required to detect within-stand peak depth (March 21, 2019) variability for effect sizes (d) ranging from 0.04 to 0.10 cm, in 0.01 m intervals were determined for each of the four study sites. Effect sizes less than 0.04 m fall within the measurement uncertainty associated with the GeoSLAM Zeb Horizon and were therefore not considered. Once these sample sizes were identified, the associated sampling distances which would allow for these sample sizes within the confines (spatial extents) of each site was determined (Table 4-2).

Two-sample t-test to identify snow depth and ablation rate differences by stand maturity

Using the two-sample t-test in the pwr package, sample sizes required to identify the measured between-site differences in averaged stand-level snow depth for all scan dates, as well as for between-stand differences in daily ablation for three (approximately) week-long time ranges were determined (Table 4-3 and Table 4-5). For these two-sample t-tests, the effect size (Cohen's d) was first calculated using Equation 4-1 (Cohen, 1988)

$$Cohen's\ d = \sqrt{\frac{\bar{x}_1 - \bar{x}_2}{\sigma'}}, \text{ where } \sigma' = \sqrt{\frac{\sigma_1^2 + \sigma_2^2}{2}} \qquad \text{(Equation 4-1)}$$

where $\bar{x}1$ and $\bar{x}2$ represent the stand-average mean (snow depth or daily ablation) for the two sites being compared, and σ' represents the pooled variance from the two sites. The pooled variance calculated in Equation 4-1 accounts for differences in variance between the two samples. Once the required sample sizes were identified, associated point sampling distances which allow for these sample sizes within the confines (spatial extents) of each of the 4 sites were determined (Table 4-4 and Table 4-6).

4.3 Results

LiDAR points from ground-level mobile terrestrial LiDAR scans, which were classified as snow/ground using the TerraScan ground classifier, show high point densities throughout much of the scan areas. Intermittent gaps near the walking path are associated with individual tree trunks, and lower point densities occur where topographic occlusion limited the site to be scanned from all angles (center of sample site in J2, Figure 4-2). The point sampling distance in a higher point density sub area (red square, Figure 4-2) has an average point spacing of 0.03 m. However, the average point sampling increases to 0.04 m in this site when considering the full site area.

4.3.1 LiDAR snow surface / ground classification

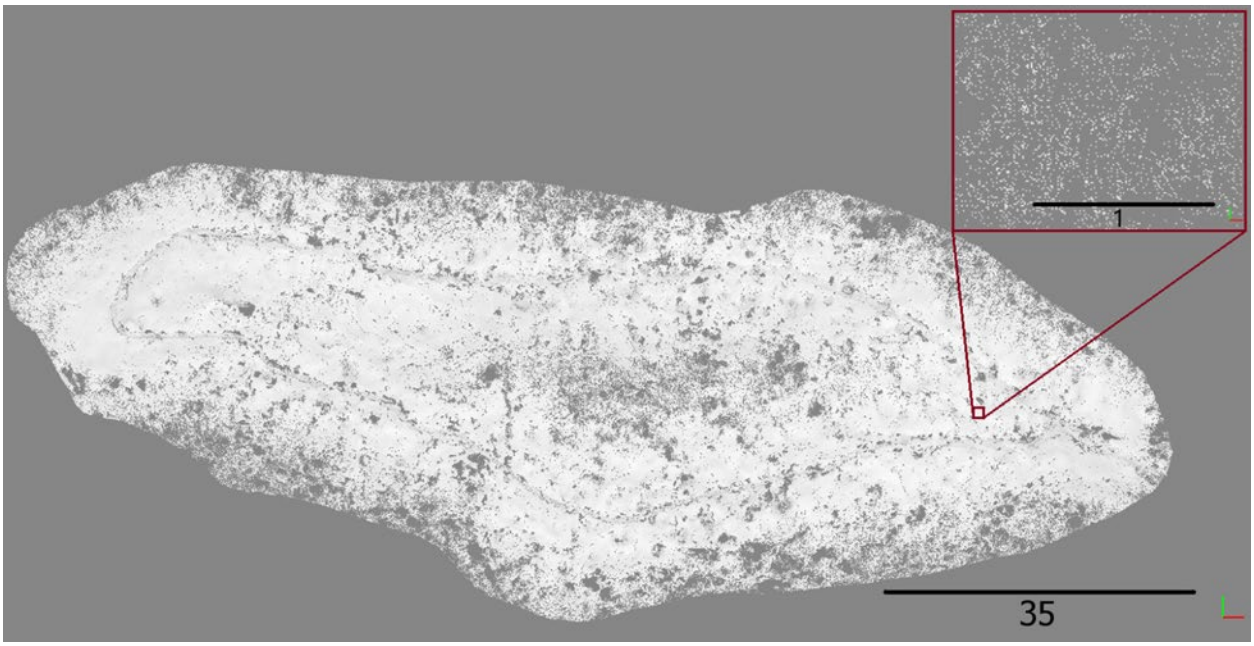

Figure 4-2 LiDAR Points representing the snow (ground) classification in the recently replanted clearcut stand (J2) at the time of peak snow accumulation (March 21, 2019). The point density of the snow surface in this LiDAR pointcloud has an average point density of 590 points per m^2, and an average point spacing of 0.04m.

Point densities at the time of peak snow accumulation (March, 21, 2019) range from 590 points/m^2 in site J2 to 1335 point / m^2 in site M (Table 4-1). The point spacing is somewhat consistent between the four sites, when averaged for the full site, although decreased point densities were observed in the interior of sites J2 and J10.

Table 4-1 LiDAR point density and spacing for the resulting snow surface classification in each study site at the time of peak snow accumulation (March 21, 2019).

Study site	Point density (points / m^2)	Point spacing (m)
J2	590	0.04
J10	810	0.03
J15	852	0.03
M	1335	0.03

4.3.2 Point sampling

Gridded models of snow depth, SWE and average daily ablation (melt) rate

LiDAR-derived models of snow depth and daily ablation gridded to 0.1 m illuminate the high degree of within-stand variability of the snowpack, particularly in the juvenile stands (Figure 4-3). Visually observing sample point locations with traditional sampling distances of 10 to 15 m (Figure 4-3, left panel) highlights the likelihood for uncertainty in stand level averages calculated from sampled snow depths measured at these sampling distances.

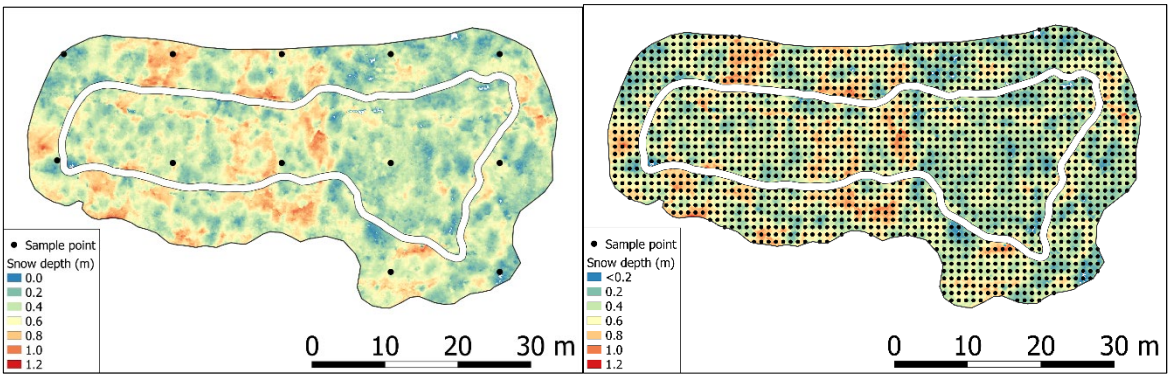

Figure 4-3 Gridded models of peak (March 21, 2019) snow depth in meters in site J15. Peak snow depths in this site range from under 0.2 m to 1.2 m. The location of point samples (black dots) show sampling distances of 15 m (left) and 1 m (right). The walking path used to perform the LiDAR scan has been masked out of the final gridded snow depth models (shown as white path)

Point sampling of peak accumulation depth

Calculations of mean peak depth and associated calculations of coefficient of variation derived through the averaging of point samples in each site differ according to point sampling distance, particularly when sampling distances exceed approximately 5 m (Figure 4-4). Sampling distances of 10 m or greater result in average stand-level snow depth values ranging from approximately 0.79 to 0.82 m in site J2, 0.45 to 0.65 m in site J10, 0.39 to 0.48 m in site J15, and from approximately 0.22 to 0.27 m in site M. The greatest range of peak snow depth averages calculated for the stand occur in the juvenile stands J10 and J15 where the within-stand snowpack variability is greatest. This variation in stand-level average snow depth decreases as the point sampling distances drop below 3 m in J2, 2 m in J10, 4 m in J15, and below 5m in site M.

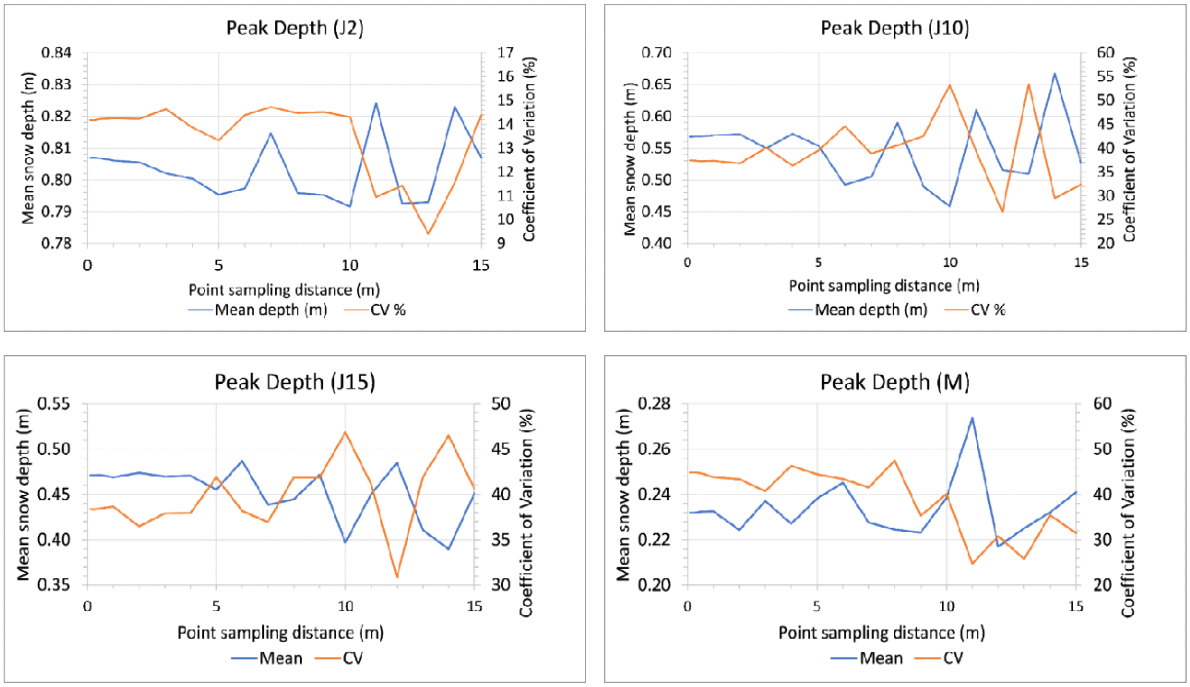

Figure 4-4 Stand averaged peak snow depth (m) and coefficient of variation % for sites J2, J10, J15, on March 21, 2019, calculated using point sampling of gridded peak snow depth rasters for point sampling distances ranging from 0.1 m to 15 m.

Point sampling of Ablation

Calculations of stand-level averages for daily ablation, and associated calculations of coefficient of variation derived through the averaging of point samples in each site differ according to point sampling distance, particularly when sampling distances exceed approximately 6 m (Figure 4-5). Sampling distances of 6 m or greater result in average stand-level daily ablation ranging from 1.54 to 1.77 cm/day in site J2, from 0.96 to 1.31 cm/day in site J10, from 0.81 to 1.09 cm/day in site J15, and from 0.82 to 1.03 cm/day in site M.

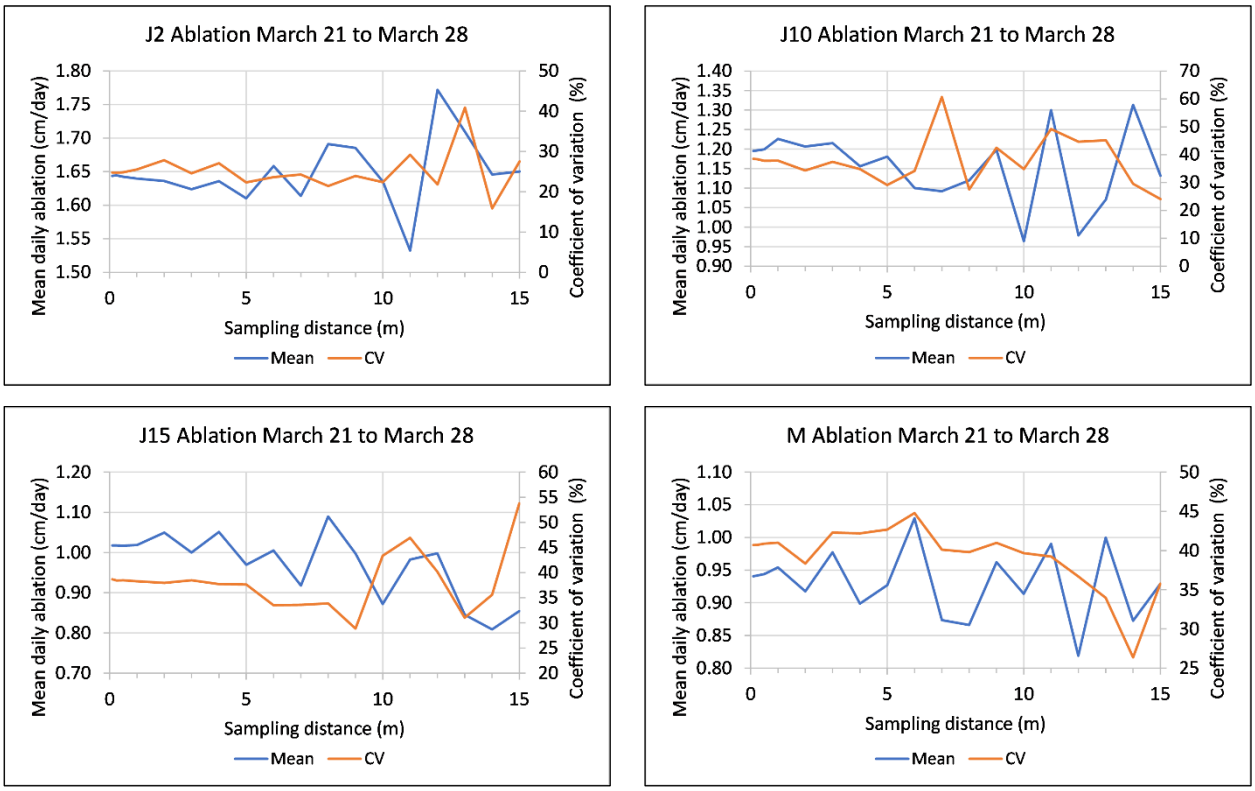

Figure 4-5 Stand averaged ablation rate in cm/day and coefficient of variation % for sites J2, J10, J15, and M from March 21 to March 28, calculated using point sampling of the gridded ablation raster for point sampling distances ranging from 0.1 to 15 m.

4.3.1 Power Analysis for determining point sample distances

Sample size and point sampling distances for identifying within stand peak depth variability

The sample sizes and point sampling distances required to identify within stand variations in snow depth (effect sizes) ranging from 4 to 10 cm at the time of peak snow accumulation (March 21, 2019) shows that for all sites, the sample size increases and the point sampling distance decreases with decreasing effect size (Table 4-2). The sample distance required to identify a 4 cm depth is 7 m in J2, 1 m in J10, 3 m in J15, and 4 m in site M. When the effect size is set to 10 cm, the point spacing increases to 15 m in J2, 4 m in J10, 7 m in J15, and 9 m in site M.

Table 4-2 Sample size (n) and point spacing required to detect within-site differences (effect sizes) in peak depth (March 21, 2019) ranging from 4 to 10 cm determined from a one-sample t-test where the power was set to 90%, with a significance of 0.05.

	J2			J10			J15			M		
Effect size	Cohen's d	n	Point spacing	Cohen's d	n	Point spacing	Cohen's d	n	Point spacing	Cohen's d	n	Point spacing
10 cm	0.91	15	15 m	0.45	54	4 m	0.55	37	7 m	0.95	14	9 m
9 cm	0.82	18	15 m	0.41	65	4 m	0.50	44	6 m	0.85	17	8 m
8 cm	0.73	22	14 m	0.36	84	3 m	0.44	57	6 m	0.76	21	7 m
7 cm	0.64	28	12 m	0.32	105	3 m	0.39	72	5 m	0.66	27	6 m
6 cm	0.60	32	11 m	0.30	119	3 m	0.36	84	4 m	0.62	30	6 m
5 cm	0.50	44	10 m	0.25	171	2 m	0.30	119	4 m	0.52	41	5 m
4 cm	0.36	83	7 m	0.18	327	1 m	0.22	220	3 m	0.38	75	4 m

Sample sizes and point sampling distances for identifying between stand differences in snow depth and ablation, according to stand maturity

Sample sizes required for detecting measured between-stand differences in snow depth according to forest maturity are presented in Table 4-3. Measured differences in snow depth between sites J2 and J10 can be detected using 12 sampling points on March 21 but require increasing sample sizes reaching 13135 points on April 14, when the two stands had an almost identical mean snow depth. For differences between sites J2 and J15, 6 sample points are able to detect measured between-stand differences on March 21 while 30 points are needed by April 16. Only 3 sample sizes are required for identifying measured differences between sites J2 and M. Between stand differences in snow depth measured in J10 and J15 require 110 points, which is the highest sample size required for detecting between-stand differences at the time of peak snow accumulation. Sample sizes are similar for detecting differences between site M and J10 or J15, with sample sizes ranging from 5 to 11 points.

Table 4-3 Sample size (n) required to detect measured differences in between-site snow depth on each LiDAR scan date from peak snow accumulation (March 21, 2019) to the end of the ablation period before the stands became snow free. Sample sizes were determined using a two-sample t-test, with the power set to 90% and with at a significance level of 0.05.

Date	J2-J10	J2-J15	J2-M	J10-J15	J10-M	J15-M
3-21-2019	12	6	3	110	8	11
3-23-2019	14	6	3	51	5	6
3-25-2019	9	5	3	63	5	6
3-28-2019	12	6	3	62	5	7
3-31-2019	13	5		29		
4-08-2019	33	7		21		
4-10-2019	39	10		30		
4-12-2019	338	12		15		
4-14-2019	13135	15		13		
4-16-2019	251	30		15		

The point sampling distances required to identify measured between-stand differences in snow depth according to forest maturity indicate that as the ablation period progresses, the required sampling distance to detect measured differences between sites J2 and J10 decreases from 8 m on March 21, 2019 (peak accumulation) to 1 m on April 16 (Table 4-4). Sampling distances for detecting differences between sites J10 and J15 increase from 3 m at peak accumulation to 8 m at the end of the ablation period. The point sampling distances required for detecting differences in snow depth between the other sites remains somewhat consistent throughout the melt period.

Table 4-4 Point sampling distances (m) required to detect measured differences in between-site snow depth on each LiDAR scan date from peak snow accumulation (March 21, 2019) to the end of the ablation period before the stands became snow free.

Date	J2-J10	J2-J15	J2-M	J10-J15	J10-M	J15-M
3-21-2019	8 m	15 m	15 m	3 m	12 m	10 m
3-23-2019	8 m	15 m	15 m	4 m	15 m	13 m
3-25-2019	10 m	15 m	15 m	4 m	15 m	13 m
3-28-2019	8 m	15 m	15 m	4 m	15 m	12 m
3-31-2019	8 m	15 m		6 m		
4-08-2019	5 m	15 m		6 m		
4-10-2019	5 m	15 m		5 m		
4-12-2019	1 m	15 m		8 m		
4-14-2019	0.25 m	11 m		8 m		
4-16-2019	1 m	7 m		8 m		

Sample sizes and sampling distances for detecting between-stand differences in ablation rate

The sample sizes required for detecting measured between-stand differences in average daily ablation decrease as the melt-season progresses (Table 4-5). Sample sizes range from 6 to 12 for detecting differences between site J2 and sites J10, J15, and M. Sample size requirements are larger for detecting measured differences between sites J10 and J15, and between either J10 or J15 and site M. The associated point sampling distances required to obtain these sample sizes ranges from 8 to 15 m for detecting differences between sites J2 and the other sites but is much smaller where larger sample sizes are required, such as for observing differences between J10 and J15, or between J15 and site M (Table 4-6).

Table 4-5 Sample size (n) required to detect measured between-site differences in daily ablation rate (cm/day) 90% of the time with a significance level of 0.05 as determined through power analyses using a two-sample t-test.

Ablation period	J2-J10	J2-J15	J2-M	J10-J15	J10-M	J15-M
March 21 to March 28	12	7	6	65	32	265
March 31 to April 8	7	5		35		
April 8 to April 16	9	6		43		

Table 4-6 Point sampling distance required to detect between-site differences in average daily ablation rate (cm/day) 90% of the time with a significance level of 0.05 (based on sample sizes shown in Table 4-4).

Ablation period	J2-J10	J2-J15	J2-M	J10-J15	J10-M	J15-M
March 21 to March 28	8 m	13 m	13 m	4 m	5 m	2 m
March 31 to April 8	13 m	15 m		5 m		
April 8 to April 16	10 m	15 m		4 m		

4.4 Discussion

This study utilized mobile terrestrial LiDAR to conduct high-precision scans of the snow surface in stands representing increasing levels of forest maturity ranging from a recently clearcut to a mature stand. These LiDAR scans were carried out below the canopy surface and at close range and resulted in point densities representing either the snow surface or bare ground (later in the melt season) averaging over 500 point/m^2, which is much higher than the approximately 4 to 15 point/m^2 observed for aerial LiDAR surveys (Broxton et al., 2019). Ground-level LiDAR scans can introduce some challenges in limiting topographic occlusion or occlusion related to high-density ground vegetation, particularly later in the season. While reductions in the LiDAR point density related to these areas of occlusion increase the uncertainty in derived measures of snow depth, the distances between LiDAR points surrounding these data holes are typically within the spatial resolution (1 m) of most DSMs produced from aerial LiDAR.

Linear interpolation was used to fill voids caused by occlusion in order to derive DSMs representing the snow/ground surface in each LiDAR scan. While this interpolation does create a continuous surface from which to derive models of snow depth and daily ablation, it should be noted that this interpolation also filled holes relating to the presence of individual tree trunks. Ideally these holes would be masked out, however identifying these area footprints can be quite difficult and would introduce another source of uncertainty in final outputs. The interpolation across these tree base footprints will have little effect on stand-averages where the basal areas are small. In the mature stand where the basal diameter of individual trees is larger, individual trees were spread further apart resulting in a small total basal area compared to the area of the stand.

The 0.1 m spatial resolution of DSMs and related models of snow depth and daily ablation created for this study offered an opportunity to investigate the influence of point sampling distance on resulting stand-averaged calculations of peak snow depth and daily ablation. Although expected, these stand-averaged values became much less variable as the point sampling distances decreased, with the largest ranges in calculations of snow depth observed in the juvenile stands, J10 and J15. In J10, the peak stand-averaged mean snow depth ranged from 0.45 to 0.65 m as the point sampling distance increased from 10 to 15 m. In site J15, the peak stand-averaged mean snow depth ranged from 0.39 to 0.48 m as the sampling distance decreased from 14 to 12 m. The large range in stand-averaged measures of snow depth for these juvenile stands using point sampling distances of 10 m or greater indicates a need to increase the sampling intensity to account for the influence these stands have on

within-stand variability. In these juvenile stands, point sampling distances less than 2 m were found to produce more consistent measures of snow depth.

Sampling distances have a similar influence on measures of daily ablation, with increased variability in stand-averaged ablation rates observed for sampling distances of 6 m or greater in all four stands. The range of values at these coarse sampling distances is similar between the four stands, with a total range of approximately 0.21 to 0.35 cm/day, with the greatest range of values observed in site J10. Although the stand-averaged ablation rate decreased according to increasing stand maturity, the variability in these calculations decreased when point sampling distances were less than 6 m.

The influences of sampling intensity on stand-averaged calculations of peak SWE and ablation rate indicate that the estimate of stand-level snow depth is highly impacted by the sampling distance used. Failure to account for within-stand snow variability in calculations of snow depth, particularly in stands where small trees may have localized impacts on snow depth, can either under or overestimate the annual water supply and may underestimate the potential for flood risk.

Power analyses using a one-sample t-test were conducted to determine the sample sizes and point sampling distances required to identify within-stand variations in peak snow depth related to stand maturity, with effect sizes ranging from 4 cm to 10 cm. Outcomes from this investigation support the findings of the point sampling analysis (above) and indicate smaller sampling distances are required to identify a 10 cm variation in snow depth in the juvenile stands (J10 and J15) than in the open (J2) or mature stand. A point sampling distance of 15 m in J2 or 9 m in site M can detect a 10 cm effect size, while in J10 or J15, a 4 m or 7 m point sampling distance is required. In order to identify a 4 cm effect size, the required point sampling distance decreased to 7 m in J2, 1 m in J10, 3 m in J15, and 4m in site M. Point sample distances chosen for surveys of snowpack depth should account for the effect size considered hydrologically significant and should also consider the distribution of forest/stand maturity in the area of interest.

Sample sizes and associated point sampling distances required to identify the between-stand differences in snow depth on each LiDAR scan date, and for the daily ablation during 3 (approximately) week-long time ranges were determined using a two-sample t-test.

Outputs from this analysis indicate that greater sample sizes and smaller point sampling distances are required for detecting differences in snow depth between stands with similar levels of maturity, such as between sites J2 and J10 or J10 and J15 than for between stands with greater

differences in stand maturity, such as J2 or J10 and M. As the ablation period progressed, the required sample size for detecting differences between J2 and J10 increased from n=12 on March 21 to n=338 on April 12 with associated point sampling distances decreasing from 8m to 0.2m, suggesting that the snowpack in these stands becomes more similar throughout the melt period. Conversely, sample sizes required to detect measured differences between sites J10 and J15 or M, or between J15 and M decrease as the ablation period progresses, indicating that the between stand differences became more pronounced. Measured snow depth differences between stands J10 and J15 require a point sampling distance of 3m on March 21, but increases to 8m by April 12.

Sample sizes required to identify between-stand differences in daily ablation are similar to those required to observe measured differences in peak (March 21, 2019) snow depth when considering differences between the open (J2) stand and sites J10, J15, and M. However, larger sample sizes are required to identify measured differences in daily ablation between M and J10 (n=32) and J15 (265), suggesting a similarity in the melt rates between these two stands.

This study used ultrafine resolution mobile terrestrial LiDAR to investigate the influence of point sampling distance on stand-averaged values of peak snow depth and daily ablation. The fine-resolution gridded snow depth and ablation models used for power analyses also present a novel approach for investigating the sampling intensity required to identify between-stand differences from peak snow accumulation through the end of the ablation period. One limitation of this study design is the time involved with performing LiDAR scans using a mobile terrestrial LiDAR unit. Although these LiDAR surveys are much faster than traditional point sampling methods, there remains a challenge in quantifying the snowpack at larger scales, or for a watershed. However, outcomes from this study, and the potential for incorporating this methodology to other elevations/aspects/forest types may be useful for determining the required spatial resolution for snow DSMs produced from aerial LiDAR surveys. The outcomes presented here suggest that a 2 m point sampling distance was generally sufficient for calculating stand-averaged snow depth and daily ablation regardless of stand maturity. As well, the 2 m point sampling distance was also generally sufficient for identifying within-stand snow depth variability with effect sizes of 4 m and greater, and for identifying the between-stand differences in snow depth and daily ablation for all four study sites. This suggests that DSMs of the snow surface produced from aerial LiDAR, at a standard spatial resolution of 1 m are likely also sufficient.

4.5 Conclusions

This study utilized very fine-resolution (0.1 m) gridded continuous models of snow depth and ablation rate produced from mobile terrestrial LiDAR to highlight the impact point sample distance has on stand-averaged calculations of snow depth, ablation rate, and variability, and to identify the sample sizes and point sampling distances required to identify within stand snow depth variability and between-stand differences in snow depth or ablation rate according to stand maturity.

For all stands assessed in this study, point sampling distances greater than 10 m for snow depth and greater than 6 m for ablation rate produced variable stand averages. The greatest range of peak snow depth averages is observed in juvenile stands J10 and J15 where young trees appear to influence greater within-stand snowpack variability. Reducing the point sampling distance in these juvenile stands greatly reduces the uncertainty in calculations of snow depth. Failure to account for within-stand variability can over or underestimate the water stored in the snowpack, which can result in poor predictions of annual water supply and flood risk.

Between-stand differences in snow depth related to differences in stand maturity indicate that higher sample sizes and smaller sampling distances are required for identifying differences between stands with similar levels of maturity. As the melt season progresses the sampling intensity required to identify differences between juvenile and open stands increases, while the sampling intensity required to identify differences between juvenile and mature stands decreases.

Outcomes from this study indicate that a 2 m point sampling distance, or a 2 m spatial resolution for LiDAR derived models of snow depth is likely sufficient for calculating stand-average snow depth, within-stand snow depth variability, and between-stand differences, regardless of stand maturity.

4.6 References

BC Ministry of Forests, Lands and Natural Resource Operations (BC FLNRO), 2021. Biogeoclimatic Ecosystem Classification Subzone/Variant District-Scale Field Maps. http://www.for.gov.bc.ca/hre/becweb/resources/maps/FieldMaps.html (Accessed August 18, 2024).

Broxton, P. D., Harpold, A. A., Biederman, J. A., Troch, P. A., Molotch, N. P., & Brooks, P. D. (2015). Quantifying the effects of vegetation structure on snow accumulation and ablation in mixed-conifer forests, *1094*(October 2014), 1073–1094. https://doi.org/10.1002/eco.1565

Champely, S. (2020). pwr: Basic Functions for Power Analysis. R package version 1.3-0. https://CRAN.R-project.org/package=pwr

Clark, J. Hendrikx, A. Slater, D. Kavetski, B. Anderson, N. Cullen, T. Kerr, E. Ö. Hreinsson, & R.A. Woods, 2011. Representing spatial variability of snow water equivalent in hydrologic and land-surface models: A review. Water Resources Research, Vol. 47.

CloudCompare (Version 2.10.2 (Zephyrus)) [GPL software]. (2019). Retrieved from http://www.cloudcompare.org/

Cohen, J. (1988). Statistical power analysis for the behavioral sciences (2nd ed.). Hillsdale, NJ: Lawrence Erlbaum.

Deems, J. S., & Painter, T. H. (2006). Lidar measurement of snow depth: accuracy and error sources. *Proceedings of the 2006 International Snow Science Workshop: Telluride, Colorado, USA, International Snow Science Workshop*, *330*, 330–338.

Dickerson-Lange, S., Howe, ER., Patrick, K., Gersonde, R., and Lundquist, J., (2023) Forest gap effects on snow storage in the transitional climate of the Eastern Cascade Range, Washington, United States. *Front. Water* 5:1115264. doi: 10.3389/frwa.2023.1115264

Dixon, D., Boon, S., & Silins, U. (2014). Watershed-scale controls on snow accumulation in a small montane watershed, southwestern Alberta, Canada, *1306*, 1294–1306. https://doi.org/10.1002/hyp.9667

Ellis, C. R., Pomeroy, J. W., Essery, R. L. H., & Link, T. E. (2011). Effects of needleleaf forest cover on radiation and snowmelt dynamics in the Canadian Rocky Mountains. *Can. J. For. Res.*, *41*, 608–620. https://doi.org/10.1139/X10-227

Egli, L., Jonas, T., & Meister, R. (2009). Cold Regions Science and Technology Comparison of different automatic methods for estimating snow water equivalent. *Cold Regions Science and Technology*, *57*(2–3), 107–115. https://doi.org/10.1016/j.coldregions.2009.02.008

Elder, K., Dozier, J., & Michaelsen, J., 1991. Snow accumulation and distribution in an Alpine Watershed. Water Resources Research, Vo. 27, No.7, 1541-1552.

Ganjkhanlo, H., Vafakhah, M., Zeinivand, H., & Fathzadeh, A. (2020). The effect of different sampling schemes on estimation precision of snow water equivalent (SWE) using geostatistics techniques in a semi-arid region of Iran. *Geocarto International*, *35*(16), 1769–1782. https://doi.org/10.1080/10106049.2019.1581267

Grünewald, T., & Lehning, M. (2015). Are flat-field snow depth measurements representative? A comparison of selected index sites with areal snow depth measurements at the small catchment scale, *1728*, 1717–1728. https://doi.org/10.1002/hyp.10295

Hedges, L. V. 1981. Distribution theory for Glass's estimator of effect size and related estimators. Journal of Educational Statistics 6: 107–128.

Hudson, R. (2000). Snowpack recovery in regenerating coastal British Columbia clearcuts. *Canadian Journal of Forest Research*, *30*(4), 548.

Kučerova and Jeniček (2014). Comparison of selected methods used for the calculation of the snowpack spatial distribution, Bystřice River Basin, Czechia. Geografie, 199, No.3 pp.199-217.

Kuchment, L. S. Ł., & Gelfan, A. N. (2001). Statistical self-similarity of spatial variations of snow cover: verification of the hypothesis and application in the snowmelt runoff generation models, *3355*(April), 3343–3355. https://doi.org/10.1002/hyp.1032

López-Moreno, J. I., Leppänen, L., Holko, L., Picard, G., Finger, E. A. D. C., Arslan, A. N., … Marty, C. (2020). Intercomparison of measurements of bulk snow density and water equivalent of snow cover with snow core samplers: Instrumental bias and variability induced by observers, (December 2019), 3120–3133. https://doi.org/10.1002/hyp.13785

Magnusson, J., D. Gustafsson, F. Husler, and T. Jonas (2014), Assimilation of point SWE data into a distributed snow cover model comparing two contrasting methods, Water Resour. Res., 50, 7816–7835, doi:10.1002/2014WR015302.

McCreight, J. L., Slater, A. G., Marshall, H. P., & Rajagopalan, B. (2014). Inference and uncertainty of snow depth spatial distribution at the kilometre scale in the Colorado Rocky Mountains: the effects of sample size, random sampling, predictor quality, and validation procedures. *Hydrological Processes*, *28*(December 2012), 933–957. https://doi.org/10.1002/hyp.9618

Murray, C. D., & Buttle, J. M. (2003). Impacts of clearcut harvesting on snow accumulation and melt in a northern hardwood forest, *271*, 197–212.

Nemec, A.F.L. 1991. Power Analysis Handbook for the design and Analysis of Forestry Trials. Biometrics Information Handbook No. 2. Ministry of Forests, Province of British Columbia, Victoria, B.C.

R Core Team (2020). R: A language and environment for statistical computing. R Foundation for Statistical Computing, Vienna, Austria. URL https://www.R-project.org/

Spittlehouse, D.L., and Winkler, R.D. (1996). Forest Canopy Effects on Sample Size Requirements in Snow Accumulation and Melt Comparisons. Presented at the 64th Western Snow Conference. Bend, Oregon.

Sturm, M., Taras, B., Listen, G., Derksen, C., Jonas, T., & Lea, J. (2010). Estimating Snow Water Equivalent Using Snow Depth Data and Climate Classes. *Journal of Hydrometeorology*, *11*, 1380–1395. https://doi.org/10.1175/2010JHM1202.1

Talbot, J., & Plamondon, A. P. (2002). The Diminution of Snowmelt Rate with Forest Regrowth as an Index of Peak Flow Hydrologic Recovery Montmorency Forest Quebec the Diminution of Snowmelt Rate with Forest Regrowth as an Index of Peak Flow Hydrologic Recovery, Montmorency Forest, Quebec, (March 2014).

Trujillo, E., and Lehning, M. (2015). Theoretical analysis of errors when estimating snow distribution through point measurements. *The Crysphere, 9,*1249-1264. doi:10.5194/tc-9-1249-2015

Trujillo, E., Rami, J. A., & Elder, K. J. (2007). Topographic, meteorologic, and canopy controls on the scaling characteristics of the spatial distribution of snow depth fields, *43*. https://doi.org/10.1029/2006WR005317

Watson, F. G. R., T. N. Anderson, W. B. Newman, S. E. Alexander, and R. A. Garott (2006), Optimal sampling schemes for estimating snow water equivalents in stratified heterogeneous landscapes, J. Hydrol., 328, 432–452.

Wetlaufer, K., Hendrikx, J., & Marshall, L. (2016). Spatial heterogeneity of snow density and its influence on snow water equivalence estimates in a large mountainous basin. Hydrology, 3(1). https://doi.org/10.3390/hydrology3010003

Winkler, R. and Spittlehouse, D. (1995). The Importance of Sample Size in Forest/Clearcut Snow Accumulation Comparisons. Proceedings of the Canadian Water Resources Association Conference. Vancouver, BC. May 16-19, 1995.

Winkler, R. D., Spittlehouse, D. L., & Golding, D. L. (2005). Measured differences in snow accumulation and melt among clearcut, juvenile, and mature forests in southern British Columbia. *Hydrological Processes*, *19*(1), 51–62. https://doi.org/10.1002/hyp.5757

Winkler, R., & Boon, S. (2015). *Revised Snow Recovery Estimates for Pine- dominated Forests in Interior British Columbia*. Kamloops, BC.

CHAPTER 5: Investigating Hydrological Recovery in Regenerating Coniferous Stands in Snow-Dominated Watersheds Using SLAM-Enabled Mobile Terrestrial LiDAR

Cydne R. Potter[1], Kim C. Green[2], Daniel L. Peters[3,1], and K. Olaf Niemann[1]

[1]Department of Geography, University of Victoria, Victoria, British Columbia, V8W2Y2, Canada
[2]Selkirk Innovates, Selkirk College, Castlegar, British Columbia, V1N4L3, Canada
[3]Watershed Hydrology and Ecology Research Division, Environment and Climate Change Canada, University of Victoria Queenswood Campus, Victoria, British Columbia, Canada V8N 1V8

Corresponding Author:
Department of Geography, University of Victoria, David Turpin Building,
99111 Ring Rd, Victoria, BC V8P 5C2
Email: cydnep@uvic.ca (Cydne R. Potter)

Cydne R. Potter cydnep@uvic.ca
Kim C. Green kgreen@selkirk.ca
Daniel L. Peters daniel.peters@ec.gc.ca
K. Olaf Niemann olaf@uvic.ca

Abstract

The return of snow accumulation and ablation processes in regenerating forests to pre-disturbance conditions, collectively referred to as hydrological recovery, has been investigated in past decades through manual snow surveys in adjacent open, juvenile, and mature stands. The outcomes of such studies provide a general understanding of hydrological recovery but lack transferability to areas where stand structure and terrain conditions differ from the reference sites. The application of mobile terrestrial LiDAR to investigate peak snow water equivalent (SWE) and ablation rates beneath regenerating trees in a space-for-time substitution study design provides new insights on the process of hydrological recovery in snowmelt forests of British Columbia, Canada. Outcomes of this study better quantify the influence of tree growth on peak SWE and ablation rate at both the tree and stand level for north aspect mixed conifer stands. Recovery of these two processes differ with recovery of Peak SWE beginning when the trees in a stand reach 3 meters in height and recovery of ablation rates beginning once trees reach 5 meters in height. Additionally, the process of negative ablation recovery in early juvenile stands reported in previous studies is herein clearly observed, providing an improved understanding of forest canopy effects on hydrological recovery in juvenile stands. The methods used in this study, which are internationally applicable, increase transferability of outcomes to stands where canopy characteristics (i.e., height, crown cover, and heterogeneity) are not represented in reference sites.

Keywords: hydrological recovery; LiDAR; snow; forest disturbance; SLAM LiDAR; negative recovery; snowpack recovery

5.1. Introduction

In snow-dominated watersheds below the treeline, annual snow accumulation, peak snow water equivalent totals (peak SWE), snowmelt rate, and snowpack longevity are largely affected by forest cover (Winkler and Boon, 2010; Varhola et al., 2010; Dickerson-Lange et al, 2015). Forest cover has been found to influence snow-water storage by reducing snow accumulation through interception, resulting in up to a 60% reduction in ground level accumulation (Hedstrom and Pomeroy, 1998; Varhola et al., 2010). Forest canopies also reduce incoming solar radiation, affecting the net energy (combined shortwave radiation (SWR) and longwave radiation (LWR)) available for driving ablation processes (snow melt and sublimation) (Boon, 2007; Ellis et al., 2010; Ellis et al., 2011; Hotovy and Jenicek, 2020). These stand-level changes in snow accumulation and melt can affect streamflow at the watershed scale. Even moderate levels of forest removal in snowmelt watersheds have been shown to alter the frequency and magnitude of peak flows (Schnorbus and Alila, 2004; Green and Alila, 2012; Grohnsdahl et al., 2019), advance the timing of spring peak flows (Moore and Scott, 2006), and increase the duration of summer low flows (Winkler et al., 2017). The ability to quantify the relationship between forest disturbance, regeneration, and the hydrologic response of a watershed is thus important for understanding how logging or natural forest disturbances might affect water-resources, aquatic habitats, and flood risk (Dickerson-Lange et al., 2021; Varhola et al., 2010).

Several studies have endeavored to quantify differences in peak snow accumulation and ablation rates between clearcut, juvenile, and mature stands (Buttle et al., 2000; Murray and Buttle, 2003; Winkler et al., 2005; Winkler and Moore, 2006; Varhola et al.,2010; Broxton et al., 2015; Konstantinos et al., 2018). These previous studies showed decreasing peak SWE with increasing canopy interception and decreasing stand-level ablation rates as stands mature (Varhola et al., 2010; Hotovy and Jenicek, 2020). The recovery of SWE and ablation processes are collectively referred to as hydrological recovery, which describes the restoration of hydrological characteristics to pre-disturbance conditions and is expressed as a positive trend increasing from 0% for clearcut to 100% for a regenerated mature stand (Winkler and Boon, 2015). However, the potential for a period of negative ablation recovery, in which very young juvenile stands display faster ablation rates than the clearcut condition has been identified in two separate studies originating in different hydroclimate regions (Winkler and Boon, 2015; Buttle et al., 2005). The process responsible for this negative recovery, and the point at which recovery transitions from negative to positive as the stand matures was not identified in either study.

The ability to estimate the hydrological recovery of a stand contributes to understanding and predicting the potential influence of forest disturbance on the timing and magnitude of snowmelt runoff. The assessment of hydrological recovery applied to individual regenerating stands is used in a cumulative manner by forest managers to estimate the current level of hydrological disturbance in a watershed (Winkler and Boon, 2017). At the watershed scale, the assumption is made that as the individual stands recover hydrologically, so to do the stream flow regime characteristics (Hudson, 2000; Buttle et al., 2005; Moore and Wondzell, 2006; Winkler & Boon, 2015).

Past studies investigating hydrological recovery relied on field surveys of snowpack depth and SWE measured along a snow course or a sampling grid within adjacent clearcut, juvenile, and mature stands (Metcalfe and Buttle, 1998, Winkler and Spittlehouse, 1995; Hudson, 2000; Winkler et al, 2005; Buttle et al., 2005). These representative site surveys were typically averaged for the entire stand and hydrological recovery values were calculated according to the mean canopy height or canopy closure. Daily ablation rates were calculated by dividing the average peak SWE for the stand by the number of days from peak accumulation to when the stand became snow-free. Applying hydrological recovery models from these prior studies to areas which differ topographically (i.e. slope, aspect, elevation) or have different vegetation characteristics can be problematic (Ellis et al., 2011; Ellis et al, 2013) as it assumes transferability of results without a full understanding of how the heterogeneity of stand height and canopy cover might affect stand-level hydrological recovery.

An additional limitation of past studies relates to manual point-based samples of snow depth and SWE, which have practical limitations associated with ease of access, the time involved in collecting a representative sample of snow depth and SWE for the site, and the inability to sample the same location twice during the ablation period due to snowpack disturbance (Winkler et al., 2005). The sample sizes and associated point densities used in some previous studies were determined according to the ability to identify between-stand differences in April 1st SWE, which is a date traditionally assumed to represent peak annual SWE in western North America regions (Winkler and Spittlehouse, 1995). When traditional sampling methods are applied to stands with a greater degree of topographic variability, or in stands with a heterogeneous vegetation distribution, the sample may not be representative. This may also be true during the ablation period if snow melt rates are variable within a stand (Winkler and Moore, 2006).

Increasingly, LiDAR is being used to investigate the spatio-temporal distribution of snowpacks at the watershed scale (Deems et al., 2006; Hopkinson et al., 2012; Deems et al., 2013; Kostadinov et al.,

2019). Continuous gridded models of snow depth produced from aerial LiDAR have a much finer spatial resolution than sampling distances employed using traditional field-based sampling methods, particularly in areas where terrain complexity limits ease of access (Deems et al., 2013; Zheng et al., 2016; Kostadinov et al., 2019). However, aerial LiDAR is susceptible to occlusion-related signal loss in areas with dense forest canopy or where topographic relief is very high (Kostadinov et al., 2019). This occlusion can influence ground level point densities and increase the uncertainty in LiDAR-derived measures of snow depth below dense forest canopy cover (Kostadinov et al, 2019).

Recent advances in LiDAR technologies, including the development of mobile terrestrial LiDAR, enable the production of very high-precision models of snow depth and average daily ablation, even in areas where dense vegetation and steep topography might reduce the number of ground returns obtained from an aerial LiDAR system. The high LiDAR point densities resulting from these ground-level surveys enable the consideration of both stand-level averages of peak snow accumulation and ablation rate, and the role that canopy cover and within-stand tree height variability might play in influencing these stand averages.

This study utilized a state-of-the-art GeoSLAM Zeb Horizon mobile terrestrial LiDAR unit to measure snow depth from the time of peak snow accumulation to the end of the ablation period to establish the relationship between forest stand maturity and hydrological recovery in mixed-coniferous stands on north aspect slopes. A key objective of this study is to better quantify the process of hydrological recovery at the scale of individual trees, allowing for potential transferability of outcomes to areas which differ topographically, or to stands where tree height, canopy cover, or within stand variability are not specifically represented in the study sites included here.

5.1.1 Study Area

The study area is located approximately 25 km southwest of the town of Nelson in the Selkirk Mountains of British Columbia, Canada (Figure 5-1). The Rover Creek watershed provided an opportunistic study design due to the proximity of a range of forest conditions, including recently harvested, juvenile, and mature stands. The study area is situated on north aspect slopes, where vegetation has been shown to have a larger influence on snow accumulation and ablation (Dickerson-Lange et al., 2023; Ellis et al., 2011). Access to the sites was maintained throughout the snow accumulation and ablation period by the nearby Snowwater Ski Lodge. Ease of access to the broad study area and individual sites was crucial for repeated (every 2-3 days) data collection from the time of peak snow accumulation through to the end of the ablation period spanning March 19 to April 24, 2019.

Four adjacent forest stands with increasing maturity were selected within walking distance of each other in order to transport equipment and carry out LiDAR scans and snow core sampling within a short (<4 hour) time window. The sites selected include one recently replanted clearcut with an average tree height of 2.7 m (J2), two juvenile stands with average heights of 11.5 m (J10) and 14.8 m (J15), and one mature stand with an average tree height of 37.6 m (M) (Table 5-1). For the purposes of this study, the cumulative openings in J2 were considered to be representative of a clearcut condition. All four sites are composed of mixed conifer species (interior Douglas fir, lodgepole pine, western larch, and western cedar) apart from the mature site M, which is primarily composed of interior Douglas fir (Table 5-1). Although species succession from the mixed-conifer stands in sites J2, J10, and J15 can not be assumed to progress to an exclusively Douglas fir stand characteristic of site M, the stands in this study represent increasing stand height and canopy cover with stand regeneration.

Sites were selected with similar topographic characteristics (slope, aspect, elevation) to control for these factors in order to measure differences in peak snow accumulation and daily ablation related to differences in stand maturity. The study sites are located on north aspect slopes, with some small variations ranging from NW to NE aspects. J10, J15, and M all have moderate median slope gradients between 54% and 60%, while J2 has a low-moderate median slope gradient of 27% (Table 5-1).

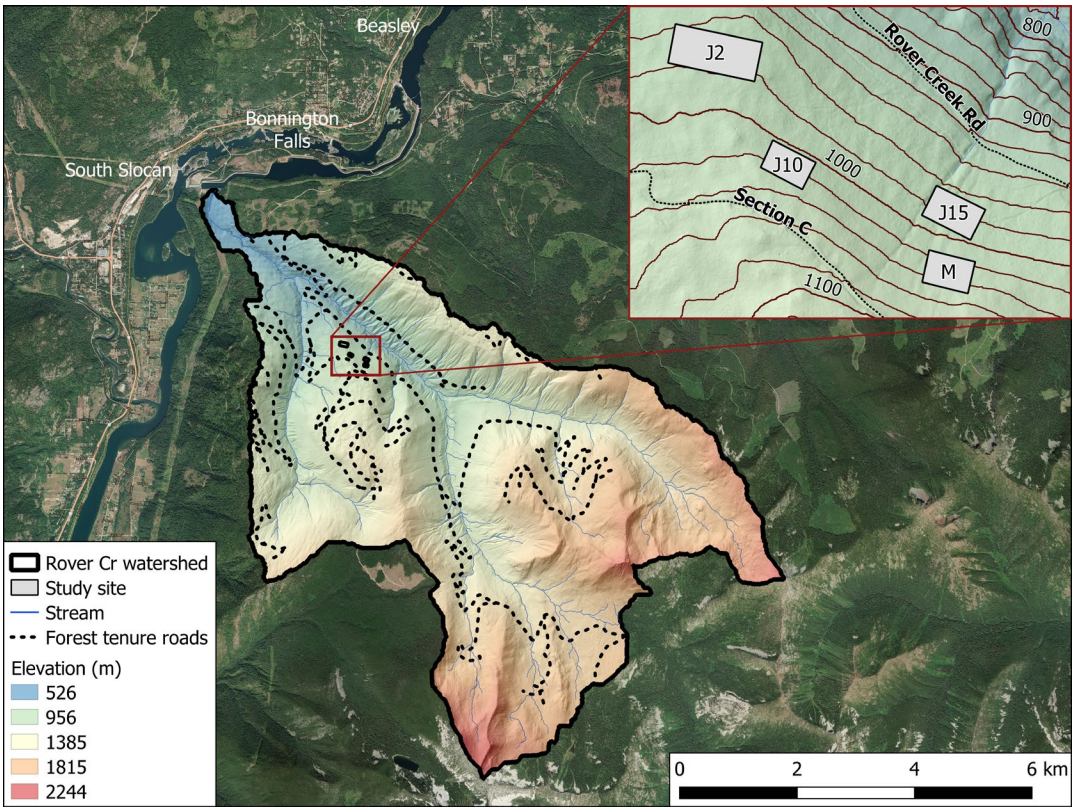

Figure 5-1 Rover Creek study area located near Castlegar, British Columbia, Canada. Study sites J2, J10, J15, and M (burgundy polygon) are located on north aspect, moderate slopes between 960 m and 1040 m elevation.

Table 5-1 Topographic and vegetation characteristics for sites J2, J10, J15, and M used for this study. Crown cover as measured on April 20th, 2019 (when western larch were still needle-free) is reported as the total crown area as a percent of the study site area.

	Elevation (m) (min/**mean**/max)	Aspect	Slope (%)	Tree height (m) (min/**mean**/max)	Crown Cover (%)	Tree Species	Understory
J2	959 / **972** / 982	N-NE-NW	27.1	(1.1 / **2.7** / 5.6)	49	Western larch (60%) Douglas fir (40%)	Open
J10	1003 / **1017** / 1032	N-NE	54.5	(4.0 / **11.5** / 18.1)	92	Douglas fir (43%), lodgepole pine (25%), western Larch (20%), cedar (9%), hemlock(3%)	Continuous low-brushy vegetation
J15	962 / **979** / 997	NE	53.7	(8.2 / **14.8** / 22.1)	97	Douglas fir (43%), lodgepole pine (25%), western Larch (20%), cedar (9%), hemlock(3%)	Open with minimal low-brushy vegetation
M	1014 / **1031** / 1048	N-NE	59.5	(32.5 / **37.6** / 42.0)	98	Douglas fir (100%)	Open with large-diameter (>25cm) woody debris

5.2. Data and Methods

5.2.1 Data Collection

LiDAR Unit and LiDAR Survey Methodology

The snow surface elevation (m), canopy height (m), and crown cover (%) in each study site was measured using a GeoSLAM ZEB-Horizon handheld mobile LiDAR scanner. The ZEB-Horizon utilizes Simultaneous Location and Mapping (SLAM) technology to produce a cohesive point cloud for the entire scanned area, with a claimed relative spatial accuracy of 1 to 3 cm. The LiDAR used on the ZEB-Horizon operates at 905 nm and has a reported operation distance of 100 m, with an effective range of approximately 40 m (https://www.faro.com/en/Products/Hardware/GeoSLAM-ZEB-Horizon-RT/). The high point density resulting from ground-level surveys using this LiDAR unit allow for the production of highly accurate, fine-resolution snow surface elevation models which effectively measure the snow surface over variable terrain and under dense forest canopy.

LiDAR survey loops were established within the four main study sites and incorporated a 100 m snow course within each site. The looped survey design is a requirement of SLAM LiDAR surveys and is employed to reduce the impact of drift error on the resulting pointclouds. For each study site, the snow course was incorporated as part of the survey loop, and the same walking path was used for all scans carried out in each survey location to limit snowpack disturbance.

The established survey loops allowed for the measurement of study areas between approximately 4000 to 9000 m^2. The loop-based scan design enabled the scanned area to be measured from multiple directions, reducing the impact of occlusion on the resulting pointclouds, and resulting in a very high LiDAR point density measure of the snow surface. The average point density resulting from LiDAR scans used in this study during the time of peak snow accumulation was ~15,000 points m^{-2} for all LiDAR returns (ground and vegetation) and ~750 points m^{-2} for points classified as ground/snow surface. LiDAR point densities from scans performed later in the season tended to be lower as the reflectivity of the snow-free ground surface was lower, and the increased topographic and vegetation complexities introduce more opportunity for occlusion.

Between 3 and 6 ground control points (GCPs) were set up along the looped walking paths in each of the study sites to facilitate co-registration of multiple scans performed from the time of peak accumulation (March 21, 2019) to the end of the ablation period. These control points consisted of styrofoam spheres with a diameter of 20 cm placed onto the end of bamboo rods. Using steel strapping,

these rods were fastened to trees within the interior of each planned scan route. The spheres remained stationary throughout the sampling period allowing for precise temporal co-registration of LiDAR pointclouds collected.

LiDAR scans were performed within a 4-hour range roughly every 2 to 3 days from the approximate time of peak snow accumulation through the end of the site-specific ablation period. Site M was snow free on March 31, J2 and J15 on April 20, 2019, and J10 on April 24, 2019. The final number of scans performed in each site varied according to the duration of snow on the ground. In site M, which was the first to become snow free, only 5 LiDAR scans were performed, while 11 scans were performed in both J2 and J15, and 12 scans were performed in J10.

Manual Snow Course Samples

Following methods described by Winkler et al. (2005), Hudson (2000), and Dixon et al. (2014), snow water equivalence (SWE) was measured using a standard Federal snow tube along snow courses established next to the LiDAR survey loop in each study site. These snow courses included 10 sample locations spread at 10 m intervals which were marked with flagging tape. Temporal snow cores were collected within 1 m of each marked sample location. Cores were collected on the upslope side of the snow course to reduce the risk of snow disturbance to the sampling area.

5.2.2 Data Processing

GeoSLAM ZEB Horizon Data Processing

The LiDAR data files collected using the GeoSLAM ZEB Horizon are viewed and processed using GeoSLAM's proprietary software (https://geoslam.com/hub/). This software was used to convert point clouds to a commonly used LAS point cloud format (ASPRS, 2019) for further analyses using CloudCompare (CloudCompare, 2019) and QGIS (QGIS.org, 2024) software.

Repeat LiDAR scans carried out on multiple dates were co-registered in CloudCompare using the styrofoam sphere GCPs placed within each study area. Aligned spheres for all co-registered scans in each site had an RMSE of less than 3 cm. For the purposes of this study, exact positioning was deemed less important than accurate repeated measures of snow depth within each site.

Global positioning system (GPS) locations for all GCPs used for co-registration of individual pointclouds were collected using a handheld Trimble GPS unit which measured GCP positions in the XY plane to within approximately +/- 5 m under dense canopy. The GPS coordinates were used to generally relate final study outputs to their associated stands. However, the GPS coordinate measures of GCP positions had a greater uncertainty than that of the co-registered LiDAR scans and were not used to georectify the individual pointclouds in order to prevent the introduction of positional uncertainty to co-registered pointclouds, and ultimately to subsequent models representing snow depth.

LiDAR Classification

The ground and snow surfaces in each of the co-registered point clouds were classified using the ground classification tools available in TerraScan (Terrasolid, 2016). Each LiDAR pointcloud was classified individually to ensure that site-specific ground classification parameters were identified which minimized the misclassification of near-ground vegetation and woody debris as part of the ground classification.

LiDAR Derivatives

Snow Depth, SWE, & Ablation

Snow surface models were created from each of the classified pointclouds by gridding the ground (snow surface) classification in each with a 0.10m grid size. This grid resolution was chosen based on both the average spacing between ground or snow-surface points within the full scan, as well as a qualitative assessment of point distributions. The walking path used to carry out the LiDAR survey loop in each site was masked out from the final snow surface models and subsequent analysis to reduce the influence of snow compaction on measured values for snow depth. In the mature stand (M) ground surface areas with large-diameter woody debris (i.e., fallen logs) were also removed from the resulting surface models.

Gridded snow depth models were created for each scan date by removing the elevation of the snow-free bare terrain from the elevation of each snow surface model according to the methods described in previous LiDAR-based snow depth studies (Deems et al., 2006; Hopkinson et al., 2012). These snow depth models were converted to gridded models of SWE using depth to SWE relationships established from the manual snow course data collected in each site. For all sites in this study, the initial scan date (March 21, 2019) was determined to be the date of peak SWE. It should be noted that the relationship between snow depth and SWE strengthens as the snowpack becomes isothermal and has a more uniform density just prior to snowmelt (Spittlehouse and Winkler, 2004). This process is reflected in Figure 5-A1 (see Appendix) with more variability in SWE observed at greater depths (earlier in the snowmelt period) prior to isothermal conditions in the snowpack.

Gridded models of average daily ablation were created by calculating the difference in SWE between gridded SWE models from two different dates and dividing this difference by the number of days between the two LiDAR scans. In order to exclude an artificial slowing of daily ablation rate where an area became snow free between the two scan dates, all grid cells which became snow free during the date range under consideration were masked out of the final gridded ablation model. Average daily ablation rate models were created for three date ranges within the ablation period: i) March 21 to 28, ii) March 31 to April 8, and iii) April 8 to April 16, 2019. The time range when all sites had snow was from March 21 to 28, 2019. This earliest date range was therefore used for comparison between the 4 sites.

The final gridded models of Peak SWE and average daily ablation were used to assess [1] stand-level differences between sites, [2] within-stand differences between the cumulative below-crown area

and openings, and [3] below crown areas of individual trees to observe within-stand variability according to tree height.

CHM, Treetop heights, Crown extents

Canopy height models (CHM) were produced using the final snow-free LiDAR scan performed in each site. Traditionally, LiDAR-derived CHMs are created from scans performed from above the canopy. While the scans in Rover Creek were conducted from below the canopy, the effective range of the Zeb Horizon LiDAR unit, paired with the ability to scan trees from multiple angles using the looped survey design resulted in high density point measures of individual tree crowns, particularly in juvenile stands where the point density of traditional airborne LiDAR scanners (ALS) can fail to fully characterize the crowns of individual trees. For the mature stand, where the top of the tree canopy is at the limit of the effective range of the Zeb Horizon, the resulting Zeb Horizon point cloud was merged with aerial (drone-based) LiDAR to better quantify the upper canopy height.

Tree crown extents and individual treetops with their associated heights were identified from the CHM in each site using the rLiDAR package in R (Silva et al., 2017). For juvenile sites J2, J10, and J15, a CHM with a 0.25 m grid size was used, while in the mature site (M) where individual branches are large enough to share physical characteristics with those of smaller trees, a 0.5 m grid size CHM was used. This coarser resolution resulted in tree crowns which were more representative of the site.

Below-Crown Peak SWE and Average Daily Ablation

Tree crown extents with their associated tree top heights were used to investigate the relationship between individual trees within each stand on below-crown SWE and daily ablation rate and to observe general trends related to tree height. This sampling design, which provides observations of below-crown snowpack dynamics for a range of tree heights within the same stand, is an example of space-for-time substitution (Pickett, 1989).

The cumulative below-crown area (CBC) within each site was used to compare differences in peak SWE and daily ablation between openings and below-canopy areas. Although the four sites in this study captured the forest cover characteristics of each stand type, the larger tree crowns in site M which contribute to a nearly continuous canopy result in a lower total sample size in both in terms of individual tree crowns and in terms of open area SWE or ablation raster pixels compared to the other sites. The distribution and magnitude of differences in peak SWE and daily ablation in the CBC and open areas were used to provide a qualitative understanding of the influence of tree crowns within each stand. The

significance of differences in both peak SWE and average daily ablation between the snowpack under the CBC area and snowpack in the opening was tested using the non-parametric Mann-Whitney U test, or Wilcox (Hollander et al., 2014) for independent samples.

In J2, where the boxplot distributions of average daily ablation in CBC and open areas highlight an inverse relationship compared to other sites, boxplot distributions were organized according to integer differences in tree height, together with open and below-crown areas in J10, to identify the height at which juvenile trees begin to positively affect ablation recovery.

Peak SWE and Ablation Recovery

Following the general methods presented by Winkler & Boon (2015), Buttle et al (2005) and Hudson (2000), both peak SWE recovery and ablation recovery were calculated for the below-crown snowpack in each site by comparing the observed peak SWE and daily ablation rates to the average values measured for the clearcut and mature snowpack using the following equation.

$$SR = [(Sc - Sy) / (Sc - Sm)] \times 100 \qquad \text{[Equation 5-1]}$$

SR describes the percent (%) snow recovery for the variables of interest; peak SWE (cm) or ablation rate (cm d-1) for the below-crown snowpack (Sy) compared to an average index value of each variable measured for the clearcut condition (Sc) assumed to be represented by the cumulative open areas in J2, and the mature stand (Sm). SR is calculated as the difference between the index value of peak SWE or average daily ablation in Sc and Sy relative to the difference in the index value between Sc and Sm. The resulting percent recovery for both peak SWE and daily ablation rate was applied to each below-crown area. Peak SWE recovery and average daily ablation recovery were plotted according to the tree height associated with each crown and a Chapman-Richards curve with an asymptote value set to 100% was fitted to the data by adjusting curve-fitting parameters which minimized the total residual error between the resulting curve and measured below-crown recovery values. A 90% confidence interval was applied to both recovery curves according to integer tree heights. Sample sizes in J15 and M are notably smaller than those in J2 and J10, as there are fewer large crowns identified in these sites which has a bearing on the resulting confidence intervals.

5.3. Results

Results from this study are presented in the order by which the LiDAR were processed, beginning with co-registered classified LiDAR pointclouds, and ultimately considering LiDAR derivatives representing peak SWE and average daily ablation. Cross-section views for aligned classified pointclouds highlight the detailed coverage of both vegetation and the snow surface resulting from ground-level scans and provide insight on vegetation influences on accumulation and melt processes. Gridded LiDAR products representing the peak SWE and average daily ablation are presented to consider differences in stand-level averages, and to investigate within-stand differences in the peak SWE and daily ablation observed in the openings and CBC areas. Finally, within-stand variability in peak SWE and average daily ablation, as well as the recovery of these two variables is considered according to tree height for the below-crown area for all trees identified in each study site.

An example of a 0.2 m depth cross-section through co-registered ground classification outputs for LiDAR scans performed in site J2 highlights the minimal influence individual trees in this site have on the snow depth (Figure 5-2). The peak snow depth surface (red points) adjacent to individual trees in J2 is similar to the peak depth in the openings. As the ablation period progressed (e.g., green surfaces), the snow depth became more variable with snowmelt close to individual tree stems exceeding that observed in the openings.

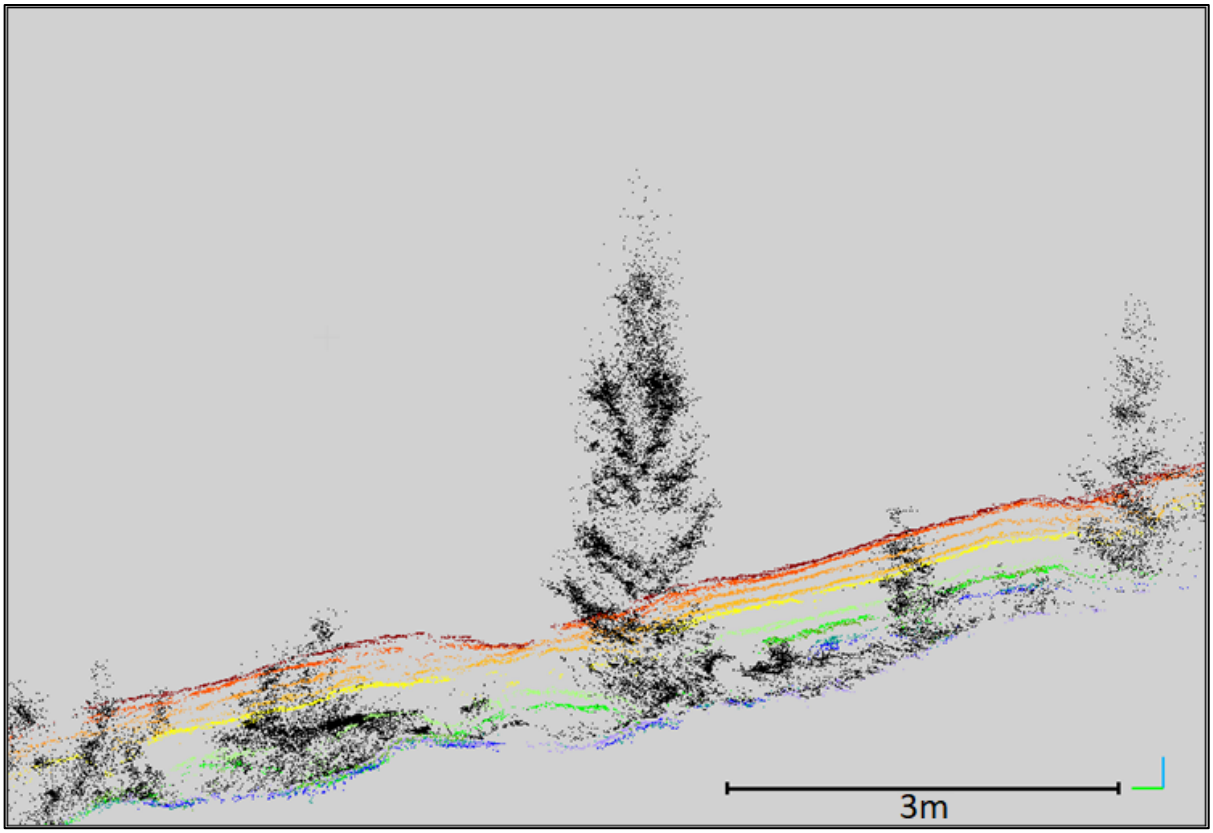

Figure 5-2 Cross section (0.2 m depth) of co-registered LiDAR pointclouds representing the snow surface from March 1, 2019 (red) through the ablation period April 20, 2019 (purple). Vegetation in J2 (black) appears to have little to no influence on the peak accumulation, while the undulating characteristics of snow surface in the later season (e.g., green surface) indicates faster melt adjacent to individual trees.

5.3.1 LiDAR Derivatives

Snow Water Equivalent (SWE)

Gridded models of SWE for four of the sampling dates beginning at the time of peak SWE (March 21) and extending through much of the ablation period (April 16) are shown below (Figure 5-3). Site M, which had the lowest peak SWE of the four sites, was snow free by March 31, 2019. For each date the measured SWE decreases with increasing stand maturity.

Peak SWE was greatest in J2 where canopy cover was minimal, and trees lacked the surface area to reduce ground-level snow accumulation through interception (Figure 5-4). In site J2 the peak SWE (March 21) in the openings was very similar to below-crown areas. However, as the ablation period progressed, the peak SWE below crowns was observed to be lower than in the surrounding openings. In sites J10 and J15 for all dates, the peak SWE was greater in the openings and decreased with proximity to the individual tree stems (treetops) (Figure 5-4). This localized control of individual crowns in these two sites resulted in deep tree wells. In J10, where the trees were taller and crowns interact collectively as a closed canopy, there are fewer visible tree wells. In site M, where the mature trees share a uniform overlying canopy, the peak SWE has a greater uniformity throughout the site, although there is some variation related to topographic variability, and possibly also to the presence of large woody debris on the ground.

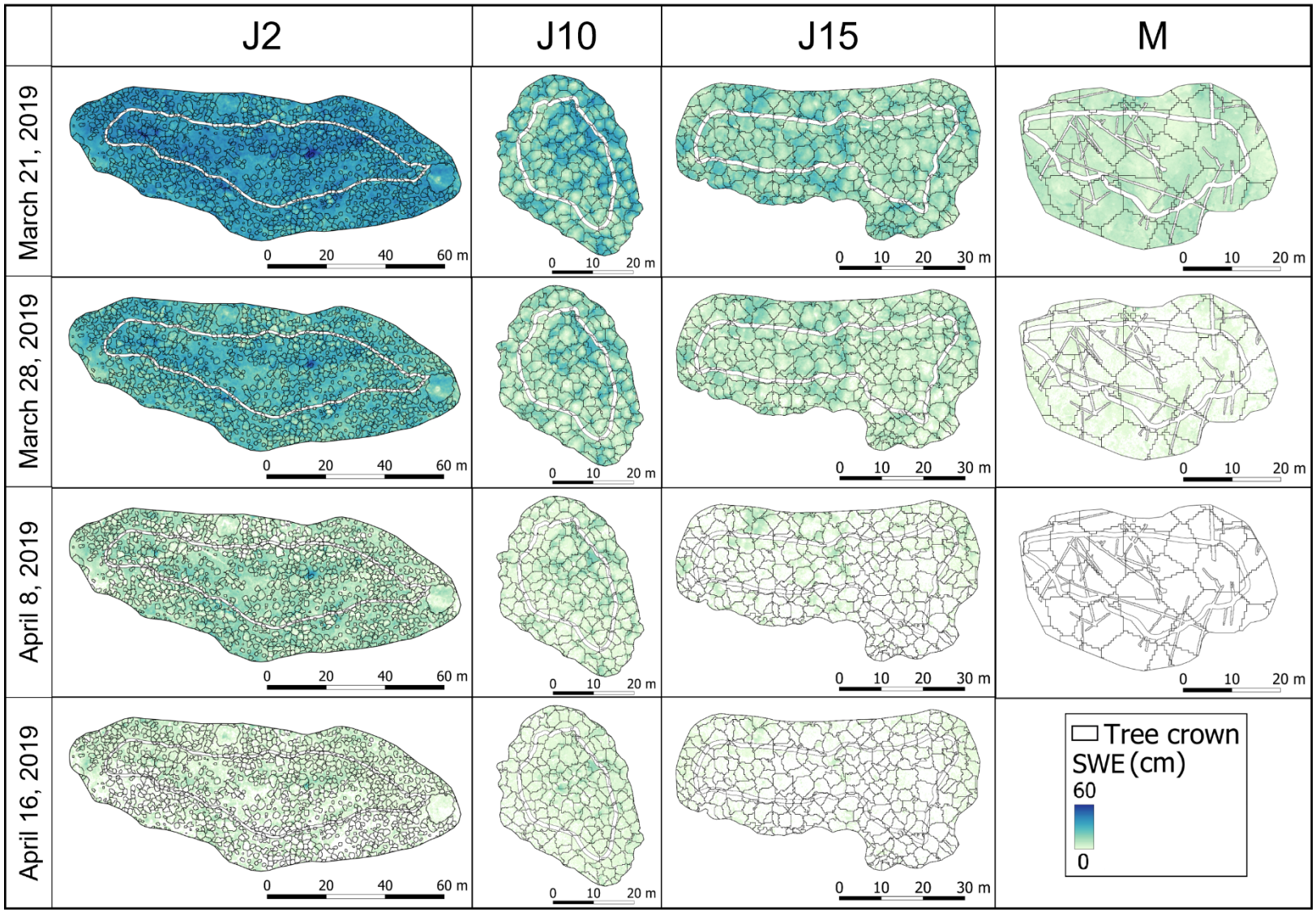

Figure 5-3 Snow water equivalent (SWE) in sites J2, J10, J15, and M. The walking path in each site has been masked out, as can be seen as a white path with no data in the middle of the study site areas. Large woody debris, specific to the mature stand (M), has also been masked out as these areas add uncertainty to snow depths measured in this site. Crown extents of individual trees are represented with black outlines.

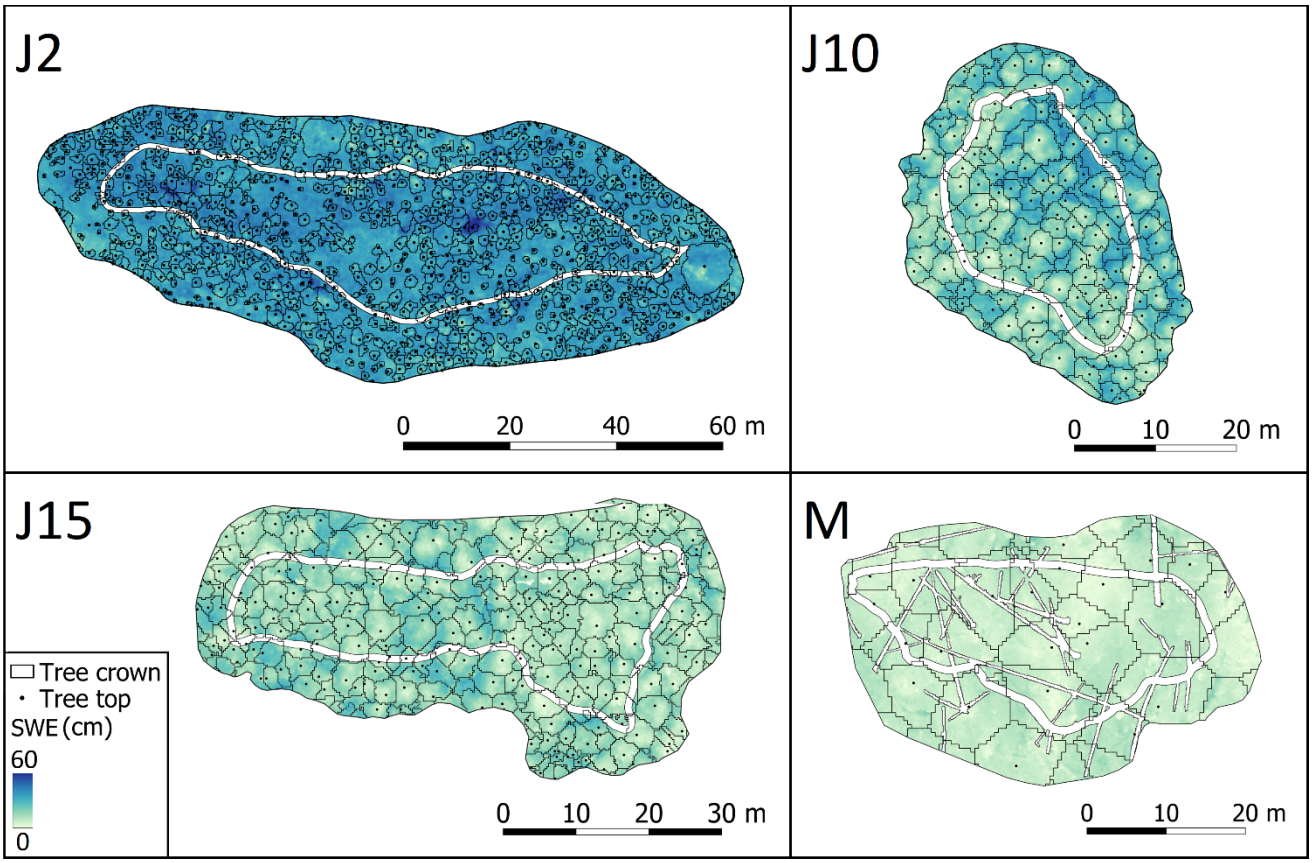

Figure 5-4 Peak Snow Water Equivalent (SWE) (March 21, 2019) in Rover Creek sites J2, J10, J15, and M. The variability in peak SWE is greatest in juvenile stands J10 and J15. The walking path in each site has been masked out, as can be seen as a white path with no data in the middle of the study site areas. Large woody debris specific to the mature stand (M) has also been masked out as these areas add uncertainty to snow depths measured in this site.

Average Daily Ablation

The average daily ablation rates during the March 21 to March 28 period were highest in J2 and decreased with increasing stand maturity (Table 5-2, Figure 5-5). In J2, the average daily ablation rate was 1.6 cm/day in the opening and 1.7 cm/day in the CBC area. In J10 these rates were 1.4 cm/day and 1.2 cm/day, respectively. J15 experienced rates of 1.2 cm/day and 1.0 cm/day. The average daily ablation rate (0.9 cm/day) was lowest in site M. The higher ablation rate observed in CBC area in J2 compared with the opening is unique to this stand. Although this difference in rate between the open and CBC area is very small and falls within the standard deviation measured for this site, this inverse relationship compared with the other sites highlights the possibility of negative ablation recovery occurring in this stand.

Table 5-2 Average daily ablation rate in cm/day observed in sites J2, J10, J15, and M for the full stand, in openings, and in the cumulative below-crown area. Yellow highlights the greater site-level ablation rate in the cumulative below-crown area compared to the openings observed in site J2. Negative minimum ablation rate values in this table result from grid cells where the SWE measured on the end date of an ablation date range is greater than at the start date. This can occur from slight misalignment of LiDAR scans, emergent vegetation affecting the ground/snow surface classification, or slight misalignments between gridded models of SWE.

	Ablation (cm/day) March 21 to March 28				
	Sample size (raster pixel count)	Min	Max	Mean	SD
J2	455,300	-1.1	4.5	1.6	0.4
J10	100,600	-1.5	5	1.2	0.5
J15	183,900	-1.6	4.2	1	0.4
M	135,300	-1.1	3.2	0.9	0.4
	Ablation in open (cm/day) March 21 to March 28				
	Sample size (raster pixel count)	Min	Max	Mean	SD
J2	229,900	0.1	4.5	1.6	0.3
J10	7,200	-0.9	4.4	1.4	0.5
J15	5,300	-0.7	3.9	1.2	0.4
M	800	-0.2	2.9	1.1	0.5
	Ablation in cumulative below-crown area (cm/day) March 21 to March 28				
	Sample size (raster pixel count)	Min	Max	Mean	SD
J2	225,400	-0.5	5.2	1.7	0.5
J10	93,400	-0.5	4.4	1.2	0.5
J15	178,600	-1.6	4.2	1	0.4
M	134,500	-0.4	2.5	0.9	0.4

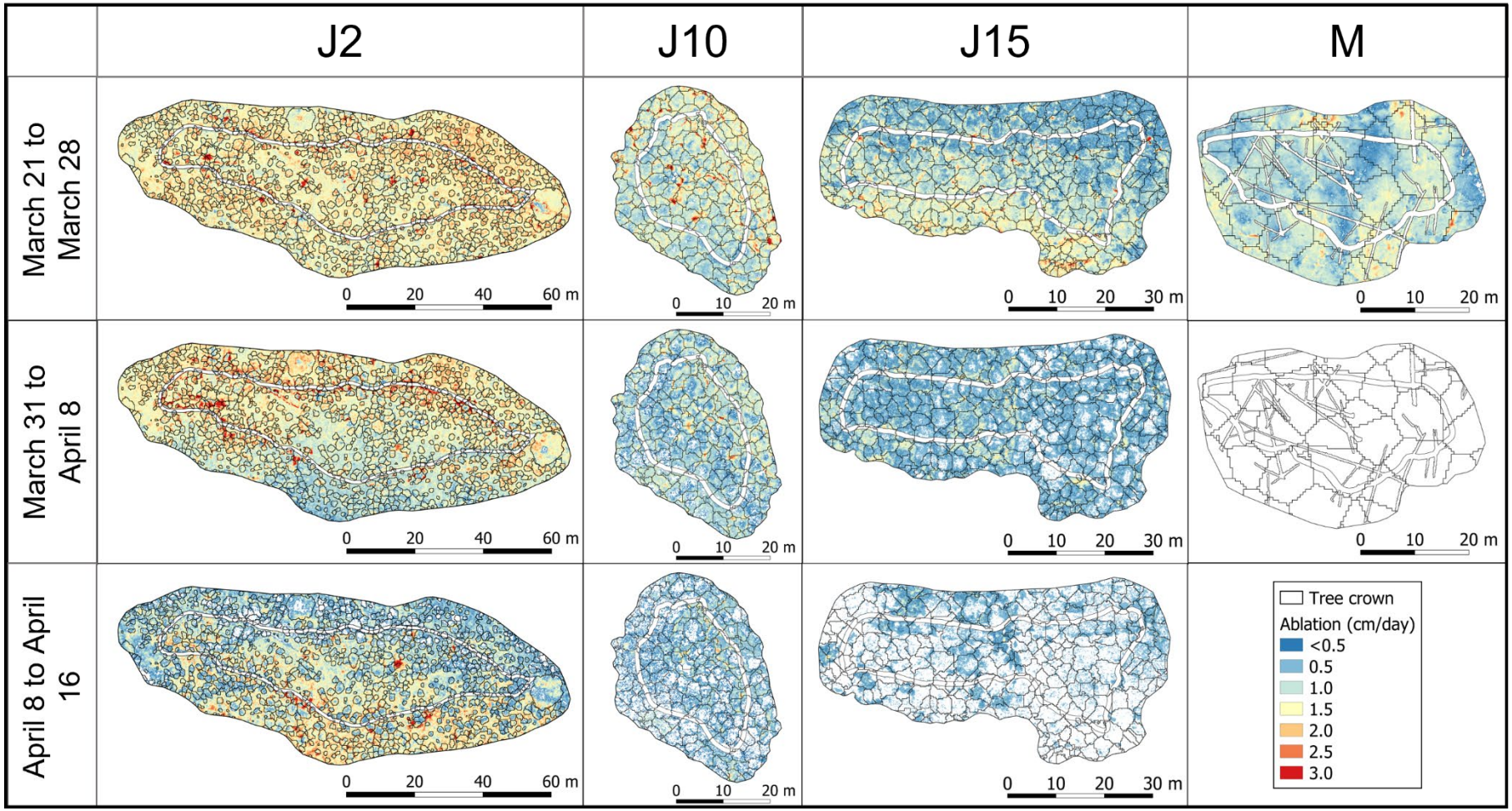

Figure 5-5 Average ablation rates (cm/day) for approximately week-long time intervals beginning at the time of peak accumulation (March 21, 2019) through the end of the ablation period (March 31, 2019, for site M, April 20th for J2 and J1, and April 24 for J10.

5.3.2 Below-Crown Peak SWE and Average Daily Ablation

Below-crown peak SWE decreases with increasing tree height within each stand and as stands mature (Figure 5-6). As trees increase in height with increasing stand-level maturity, the range in peak SWE is reduced, with a greater range in SWE observed in recently replanted juvenile stands.

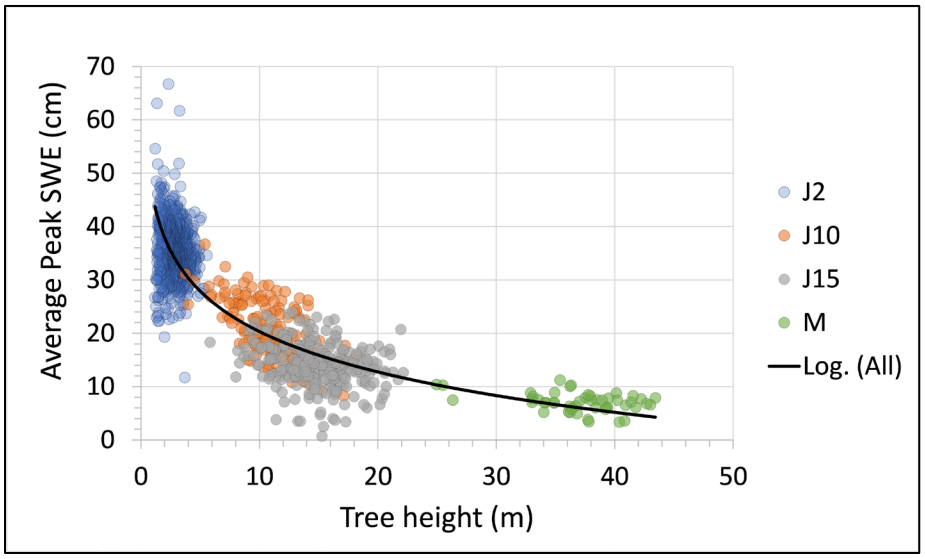

Figure 5-6 Peak Snow Water Equivalent (SWE) measured for below-crown areas of each tree identified in sites J2, J10, J15, and M. Peak SWE is shown to decrease as trees increase in height, with the greatest decrease observed for trees below 10m in height.

Below-crown peak daily ablation rates between March 21 and March 28, 2019 decreased with increasing tree height within each stand and stand maturity. The greatest reduction in average daily ablation occurred between sites J2 and J10 (Figure 5-7).

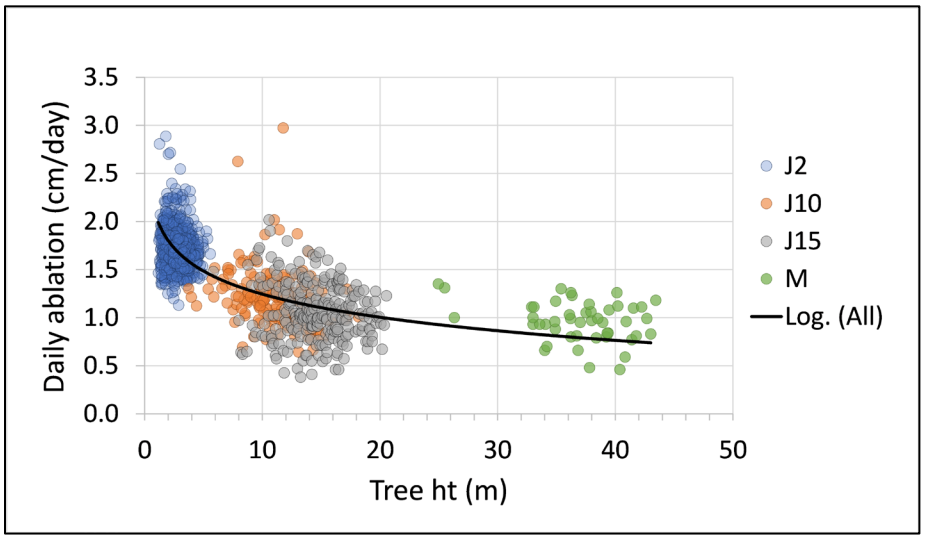

Figure 5-7 Normalized (averaged) below-crown daily ablation rates in cm/day for trees in J2 (blue), J10 (orange), J15 (grey) and M (green).

5.3.3 Peak SWE and Average Daily ablation in Openings (gaps) versus cumulative below-crown areas

Boxplots representing the distribution of peak SWE and average daily ablation for the full site, openings, and CBC areas are shown in Figures 5-8 and 5-9. As stands mature, the range of both peak SWE and average daily ablation decreases, with the smallest range of values observed in the mature stand where the continuous canopy controls both stand-level accumulation and amount of incoming solar radiation available to drive ablation.

Peak SWE in openings (gaps) and cumulative below-crown area

Although there is a general stand level decrease in peak SWE as stands mature, it is more pronounced in the CBC areas than in the openings (Figure 5-8). In J2, there is very little difference between peak SWE in the openings compared with the CBC. In sites J10 and J15, the CBC area had a noticeably reduced peak SWE than in in the openings. In site M, the peak SWE in the opening is similar to that observed in the CBC area.

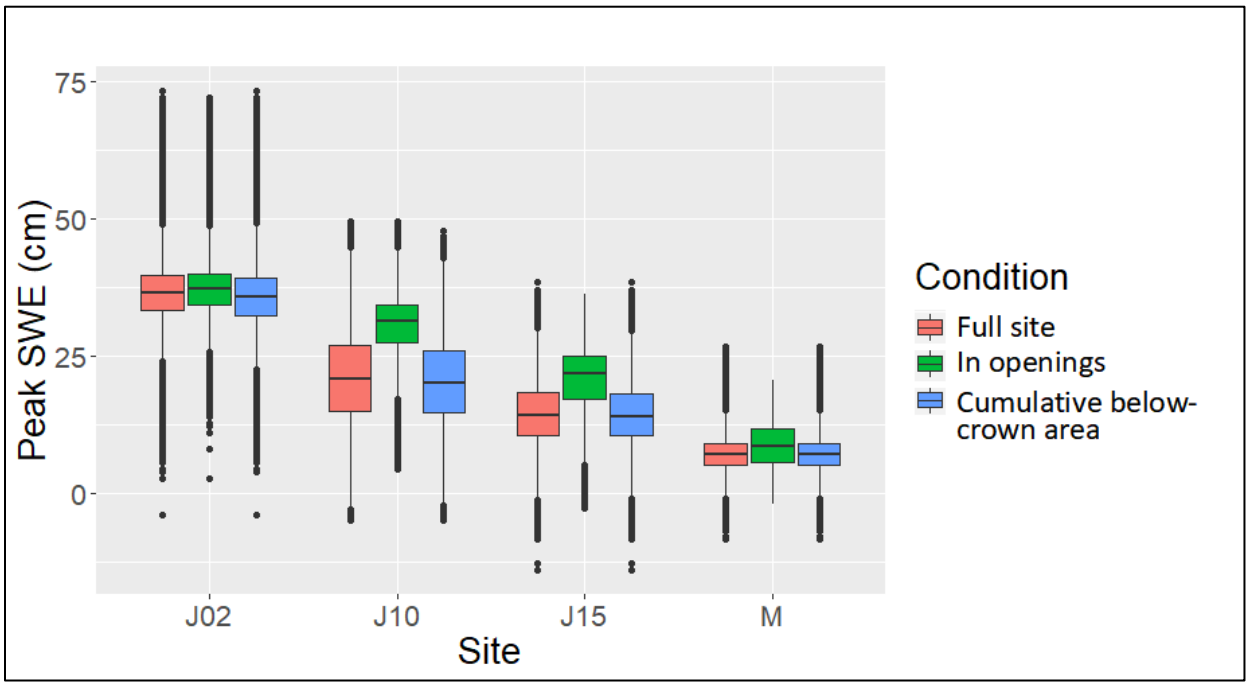

Figure 5-8 Boxplots showing Peak SWE on March 21, 2019, for the full site (red), openings (green), and cumulative below-crown area (blue) in sites J2, J10, J15, and M. Boxplots include the 25th to 75th percentiles, as well as the median (50th percentile) represented as a line.

In J2, the mean peak SWE was 1.4 cm lower in the CBC area than in the openings (Table 5-3). In sites J10 and J15, the reduction in average sub-canopy snow compared to the clearcut condition is 9.2 cm and 6.5 cm respectively. In these two sites, the trees crowns are large enough to intercept snow and reduce ground-level accumulation. However, the crowns in these juvenile sites have yet to share the interception capability of the closed canopy found in the mature stand (M), and the control these juvenile trees play on below crown snow is highly localized. In site M, peak SWE is more evenly distributed throughout the site.

Table 5-3 Minimum, maximum, and mean Peak SWE (cm), and standard deviation (SD) measured in the openings and in cumulative below-crown area in sites J2, J10, J15, and M on March 21, 2019. The difference in mean peak SWE in each site is highlighted in yellow.

	Peak SWE in open areas (cm)				Peak SWE in cumulative below-crown area (cm)				
	Min	Max	Mean	SD	Min	Max	Mean	SD	Diff (cm)
J2	16.5	66.5	37.2	4.8	10.6	61.9	35.8	5.4	1.4
J10	4.4	49.6	30.3	6.8	0.3	44.1	21.1	7.2	9.2
J15	-2.6	36.4	21.0	5.8	-12.8	33.6	14.5	5.4	6.5
M	-2.0	20.6	8.9	3.9	-2.4	17.7	7.1	3.0	1.8

The Mann-Whitney U test identified a significance in the difference in peak SWE between the opening and CBC in all sites (Table 5-4).

Table 5-4 Mann Whitney U test outputs comparing peak SWE in the opening and cumulative below-crown areas in sites J2, J10, J15, and M.

	W	p-value
J2	2.19E+10	< 2.2e-16
J10	1.07E+08	< 2.2e-16
J15	1.95E+08	< 2.2e-16
M	7.39E+07	< 2.2e-16

Average daily ablation in openings (gaps) and sub-canopy areas

In sites J10, J15, and M, where tree crowns reduce the amount of incoming solar radiation reaching the snowpack, the average daily ablation rate is observed to be higher in openings/gaps than in the CBC (Figure 5-9). In J2, where tree crowns are in contact with or sometimes within the snowpack, the ablation rate is observed to be greater in the CBC than in openings. This observed increase in ablation rate falls within the standard deviation of ablation rates for the full stand but includes all trees within the site. A more complete breakdown of average daily ablation rates according to tree height for sites J2 and J10 is shown in Figure 5-10.

The Mann-Whitney U test shows a significant difference in the average daily ablation rates observed in the opening compared to the sub canopy area in all sites (Table 5-5), although the sample size for open areas in site M limits confidence in this test output.

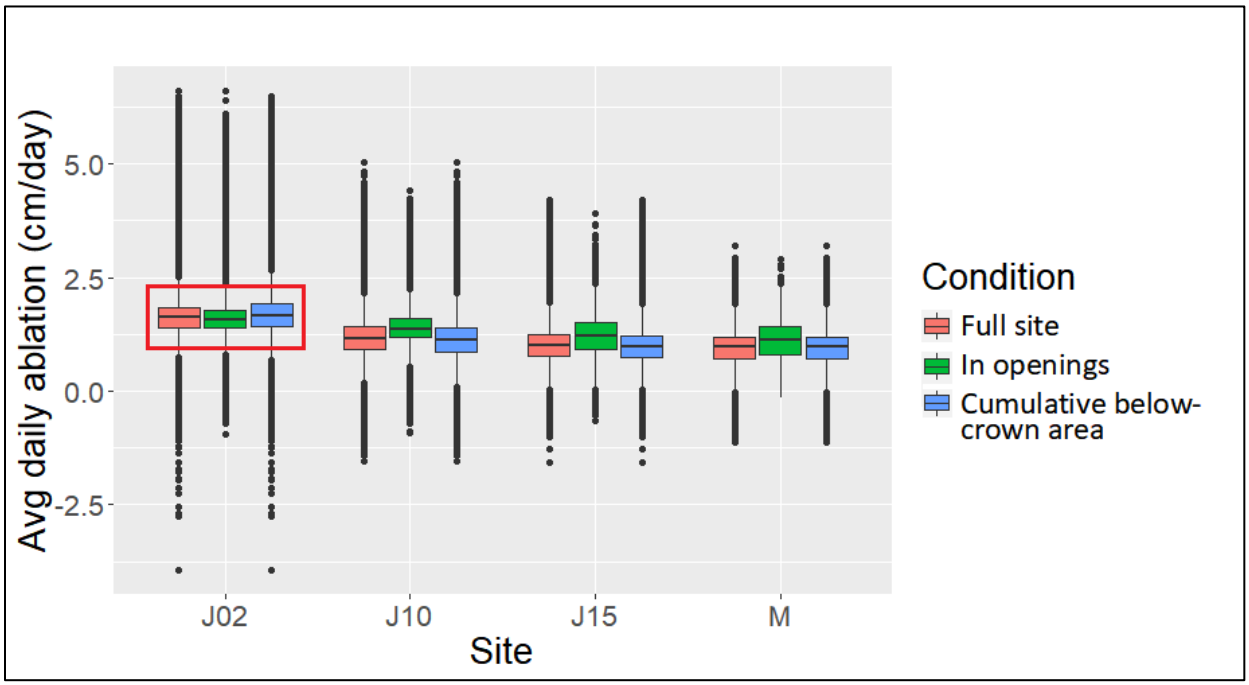

Figure 5-9 Boxplots showing the distribution of average daily ablation (in cm/day) from March 21 to March 28, 2019, in all sites (J2, J10, J15, and M). The ablation rates in the cumulative below-crown areas (blue) are lower than in the openings (green) for sites J10, J15, and M. In J2 (outlines in red) there is a reverse relationship, with CBC showing a faster ablation rate than in the opening.

Table 5-2 Mann-Whitney U test outputs comparing the average daily ablation rates in the opening and cumulative below-crown areas in sites J2, J10, J15, and M. The sample area for openings in site M is very small.

	March 21 – March28	
	W	p-value
J2	2.98E+10	< 2.2e-16
J10	2.27E+08	< 2.2e-16
J15	1.09E+09	< 2.2e-16
M*	1.22E+08	< 2.2e-16

Boxplots representing the distribution of average daily ablation (cm/day) in the openings and under-crown areas for trees in sites J2 and J10 are shown in Figure 5-10. In general, there is a decrease in the ablation rate as tree height increase. However, an initial increase in the ablation rate compared to the clearcut condition is observed in J2, with ablation rates in the sub crown area for trees less than 5 m in height exceeding the melt rates observed in the openings. This increased ablation rate slows as the trees increase in height. As trees approach 5m in height the ablation rate in the below-crown area begins to approximate the clearcut condition, indicating that trees begin to positively affect below crown ablation rates above this 5 m height threshold.

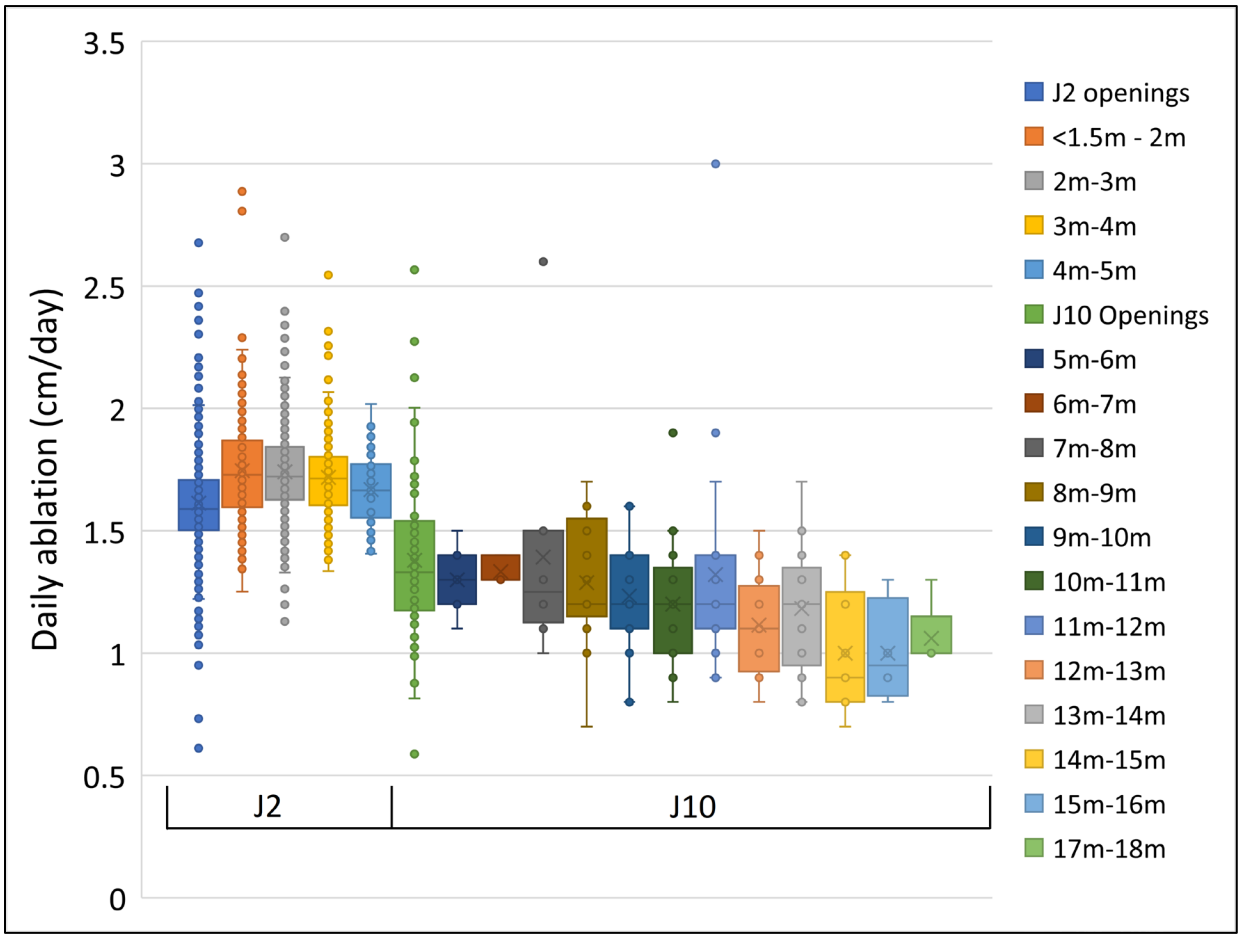

Figure 5-10 Boxplots representing the distribution of average daily ablation in cm/day from March 21, 2019 to March 28, 2019 for openings and below-crown areas according to tree height in sites J2 and J10. Boxplots include the 25th to 75th percentiles, as well as the median (50th percentile, represented as a line) and mean (represented as an X). Note the initial increase in ablation rate observed in the below-crown area of small (<5m) trees in J2 compared to openings in J2 which were used to represent the clearcut condition. This initial increased ablation rate in J2 is an example of negative recovery, where small trees adjacent to, or within the snowpack act to increase the ablation rate.

5.3.4 Hydrological Recovery

Peak SWE Recovery

Peak SWE recovery % (SR, Equation 5-1) applied to below-crown snowpack for all identified trees in sites J2, J10, J15, and M) are shown below (Figure 5-11). The 90% confidence interval on the fitted Chapman-Richards curve indicates a strong relationship between this curve output and measured below-crown values of peak SWE. When considering peak SWE recovery % according to tree height, the resulting curve indicates that peak SWE recovery begins when juvenile trees reach approximately 3 m in height. Peak SWE recovers approximately 50% when trees reach 10 m in height, 75% at approximately 15 m, and approach 100% (fully recovered) when trees are greater than 30 m in height. The spread of recovery values (-50% to 50%) for below-crown areas relating to small trees in J2 is a function of the recovery equation (Equation 5-1) and results when measured below-crown SWE values are similar (slightly larger or smaller) to that of the average SWE representing the clearcut condition. The spread in recovery around 0% for trees less than 3 m in height indicates no measurable hydrological recovery.

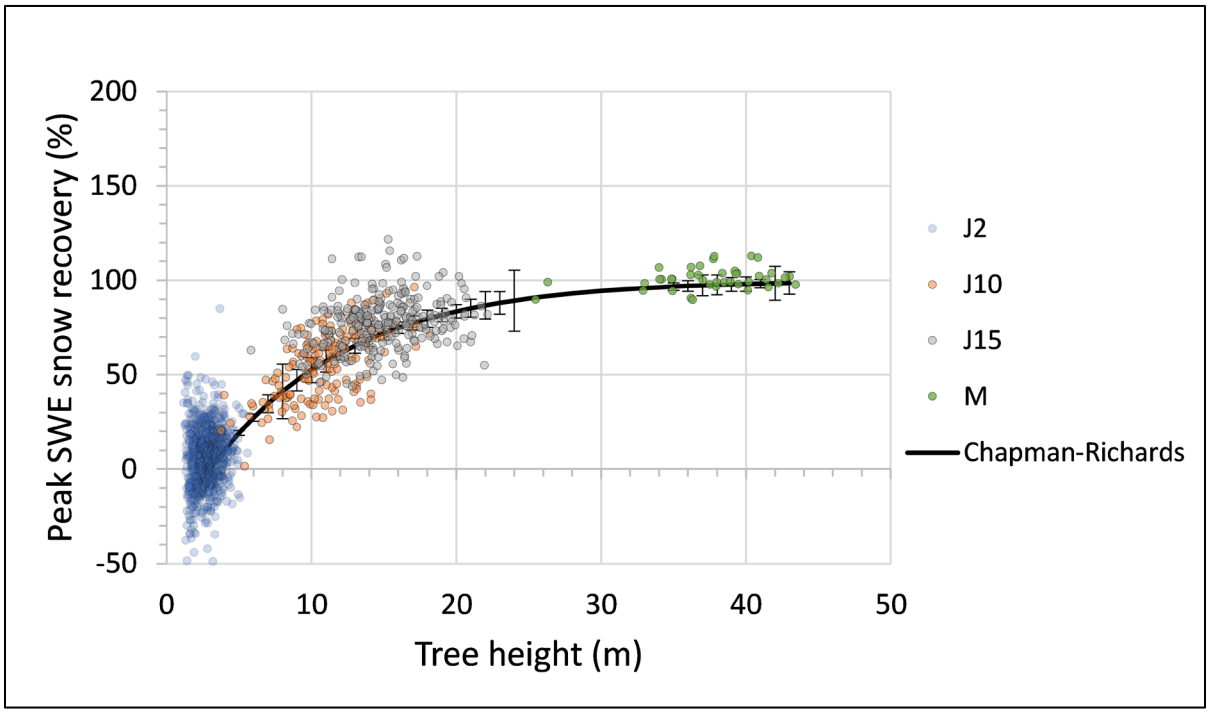

Figure 5-11 Peak snow water equivalent (SWE) recovery for below-crown snowpack in sites J2 (blue), J10 (orange), J15 (grey) and M (green) with a fitted Chapman-Richards curve. Error bars indicate the 90% confidence interval on the curve.

Ablation recovery

Ablation recovery % (SR, Equation 5-1) applied to CBC snowpack for all identified trees in sites J2, J10, J15, and M) are shown below in Figure 5-12. The Chapman-Richards curve fitted to the below-crown measures of average daily ablation according to tree height for all stands indicates that ablation recovery begins when stands reach approximately 3 m in height. However, the distribution of below-crown ablation rate according to tree height shown in Figure 5-10 suggests this recovery should start when trees reach a height of 5 m. A 5 m stand height initiation of ablation recovery is more likely than the 3 m stand height for initial recovery identified using the fitted Chapman-Richards curve due to the limitations of curve fitting. Error bars representing the 90% confidence interval according to integer tree height indicate that the relationship between tree height and average daily ablation recovery is less robust than was observed for the relationship between tree height and peak SWE recovery. The resulting curve indicates that ablation recovery reaches 50% when trees reach a height of approximately 9 m, 75% at approximately 12 m, and approach 100% recovery when trees are greater than 30 m. Similar to SWE recovery, small trees in J2 display a range of ablation recovery values from -50% to 50% for reasons explained above.

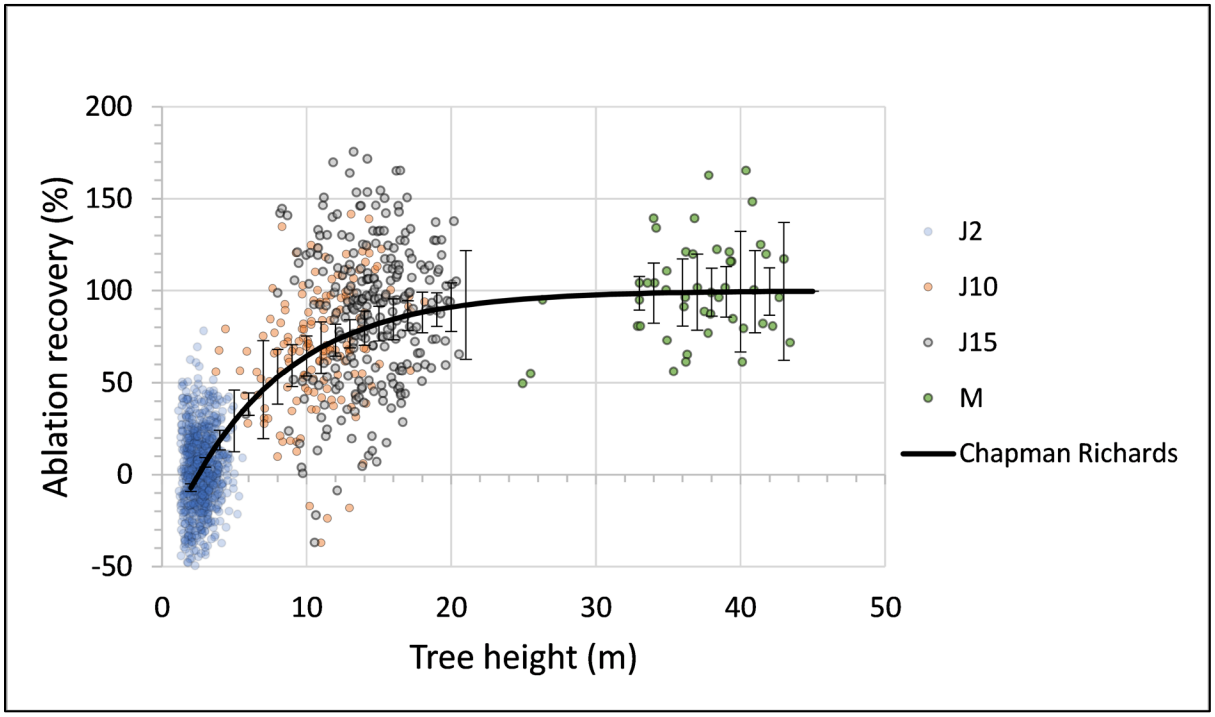

Figure 5-12 Ablation recovery by tree height calculated from average below-crown daily ablation rates compared to stand-level mean daily ablation rate for the same time range (March 21, 2019, to March 28, 2019). Error bars represent the 90% confidence interval on the curve.

5.4. Discussion

Fine resolution gridded models of snow depth, SWE, and average daily ablation produced from high precision mobile terrestrial LiDAR scans provided a unique ability to consider not only stand-level averages of peak SWE and ablation recovery, but also the variability of within-stand recovery related to the influence of individual tree crowns. By considering below-crown snowpack for trees within each stand, we were able to better understand the process by which hydrological recovery progresses as a replanted stand matures, and a continuous canopy develops.

While significant differences in both peak SWE and daily ablation existed between the openings and CBC areas in each stand, this significance when considered alone, fails to identify the drivers or reasons behind this difference. Although there was a decrease in peak SWE in the CBC area with increasing stand maturity, the magnitude of this difference in each site changes as trees grow. As the trees mature, there was a stand-level reduction in the peak SWE related to increasing canopy cover and interception ability which affects not only the CBC area, but also the accumulation in the openings. However, the reduction in peak SWE observed between sites is much more pronounced in CBC areas than in the openings.

In J2, where trees have small diameter crowns, individual trees are less effective at reducing ground-level snow accumulation through interception, and the peak SWE is similar in the openings and below-crown areas. In J10, where individual trees have a greater interception capacity than trees in J2 due to their larger crown diameter, there was a greater decrease in the below-crown peak SWE. However, in this site the canopy is still non-continuous, and the control on the below-crown snowpack is still highly localized. In this site, below-crown reduction in peak SWE is observable as deep tree wells, where openings (areas beyond the crown extent) still have a comparable snow accumulation depth to openings in J2.

In J15, the magnitude of the difference in peak SWE between the openings and below-crowns was similar to that seen in J10. However, there were fewer openings overall as the individual crowns in this site began to behave collectively as a continuous canopy. This process of increasing interception capacity with increasing canopy cover progresses as the stand matures. In the mature site (M) where the canopy was continuous, the snowpack in any remaining small openings is controlled by the stand level canopy cover, and the peak SWE in this site was much more uniform throughout the stand.

The average daily ablation rate decreased with increasing stand maturity, with significant differences between the opening and CBC areas in each site. The total range in average daily ablation also decreased with increasing stand maturity, as the individual tree crowns coalesce to form a more uniform canopy cover. The greatest decrease in daily ablation rate was observed between sites J2 and J10. The ablation rate in the openings in J2 was lower than in the CBC area. This observation in J2 is contrary to the taller juvenile and mature stands, where the individual crowns display reduced melt rates in the below-crown area. In J2, comparisons of daily ablation in the combined open area to below-crown areas, grouped according to tree height, highlights a period when trees smaller than 5 m correspond with an increased ablation rate compared to the adjacent openings. Longwave radiation emitted from these small trees may be driving this increase and is consistent with observations of LWR emission by trees under 5 m in height observed by Hotovy and Jenicek (2020). This finding is an example of negative ablation recovery and describes a period of time when juvenile trees act to increase the below-crown melt rate relative to the clearcut condition. While negative recovery has been observed in previous studies (Buttle et al, 2005; Winkler and Boon, 2015), the space-for-time substitution design used here provides new insights of the process by which a recently replanted stand in a snow-dominated watershed transitions from a period of negative to positive hydrological recovery.

Peak SWE and daily ablation in regenerating juvenile stands recover at different rates. The recovery of ablation rate begins later than for peak SWE due to an initial period of negative ablation recovery but progresses more quickly than recovery of peak SWE. Higher stocking densities in recently replanted stands may exacerbate the negative recovery ‘effect’ as the below-crown area of many individual trees cumulatively increase the ablation rate of the stand. Minimal peak SWE recovery in a recently replanted stand, paired with this period of negative recovery could have hydrological implications at a watershed scale. The negative recovery ‘effect’ is of greatest concern for watersheds where the majority of harvest has occurred over a narrow time span. In these watersheds progressively larger increases in stand level ablation rates as the juvenile stand grows through the 5 m height threshold has the potential to cause progressively larger changes in stream flow during the first decade or more of regrowth.

This study primarily focused on recovery of north aspect stands according to tree height, rather than canopy cover. While other studies (Buttle et al, 2005; Hudson, 2000; Winkler and Boon, 2015) have considered the influence of canopy cover to quantify hydrological recovery at a stand level, the sites used in this study were too small to establish these relationships. However, by quantifying the influence

of individual trees on hydrological recovery according to tree height, differences in canopy cover, either naturally occurring or related to selective harvest or post-harvest restocking density, could potentially be accounted for by adjusting the total CBC area within the stand. This ability to combine the influence of individual trees enables potential transferability of the applied recovery to stands with a high degree of internal variability in vegetation height and density. However, the transferability of recovery curves developed from this study to stands with different topographic characteristics such as elevation or slope aspect, or to stands with different species composition, would require further study.

Although individual tree crowns may influence the below-crown snowpack of neighboring trees and adjacent openings, this 'neighbor' effect was not specifically investigated in this study. The general trends observed here, which show a stand-level decrease in both peak SWE and ablation rate not only for the full stand, but also for cumulative open areas as stands mature, suggest that this effect may be significant. Additionally, the large range of below-crown ablation recovery values observed for juvenile 10 m – 20 m trees (Figure 5-12) suggests that individual tree crowns are unlikely be the sole factor influencing measures of below-crown ablation recovery in these juvenile stands.

The opportunistic study design employed here utilized the cumulative open areas in J2 to represent the clearcut condition. The total open area in J2 accounted for approximately 50% of the site and was assumed to act as an effective proxy for a clearcut, as the very small trees lacked interception capacity and were largely needle-free western larch. The extent to which the small trees in this site may have contributed to the net energy balance in the adjacent openings is unknown. Quantifying their influence on peak SWE and ablation would require a more rigorous study comparing J2 openings to a fully clearcut area.

The use of mobile terrestrial LiDAR allowed for the development of exceptionally high-resolution snow surface, terrain models, and forest delineation, even under dense forest canopy where aerial point clouds from aerial LiDAR are sparse. The presence of understory brush in J10 introduced uncertainty for surface models representing bare ground and low-snow conditions. Clearing understory brush in the fall, prior to the start of snow accumulation would have reduced this uncertainty. The range of the LiDAR unit was effective for measuring canopy height and structure in trees up to approximately 25m in height. Above this height, occlusion by lower branches reduced the point density of the upper canopy, resulting in lower-resolution canopy height model.

This study focused on north aspect slopes, where vegetation has been shown to play a larger role in determining differences in the energy balance between forested areas and openings. On north aspects, differences in peak snow accumulation between openings and CBC areas was greatest in juvenile stands where the canopy is non-continuous, and where trees crowns were smaller and lack the interception ability of a mature stand. Individual tree crowns in these juvenile stands have a strong but localized control on both peak SWE and ablation. Recovery of peak SWE on north aspects in the Rover Creek begins when trees reach a height of approximately 3 m, while ablation recovery begins at approximately 5 m, with both peak SWE and ablation reaching full recovery when stands are approximately 30 m in height. These study outputs are similar to those found by Winkler and Boon (2015), although the start of recovery was delayed and reaches full recovery when stands are 5 m taller than those included in this prior study.

5.5. Conclusions

Previous studies (Hudson, 2000; Buttle et al., 2005; Winkler and Boon, 2015) investigated the process of hydrological recovery by comparing the stand-average peak SWE or daily ablation, resulting in generalized stand-level recovery curves. These simplified models of recovery lack transferability to stands where forest cover characteristics differ greatly from reference sites. The fine-resolution snow depth and vegetation models derived from LiDAR used in this study allowed for the investigation of hydrological recovery at both the stand level and at the scale of the individual tree. By considering the influence of individual tree crowns on below-crown snowpack measures of peak SWE and ablation rate, hydrological recovery at a stand level can be estimated by aggregating the effect of individual trees, regardless of unique stand characteristics and within-stand variability.

The results from this study indicate a period of negative ablation recovery for juvenile trees less than 5m in height. These findings support those observed by Buttle et al (2005) and Winkler and Boon (2015). Although negative recovery has been reported previously, the height at which trees transition from having a negative to positive influence on the stand's hydrological recovery is newly identified. In recently replanted clearcut stands where trees are smaller than approximately 5 m in height, individual trees have very little control on peak SWE but do increase the below-crown ablation rate compared to open areas. Depending on the stocking density of these smaller trees, and the total area of recently replanted blocks, the potential cumulative influence on the stand-wide ablation rate could have implications for annual stream flow including peak flows within a watershed.

This study focused on north aspects between 950 m and 1050 m elevation, while the individual sites included in this study were limited to primarily Douglas fir, lodgepole pine, western larch, cedar, and hemlock-dominated stands, where much of the forestry-related disturbance in the Kootenay region of British Columbia is focused. To better understand how hydrological recovery processes differ throughout a watershed, and to improve predictions of watershed-scale hydrological response to current and projected levels of forest disturbance, the outcomes from this study should be supplemented with a more comprehensive assessment of tree-scale and stand-scale recovery in juvenile and recovering stands representing a more complete range of species, slope gradient, aspect, and elevation.

Declaration of Competing Interest

The authors declare that they have no known competing financial interests or personal relationships that could have appeared to influence the work reported in this paper.

Acknowledgements

Funding for this work was provided by the Natural Sciences and Engineering Research Council of Canada CCIP grant 517639-2017 - Building an Innovative Forestry Technology Sector, Selkirk Innovates, and Innovate BC. Selkirk Innovates is gratefully acknowledged for providing fieldwork equipment and support staff. We thank Tina Deenik for her insightful discussion and editorial support.

References

American Society for Photogrammetry and Remote Sensing (ASPRS) (2019). LAS Specification 1.4 – R15. *https://www.asprs.org/wp-content/uploads/2019/07/LAS_1_4_r15.pdf*

Boon, S (2007). Snow accumulation and ablation in a beetle-killed pine stand in Northern Interior British Columbia. *BC Journal of Ecosystems and Management* 8(3):1–13. url: http://www.forrex.org/publications/jem/ISS42/vol8_no3_art1.pdf

Broxton, P. D., Harpold, A. A., Biederman, J. A., Troch, P. A., Molotch, N. P., & Brooks, P. D. (2015). Quantifying the effects of vegetation structure on snow accumulation and ablation in mixed-conifer forests, 1094(October 2014), 1073–1094*. https://doi.org/10.1002/eco.1565*

Buttle, J.M., Creed, J. M.., & Pomeroy, J. W. (2000). Advances in Canadian forest hydrology, 1995 – 1998. Hydrological Processes, 14, 1551-1578.

Buttle, J, M., Oswald, C.J., and Woods, D.T. (2005). Hydrologic Recovery of Snow Accumulation and Melt Following Harvesting in Northeastern Ontario. *62nd Eastern Snow Conference. Waterloo, ON, Canada 2005*.

CloudCompare (version 2.10.2 (Zephyrus)) [GPL software]. (2019). Retrieved from http://www.cloudcompare.org/

Deems, J. S., & Painter, T. H. (2006). Lidar measurement of snow depth: accuracy and error sources. *Proceedings of the 2006 International Snow Science Workshop: Telluride, Colorado, USA, International Snow Science Workshop*, *330*, 330–338.

Deems, J. S., Painter, T. H., & Finnegan, D. C. (2013). Lidar measurement of snow depth: A review Lidar measurement of snow depth: a review. *Journal of Glaciology*, *59*, 467–479. https://doi.org/10.3189/2013JoG12J154

Dickerson-Lange, S. E., Lutz, J. A., Gersonde, R., Martin, K. A., Forsyth, J. E., & Lundquist, J. D. (2015). Water Resources Research. https://doi.org/10.1002/2015WR017873.Received

Dickerson-Lange, S. E. (2021). Ranking Forest Effects on Snow Storage: A Decision Tool for Forest Management Water Resources Research. https://doi.org/10.1029/2020WR027926

Dickerson-Lange SE, Howe ER, Patrick K, Gersonde R and Lundquist JD (2023) Forest gap effects on snow storage in the transitional climate of the Eastern Cascade Range, Washington, United States. Front. Water 5:1115264. doi: 10.3389/frwa.2023.111526

Dixon, D., Boon, S., & Silins, U. (2014). Watershed-scale controls on snow accumulation in a small montane watershed, southwestern Alberta, Canada, *1306* (January 2013), 1294–1306. https://doi.org/10.1002/hyp.9667

Ellis, C. R., Pomeroy, J. W., Brown, T., & Macdonald, J. (2010). Simulation of snow accumulation and melt in needleleaf forest environments, (1995), 925–940. https://doi.org/10.5194/hess-14-925-2010

Ellis, C. R., Pomeroy, J. W., Essery, R. L. H., & Link, T. E. (2011). Effects of needleleaf forest cover on radiation and snowmelt dynamics in the Canadian Rocky Mountains. *Can. J. For. Res.*, *41*, 608–620. https://doi.org/10.1139/X10-227

Ellis, C. R., Pomeroy, J. W., & Link, T. E. (2013). Modeling increases in snowmelt yield and desynchronization resulting from forest gap-thinning treatments in a northern mountain headwater basin, *49*, 936–949. https://doi.org/10.1002/wrcr.20089

Green, K. C., & Alila, Y. (2012). A paradigm shift in understanding and quantifying the effects of forest harvesting on floods in snow environments. *WATER RESOURCES RESEARCH*, *48*(August), 1–21. https://doi.org/10.1029/2012WR012449

Gronsdahl, S., Moore, R. D., Winkler, R., Rosenfeld, J., & Mccleary, R. (2019). Effects of forestry on summertime low flows and physical fish habitat in snowmelt-dominant headwater catchments of the Pacific Northwest, (August), 3152–3168. https://doi.org/10.1002/hyp.13580

Hedstrom, N.R. and Pomeroy, J.W. (1998). Measurements and modelling of snow interception in the boreal forest. Hydrol. Process., 12: 1611-1625. https://doi.org/10.1002/(SICI)1099-1085(199808/09)12:10/11<1611::AID-HYP684>3.0.CO;2-4

Hollander, M., Chicken, E., & Wolfe, D. A. (2014). *Nonparametric statistical methods* (Third edition.). John Wiley & Sons, Inc.

Hopkinson, C., Collins, T., Anderson, A., Pomeroy, J., and Spooner, I. (2012). Spatial Snow Depth Assessment Using LiDAR Transect Samples and Public GIS Data Layers in the Elbow River Watershed, Alberta. *Canadian Water Resources Journal/Revue Canadienne Des Ressources Hydriques,* 37(2), 69-87, DOI : 10.4296/cwrj3702893

Hotovy, O., & Jenicek, M. (2020). The impact of changing subcanopy radiation on snowmelt in a disturbed coniferous forest, (October), 5298–5314. https://doi.org/10.1002/hyp.13936

Hudson, R. (2000). Snowpack recovery in regenerating coastal British Columbia clearcuts. *Canadian Journal of Forest Research*, *30*(4), 548.

Konstantinos, A.M., Storck, P., & Lettenmaier, D. P. (2009). Modeling snow accumulation and ablation processes in forested environments, *45*(February), 1–13. https://doi.org/10.1029/2008WR007042

Kostadinov, T. S., Schumer, R., Hausner, M., Bormann, K. J., Ga, R., Mcgwire, K., … Harpold, A. A. (2019). Remote Sensing of Environment Watershed-scale mapping of fractional snow cover under conifer forest canopy using lidar, *222*(November 2018), 34–49. https://doi.org/10.1016/j.rse.2018.11.037

Moore, R. D., & Wondzell, S. M. (2006). Physical Hydrology and the Effects of Forest Harvesting in the Pacific Northwest: A Review. *Journal of the American Water Resources Association,* 04065, 763–784.

Murray, C. D., & Buttle, J. M. (2003). Impacts of clearcut harvesting on snow accumulation and melt in a northern hardwood forest, *271*, 197–212.

Pickett, S.T.A. (1989). Space-for-Time Substitution as an Alternative to Long-Term Studies. In: Likens, G.E. (eds) Long-Term Studies in Ecology. Springer, New York, NY. https://doi.org/10.1007/978-1-4615-7358-6_5

QGIS.org, 2024. QGIS Geographic Information System. QGIS Association. http://www.qgis.org

R Core Team (2020). R: A language and environment for statistical computing. R Foundation for Statistical Computing, Vienna, Austria. URL https://www.R-project.org/

Schnorbus, M., and Y. Alila (2004), Forest harvesting impacts on the peak flow regime in the Columbia Mountains of southeastern British Columbia: An investigation using long-term numerical modeling, Water Resour. Res., 40, W05205, doi:10.1029/2003WR002918.

Silva, C.A., Crookston, N.L., Hudak, A.T., Vierling, L.A., Carine Klauber, C., and Cardil, A. (2017). rLiDAR: LiDAR Data Processing and Visualization. R package version 0.1.1. https://CRAN.R-project.org/package=rLiDAR

Spittlehouse, D.L. and R.D. Winkler (2004). Snowmelt in a forest and clearcut. Proceedings 72nd Western Snow Conference, Vancouver, BC, pp. 33-43.

Soininen, A. Terrasolid (2016). TerraScan (V.16) [computer software.

Varhola, A., Coops, N. C., Weiler, M., & Moore, R. D. (2010). Forest canopy effects on snow accumulation and ablation: An integrative review of empirical results. *Journal of Hydrology*, *392*(3–4), 219–233. https://doi.org/10.1016/j.jhydrol.2010.08.009

Winkler, R. D., & Moore, R. D. (2006). Variability in snow accumulation patterns within forest stands on the interior plateau of British Columbia, *3695*, 3683–3695. https://doi.org/10.1002/hyp

Winkler, R.D., Spittlehouse, D.L. and Golding, D.L. (2005), Measured differences in snow accumulation and melt among clearcut, juvenile, and mature forests in southern British Columbia. Hydrol. Process., 19: 51-62. https://doi.org/10.1002/hyp.5757

Winkler, R.D., Spittlehouse, D.L. and Golding, D.L. (1995), The Importance of Sample Size in Forest/Clearcut Snow Accumulation Comparisons. *Mountain hydrology, Peaks and Valleys in Research and Applications*. Proceedings from a conference, May 16-19, 1995, Vancouver, British Columbia.

Winkler, R., Boon, S., Zimonick, B., & Baleshta, K. (2010). Assessing the effects of post-pine beetle forest litter on snow albedo, *812*(April 2009), 803–812. https://doi.org/10.1002/hyp.7648

Winkler R.D. and Boon, S., (2015), Revised Snow Recovery Estimates for Pine-Dominated Forests in Interior British Columbia. B.C. Ministry of Forests, Lands and Natural Resource Operations, Extension Note 116 (https://www.for.gov.bc.ca/hfd/pubs/docs/en/EN116.PDF).

Winkler, R., Spittlehouse, D., & Boon, S. (2017). Streamflow response to clear-cut logging on British Columbia's Okanagan Plateau. *Ecohydrology*, *10*(2), 1–15. https://doi.org/10.1002/eco.1836

Zheng, Z., Kirchner, P. B., & Bales, R. C. (2016). Topographic and vegetation effects on snow accumulation in the southern Sierra Nevada: a statistical summary from lidar data, 257–269. https://doi.org/10.5194/tc-10-257-2016

Appendix

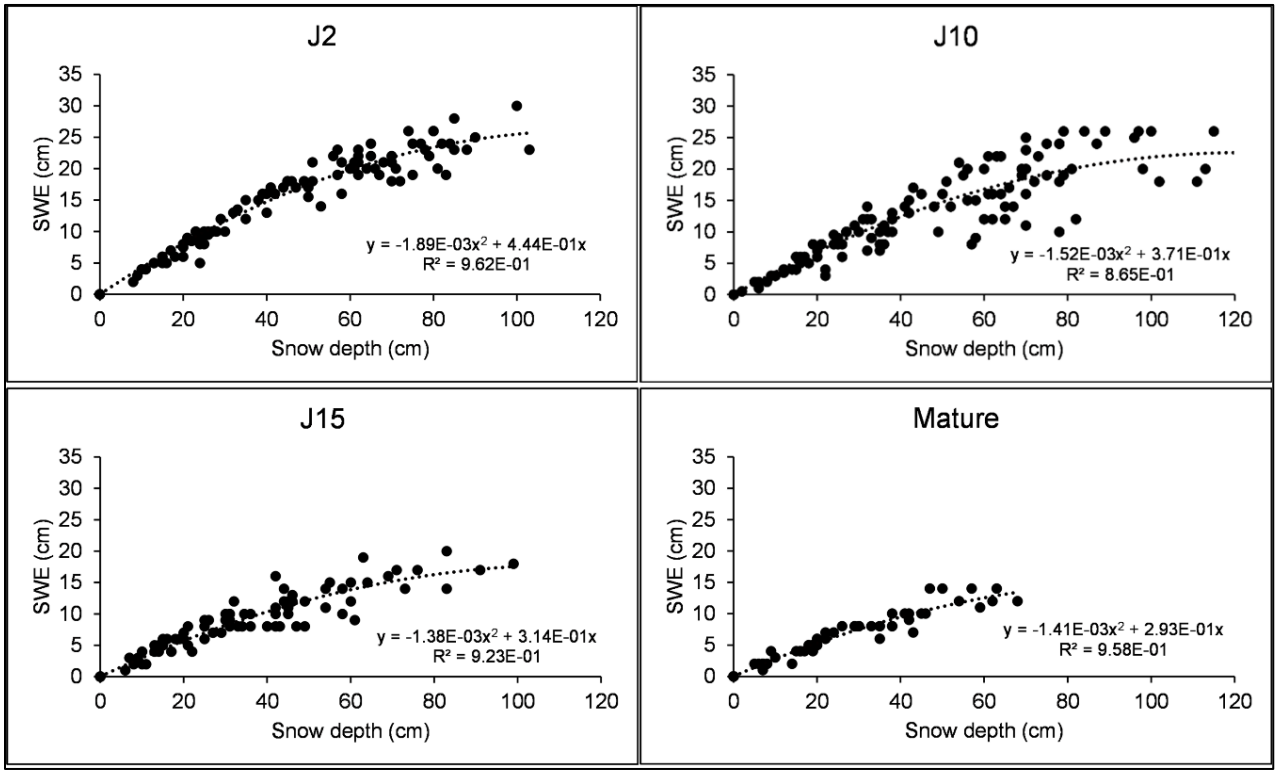

Figure 5-A1 Snow depth to Snow Water Equivalent (SWE) relationships derived from snow core sampling using a standard Federal snow tube in study sites J2, J10, J15, and M undertaken from March 14, 2019, through the stand specific end of the ablation period (March 31-April 24) in each site.

CHAPTER 6: Conclusions and future work

This thesis presents the first LiDAR-based analysis of the recovery of hydrological processes according to forest stand regeneration. Utilization of mobile terrestrial LiDAR scans for investigations of sub-canopy snow processes allow for the quantification of peak SWE and ablation rate to be considered at spatial resolutions not possible in prior studies.

In Chapter 4, these fine-resolution models were used as a proxy for a snowpack to investigate how point sampling distances might impact stand-averaged estimations of peak snow depth and melt rate. Stand-averaged calculations from point samples collected at traditional 10 m to 15 m point sampling distances were compared to stand averages resulting from increasingly smaller sampling distances. For snow depth, sampling distances greater than 10 m, and for daily ablation, distances of greater than 6 m were shown to produce a larger range of values. Below these sampling distances, the calculated values were less variable. The greatest range in stand-averaged peak snow depth was observed in juvenile 10 m and 15 m stands where the within-stand snow variability is greatest. In J10, the range in derived stand-level snow depth differed by 20 cm depending on the sampling distance used. This suggests that for areas where small trees and vegetation contribute to greater within-stand depth variability, much higher sampling intensity is required to accurately quantify the snowpack. Decreasing the sampling distances to 1 m in J10 and to 2 m in J15 reduced the uncertainty in derived snow depths.

Between-stand differences in snow depth related to differences in stand maturity indicate that higher sample sizes and smaller sampling distances are required for identifying differences between stands with similar levels of maturity. As the melt season progresses the sampling intensity required to identify differences between juvenile and open stands increases, while the sampling intensity required to identify differences between juvenile and mature stands decreases.

Individual tree crowns and their associated treetop heights were derived from canopy height models produced from the mobile terrestrial LiDAR scans performed at the end of the snow melt period in each site. The footprints of these trees were used in Chapter 5 to assess both stand-level relationships between peak SWE and daily ablation according to stand maturity, as well as to investigate how individual trees within each stand influence the below-crown snowpack and stand-level snowpack variability.

Previous studies undertaken to quantify the process of hydrological recovery compared stand-average peak SWE or daily ablation, resulting in generalized stand-level recovery curves. These simplified models of recovery lack transferability to stands where forest cover characteristics differ greatly from reference sites. The fine-resolution snow depth and vegetation models derived from LiDAR used in this study allowed for the investigation of hydrological recovery at both the stand level and at the scale of the individual tree. By considering the influence of individual tree crowns on below-crown snowpack measures of peak SWE and ablation rate, hydrological recovery at a stand level can be estimated by aggregating the effect of individual trees, regardless of unique stand characteristics and within-stand tree height and crown cover variability.

This study reveals a much more complicated relationship between stand maturity and the process of hydrological recovery, particularly in juvenile stands where individual tree crowns act to control sub-crown snowpack. Outputs presented here highlight a period of negative ablation recovery for juvenile trees less than 5 m in height. These findings support those observed by Buttle et al (2005) and Winkler and Boon (2015). Although negative recovery has been reported previously, the height at which trees transition from having a negative to positive influence on the stand's hydrological recovery is newly identified. In recently replanted clearcut stands where trees are smaller than approximately 5 m in height, individual trees have very little control on peak SWE, but do increase the below-crown ablation rate compared to open areas. Depending on the stocking density of these smaller trees, and the total area of recently replanted blocks, the potential cumulative influence on the stand-wide ablation rate could have implications for annual stream flow including peak flows within a watershed.

Limitations and Future Work

This limited study focused exclusively on north aspects between 950 and 1050 m elevation within a single biogeoclimatic subzone characterized Douglas fir, lodgepole pine, western larch, cedar, and hemlock-dominated stands. To better understand how hydrological recovery processes differ throughout a watershed, and to improve predictions of watershed-scale hydrological response to current and projected levels of forest disturbance, the outcomes from this study should be supplemented with a more comprehensive assessment of tree-scale and stand-scale recovery in juvenile and recovering stands representing a more complete range of species, slope gradient, aspect, and elevation. An investigation of the relationship between canopy cover and hydrological recovery should also be incorporated into any future works as canopy cover acts to control the net energy reaching the snow surface.

To better understand the potential implications of the initial period of negative ablation recovery observed in the below-crown snowpack associated with trees less than 5m in height, the influence of these small trees on below-crown peak SWE and ablation rate should be investigated on south aspects, and across a range of elevations. A more comprehensive understanding of the timing and height at which regenerating stands throughout the watershed transition from negative to positive recovery may be useful for adjusting forestry planning procedures to mitigate a possible period of increased flooding risk due to faster melt.

Aerial LiDAR surveys offer an opportunity to investigate hydrological recovery across a full watershed basin using methodologies presented here, although an improved methodology for determination of depth to SWE relationships across a range of elevations and aspects is required. For this study, depth to SWE relationships were developed from direct sampling of the snowpack. This labour and time-intensive approach is unrealistic in a large or topographically complex watershed where elevation and aspect will influence snowpack density. The accuracy of any aerial lidar-based assessment should be calibrated using finer-precision mobile terrestrial LiDAR scans, as ground point densities and positional accuracies from an aerial platform are typically much lower than from terrestrial LiDAR scans, particularly in areas with thick vegetation or topographic relief.